University of New Hampshire
University of New Hampshire Scholars' Repository

Doctoral Dissertations | Student Scholarship

Fall 2006

CUPOLETS: Chaotic unstable periodic orbits theory and applications

Kourosh Zarringhalam
University of New Hampshire, Durham

Follow this and additional works at: https://scholars.unh.edu/dissertation

Recommended Citation
Zarringhalam, Kourosh, "CUPOLETS: Chaotic unstable periodic orbits theory and applications" (2006). *Doctoral Dissertations*. 349.
https://scholars.unh.edu/dissertation/349

This Dissertation is brought to you for free and open access by the Student Scholarship at University of New Hampshire Scholars' Repository. It has been accepted for inclusion in Doctoral Dissertations by an authorized administrator of University of New Hampshire Scholars' Repository. For more information, please contact nicole.hentz@unh.edu.

CUPOLETS: Chaotic Unstable Periodic Orbits Theory and Applications

BY

Kourosh Zarringhalam

B.S., Razi University, 1999
M.S., Isfahan University of Technology, 2001

DISSERTATION

Submitted to the University of New Hampshire
in partial fulfillment of
the requirements for the degree of

Doctor of Philosophy

in

Mathematics

September 2006

Reproduced with permission of the copyright owner. Further reproduction prohibited without permission.

UMI Number: 3231362

INFORMATION TO USERS

The quality of this reproduction is dependent upon the quality of the copy submitted. Broken or indistinct print, colored or poor quality illustrations and photographs, print bleed-through, substandard margins, and improper alignment can adversely affect reproduction.

In the unlikely event that the author did not send a complete manuscript and there are missing pages, these will be noted. Also, if unauthorized copyright material had to be removed, a note will indicate the deletion.

UMI®

UMI Microform 3231362

Copyright 2006 by ProQuest Information and Learning Company.

All rights reserved. This microform edition is protected against unauthorized copying under Title 17, United States Code.

ProQuest Information and Learning Company
300 North Zeeb Road
P.O. Box 1346
Ann Arbor, MI 48106-1346

Reproduced with permission of the copyright owner. Further reproduction prohibited without permission.

This dissertation has been examined and approved.

Kevin M. Short

Dissertation Director, Kevin M. Short
Professor of Mathematics

Eric Grinberg

Eric L. Grinberg, Professor of
Mathematics

Marianna Shubov

Marianna Shubov, Professor of
Mathematics

Don Hadwin

Donald W. Hadwin, Professor of
Mathematics

Michael J. Carter

Michael J. Carter, Associate Professor of
Electrical Engineering

July 19, 2006
Date

Reproduced with permission of the copyright owner. Further reproduction prohibited without permission.

DEDICATION

With love, to my family.

Reproduced with permission of the copyright owner. Further reproduction prohibited without permission.

ACKNOWLEDGMENTS

I wish to thank a number of people without whom this thesis would have been impossible. I am sincerely in debt to my advisor professor Kevin Short for providing me with lots of research opportunities and guiding me through this dissertation. Professor Short is an enthusiastic and creative researcher who sincerely shares his knowledge with his students and I am very grateful to have the privilege of being his student. I would also like to thank Professor Don Hadwin for all the things he taught me and all the unconditional support that I have got from him.

Also I would like to express my gratitude to the rest of my dissertation committee members, Professor Mariana Shubov, Professor Michael Carter and especially Professor Eric Grinberg for all their support and mentoring.

Thanks to my friend Ian Berry for all the useful discussions we had and all the help with computations.

Finally I would like to thank my wife Glareh who has always been there for me and has given me her unconditional love and support.

Reproduced with permission of the copyright owner. Further reproduction prohibited without permission.

TABLE OF CONTENTS

Page

DEDICATION iii

ACKNOWLEDGMENTS iv

LIST OF TABLES vii

LIST OF FIGURES viii

ABSTRACT xi

CHAPTER

1. BACKGROUND 1

1.1 Introduction 1

1.1.1 Asymptotic Behavior 6

2. CUPOLETS 14

2.1 Introduction 14
2.2 Generating Controlled Stabilized Periodic Orbits 15

3. ADAPTIVE MULTIRESOLUTION ANALYSIS 24

3.1 Introduction 24
3.2 A Walsh Transform-like approach 27
3.3 Partial Periodic Multiresolution Analysis 36
3.4 Scaling and Shifting 47

Reproduced with permission of the copyright owner. Further reproduction prohibited without permission.

4. THEORETICAL RESULTS **55**

4.1 Introduction 55
4.2 Background Materials 57

4.2.1 Definitions 58
4.2.2 Fixed Point Theorems 64
4.2.3 Method of containment 67
4.2.4 A fixed point method 71

4.2.4.1 Non-periodic shadowing 71
4.2.4.2 Periodic shadowing 77

4.3 Finite time shadowing theorem 80

4.3.1 Non-periodic shadowing theorem 81
4.3.2 Periodic shadowing theorem 91

5. CONCLUSION **100**

BIBLIOGRAPHY **102**

Reproduced with permission of the copyright owner. Further reproduction prohibited without permission.

LIST OF TABLES

Table **Page**

1.1 Period doubling bifurcation in Logistic map. 4

Reproduced with permission of the copyright owner. Further reproduction prohibited without permission.

LIST OF FIGURES

Figure **Page**

1-1 Time series of the Logistic map for different values of the parameter r. The r values are, (a) $r = 2.8$, (b) $r = 3.3$, (c) $r = 3.5$ and (d) $r = 3.9$ respectively. 3

1-2 Bifurcation diagram of the logistics map. 5

1-3 The solution $x(t)$ of the Lorenz system. 6

1-4 (a) The attractor of the Lorenz system and its projections to (b) $x - y$, (c) $x - z$ and (d) $y - z$ planes. 7

1-5 The Poincaré map. 11

2-1 Double scroll oscillator. (a) Electrical schematic and (b) nonlinear negative resistance g. 16

2-2 (a) The Attractor of the Double Scroll oscillator and its projections to (b) $x - y$, (c) $x - z$ and (d) $y - z$ planes. Here $x = v_{c_1}$, $y = v_{c_2}$ and $z = i_L$. The straight lines in part (c) of the figure are the Poincaré cross sections. 17

2-3 Top view of the intersection of the Poincaré surface with one of the lobes of the double scroll attractor. The asterisks show the places where the trajectory pierces the Poincaré surface. 19

2-4 Coding function $r(x)$ 20

2-5 This figure shows a few of the cupolets of the double scroll system with different periods. The control sequences applied to obtain the cupolets are, (a)00, (b)11, (c) 01 and (d) 001. 23

Reproduced with permission of the copyright owner. Further reproduction prohibited without permission.

3-1 The compact cupolets in the second column of this figure are created by using the phase transformation to compact form of the corresponding cupolets in the first column of the figure. 28

3-2 Basis element for the space V^2. 30

3-3 An arbitrary signal f is approximated using the compact cupolets shown in (a). There are 256 sample points in the signal f. The approximations are done at levels 0, 4, and 8. The number of basis elements for each of these resolution-level is 1, 16, and 256 respectively. 34

3-4 An arbitrary signal f is approximated using the compact cupolets shown in (a). There are 256 sample points in the signal f. The approximations are done at levels 0, 4, and 8. The number of basis elements for each of these resolution-level is 1, 16, and 256 respectively. 35

3-5 (a) Original 256×256 Image, (b) fourth resolution-level with 16 basis elements, (c) Sixth resolution-level with 63 basis elements and (d) eighth resolution-level with 254 basis elements. The size of the windowed data is one scan line (256). 37

3-6 The functions in the first column of the figure represent examples of compact cupolets at the coarsest resolution. The versions in the second column of the figure, correspond to the level 4 scaling function. 40

3-7 These figures illustrate approximations of an arbitrary signal f. There are 4 different available resolution-levels and the number of basis elements in the resolution-levels are 32, 64, 128 and 256 respectively. 44

3-8 These figures illustrate spectral values as well as the enclosing envelop function of the signal f in Figure (3-7) in the 4 available resolution-levels. 45

3-9 The total number of basis elements used is 4, 8 and 16 respectively. 48

Reproduced with permission of the copyright owner. Further reproduction prohibited without permission.

3-10 (a) Original 256×256 Image, (b) level 2, (c) level 3 and (d) level 4. The size of the windowed data is 256 and the number of basis elements used in each resolution-level is 24, 54 and 120 per window. 49

3-11 The length of the signal f is 256 and the approximations are done up to resolution-levels (a) 3, (b) 5 and (c) 7. The number of basis elements used in each case is 7, 31 and 127 respectively. 51

3-12 (a) Original 256×256 Image, (b) reconstruction up to resolution level 4, (c) reconstruction up to resolution-level 6 and (d) reconstruction up to resolution-level 7. The length of the windowed data is 256 and the number of basis elements used in each resolution-level is 15, 63 and 127 per windowed data respectively. 52

4-1 Geometric interpretation of the Browder fixed point theorem. For example if the point u on the boundary of the box C lives on the upper edge of the box as shown in part (a) of the figure, then the map $u - f(u)$ has to live in the upper half plane in $\mathbb{R}^2$, i.e., the dashed area shown if part (b) of the figure. 68

4-2 Containment Method 70

4-3 Pseudo orbit y_k and shadowing orbit x_k. 74

4-4 The convex set U containing the $\delta-$ pseudo orbit $\{y_k\}_{k=0}^{N}$. 76

4-5 Pseudo orbit y_k and shadowing orbit x_k. 83

Reproduced with permission of the copyright owner. Further reproduction prohibited without permission.

ABSTRACT

CUPOLETS: Chaotic Unstable Periodic Orbits Theory and Applications

by

Kourosh Zarringhalam
University of New Hampshire, September, 2006

Recent theoretical work suggests that periodic orbits of chaotic systems are a rich source of qualitative information about the dynamical system. The presence of unstable periodic orbits located densely on the attractor is a typical characteristic of chaotic systems. This abundance of unstable periodic orbits can be utilized in a wide variety of theoretical and practical applications [19]. In particular, chaotic communication techniques and methods of controlling chaos depend on this property of chaotic attractors [12, 13].

In the first part of this thesis, a control scheme for stabilizing the unstable periodic orbits of chaotic systems is presented and the properties of these orbits are investigated. The technique allows for creation of thousands of periodic orbits. These approximated chaotic unstable periodic orbits are called *cupolets (Chaotic Unstable Periodic Orbit-lets)*. We show that these orbits can be passed through a phase transformation to a *compact cupolet* state that possesses a wavelet-like structure and can be used to construct adaptive bases. The cupolet transformation can be regarded as an alternative to Fourier and wavelet transformations. In fact, this new framework

Reproduced with permission of the copyright owner. Further reproduction prohibited without permission.

provides a continuum between Fourier and wavelet transformations and can be used in variety of applications such as data and music compression, as well as image and video processing.

The key point in this method is that all of these different dynamical behaviors are easily accessible via small controls. This technique is implemented in order to produce cupolets which are essentially approximate periodic orbits of the chaotic system. The orbits are produced with small perturbations which in turn suggests that these orbits might not be very far away from true periodic orbits. The controls can be considered as external numerical errors that happen at some points along the computer generated orbits. This raises the question of shadowability of these orbits. It is very interesting to know if there exists a true orbit of the system with a slightly different initial condition that stays close to the computer generated orbit. This true orbit, if it exists, is called a shadow and the computer generated orbit is then said to be shadowable by a true orbit.

We will present two general purpose shadowing theorems for periodic and non-periodic orbits of ordinary differential equations. The theorems provide a way to establish the existence of true periodic and non-periodic orbits near the approximated ones. Both theorems are suitable for computations and the shadowing distances, i.e., the distance between the true orbits and approximated orbits are given by quantities computable form the vector field of the differential equation.

Reproduced with permission of the copyright owner. Further reproduction prohibited without permission.

CHAPTER 1

BACKGROUND

1.1 Introduction

Periodic orbits of chaotic systems are a rich source of qualitative information about the dynamical system. The presence of unstable periodic orbits located densely on the attractor is a typical characteristic of chaotic systems. In this chapter we provide the necessary background materials and discuss a control scheme for stabilizing the unstable periodic orbits of chaotic systems.A nonlinear dynamical system is a system that can be modeled by nonlinear algebraic or differential equations. The state of a dynamical system evolves with time t, which could be a continuous or a discrete variable. A discrete time system is usually described by a map and a continuous time system is described by a set of differential equations. As $t \to \infty$, the system may reach a steady state which is often a fixed point, a periodic solution or some other bounded set. One of the greatest breakthroughs in mathematics in the last century has been the realization that even the simplest dynamical systems may behave extremely unpredictably, where the dynamics is deterministic but aperiodic and sensitive dependence on initial conditions and noise means that long term pre-

Reproduced with permission of the copyright owner. Further reproduction prohibited without permission.

diction is impossible. For instance consider the Logistics map

$$x_{n+1} = r\,(1 - x_n)\,, \tag{1.1}$$

where $0 \leq r \leq 4$ is a parameter and $n \geq 0$. Fig. 1-1 shows some plots of the time series $\{x_n\}_{n=0}^{\infty}$ for different values of the parameter r and a fixed initial condition x.

For $r < 1$, $x_n \to 0$ as $n \to \infty$ for any given initial condition x. For $1 < r < 3$, the time series x_n grows until it reaches some steady state that varies as a function of r. As r increases above 3, the time series x_n will produce a *period-2 cycle*, a period-4 cycle and so on. Here we use the term 2 cycle to indicate that the steady state behavior jumps between 2 points in a cyclic fashion. This phenomena is called *period-doubling bifurcation, cascade* or *route to chaos.* Table 1.1 shows the values of r, where 2^n-cycle first appears. Note that the successive bifurcations appear faster and faster until r_n converges to a limiting value r_∞. For large values of n, the distance between the successive transitions shrinks by a constant factor

$$\delta \;=\; \lim_{n\to\infty} \frac{r_n - r_{n-1}}{r_{n+1} - r_n} \;=\; 4.669\cdots\,. \tag{1.2}$$

The number δ is a universal constant called the *Feigenbaum constant.* The period doubling is not unique to the Logistics map. In fact, Metropolis et al. [16] proved that all unimodal maps of the form $x_{n+1} = rf(x_n)$, where $f(x)$ satisfies $f(0) = f(1) = 0$

Reproduced with permission of the copyright owner. Further reproduction prohibited without permission.

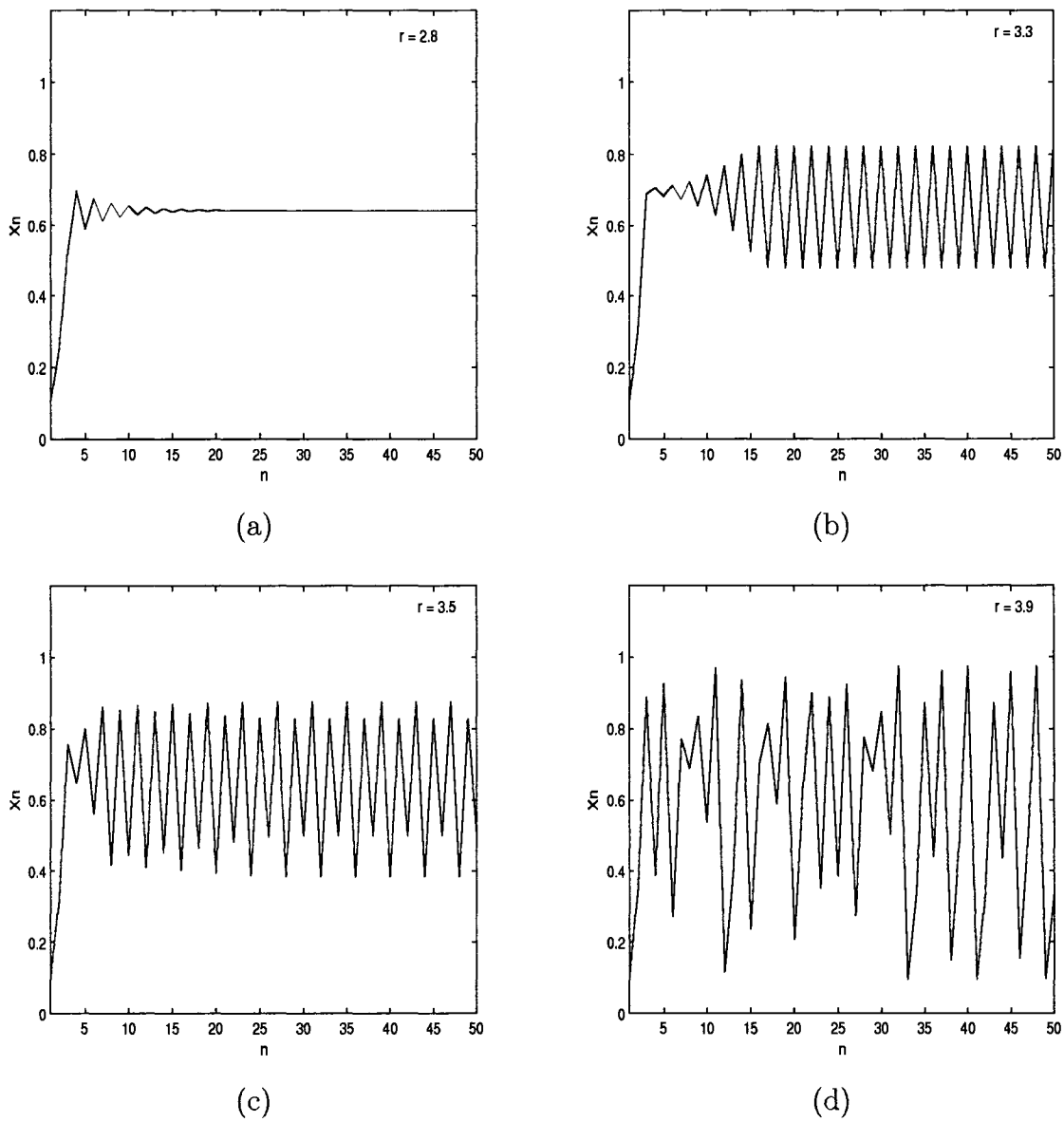

Figure 1-1. Time series of the Logistic map for different values of the parameter r. The r values are, (a) $r = 2.8$, (b) $r = 3.3$, (c) $r = 3.5$ and (d) $r = 3.9$ respectively.

Reproduced with permission of the copyright owner. Further reproduction prohibited without permission.

r	value	periods
r_1	3	(period 2 is born)
r_2	$3.449\cdots$	(period 4 is born)
r_3	$3.54409\cdots$	(period 8 is born)
r_4	$3.5644\cdots$	(period 16 is born)
r_5	$3.568759\cdots$	(period 32 is born)
$\vdots$		$\vdots$
r_∞	$3.569946\cdots$	(period ∞ is born)

Table 1.1. Period doubling bifurcation in Logistic map.

have the same property. As r is varied, the order in which the stable periodic solutions appear is independent of the unimodal map used.

For values of $r > r_\infty$, the sequence $\{x_n\}$ never settles down to a fixed point or a periodic orbit. This can be very well illustrated by the *bifurcation diagram* of the logistics map. Fig.1-2(a) shows the interesting part of the diagram where $3.4 \leq r \leq 4$. At $r = 3.4$, the attractor is a period-2 cycle as indicated by the two branches. As r increases, both branches split simultaneously, yielding a period-4 cycle. a cascade of future period doublings occurs as r increases, yielding period-8, period-16, and so on, until at $r = r_\infty \approx 3.57$, the map becomes chaotic and the attractor changes from a finite to an infinite set of points.

For $r > r_\infty$, the diagram shows a mixture of order and chaos with periodic windows between chaotic clouds of dots. The large window beginning near $r \approx 3.83$ contains a stable period-3 cycle. A blow up of part of the period-3 window is shown in Fig.1-2(b).

Reproduced with permission of the copyright owner. Further reproduction prohibited without permission.

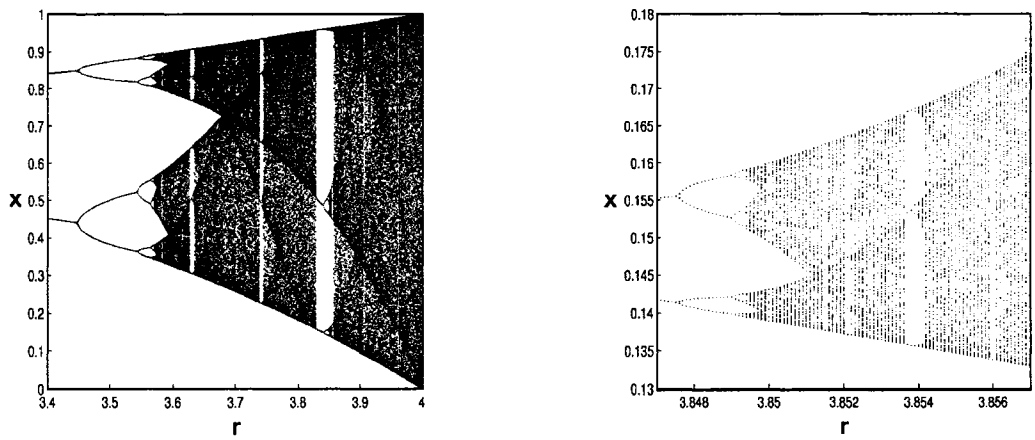

(a) (b)

Figure 1-2. Bifurcation diagram of the logistics map.

A famous example of a continuous time chaotic system is the Lorenz system. The differential equations describing the Lorenz system are:

$$\begin{aligned} \dot{x} &= \sigma(y - x), \\ \dot{y} &= \rho x - y - xz, \\ \dot{z} &= -\beta z + xy, \end{aligned} \tag{1.3}$$

where $(x, y, z) \in \mathbb{R}^3$, σ and β are positive constants and ρ is a parameter. For certain values of parameters, this system appears to behave unpredictably. For example if we numerically integrate this system with parameter values $\sigma = 10$, $\beta = \frac{8}{3}$ and $\rho = 28$, we observe that after an initial transient, the solutions settle into an irregular, aperiodic oscillation that persists as $t \to \infty$. Figure 1-3 shows a plot of $x(t)$ for a typical initial condition.

Reproduced with permission of the copyright owner. Further reproduction prohibited without permission.

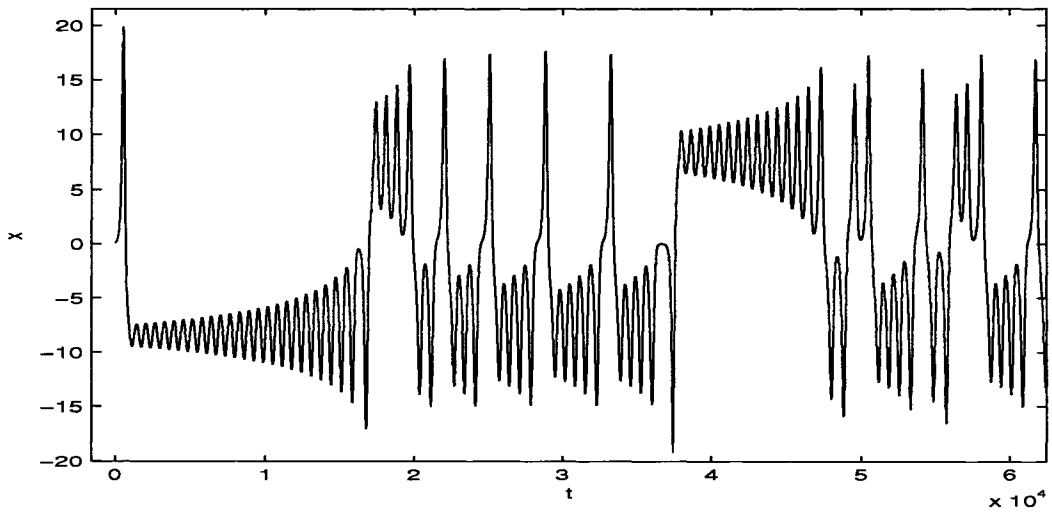

Figure 1-3. The solution $x(t)$ of the Lorenz system.

When we view the trajectories of the Lorenz system in three dimensions in the phase space, it appears that the trajectories settle onto a thin set. This limiting set is an attracting set of zero volume but infinite surface area. In fact numerical experiments suggest that this set has a fractal dimension of about 2.05. Figure 1-4 shows the limiting behavior of a typical trajectory of the Lorenz system in two and three dimensions.

1.1.1 Asymptotic Behavior

In this section we present the necessary definitions to deal with the notion of "long-term" behavior of dynamical systems. We will consider only C^r, $(r \geq 1)$ maps and autonomous vector fields on $\mathbb{R}^n$,

Reproduced with permission of the copyright owner. Further reproduction prohibited without permission.

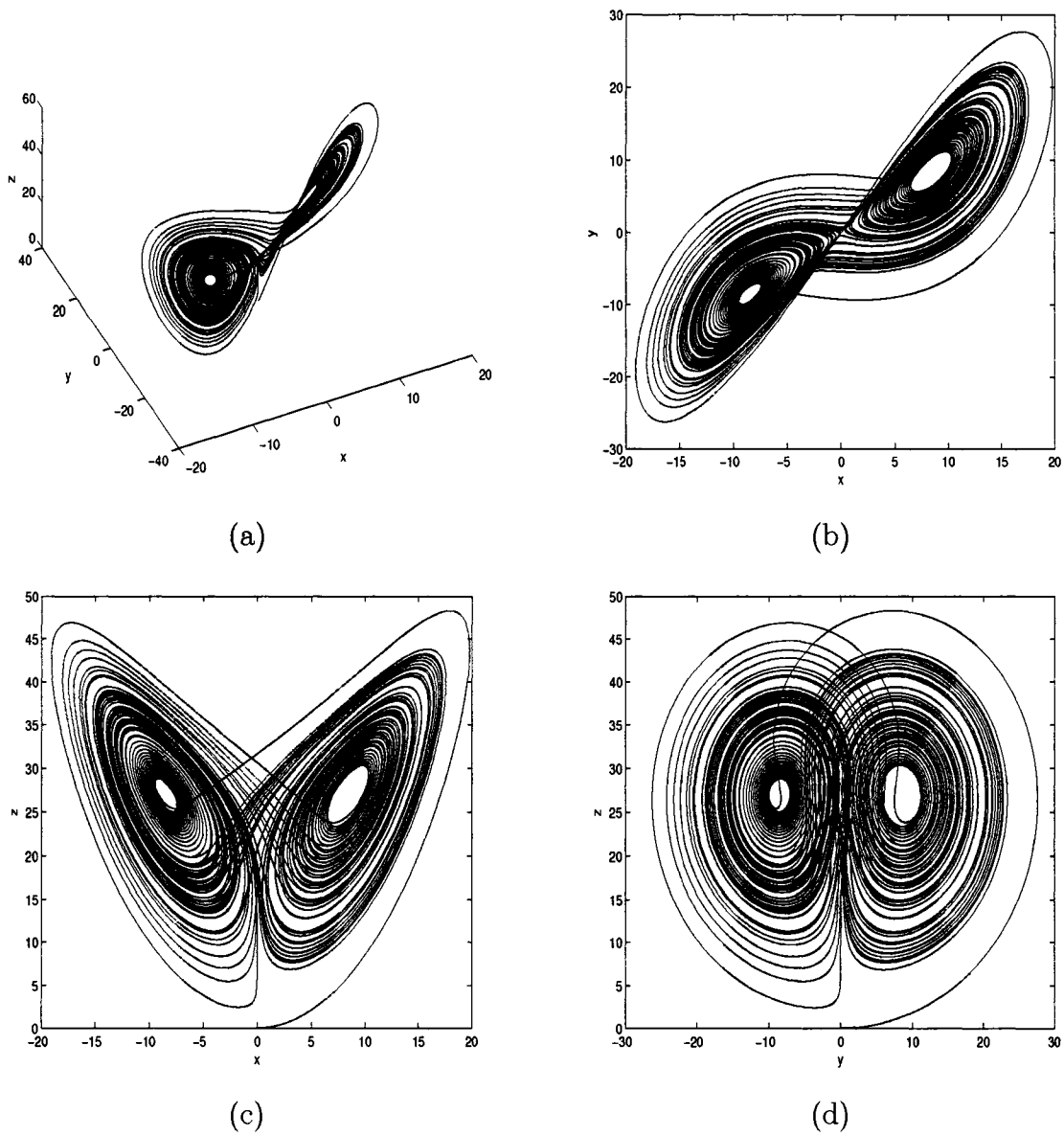

Figure 1-4. (a) The attractor of the Lorenz system and its projections to (b) $x-y$, (c) $x-z$ and (d) $y-z$ planes.

Reproduced with permission of the copyright owner. Further reproduction prohibited without permission.

$$\begin{aligned} \textit{Vector Field} \quad &: \quad \dot{x} = f(x), \quad x \in \mathbb{R}^n, \\ \textit{Map} \quad &: \quad x \mapsto g(x), \quad x \in \mathbb{R}^n. \end{aligned}$$

The flow generated by the above vector field will be denoted by $\varphi(t, x) = \varphi_t(x)$. If we think of the initial condition x_0 as being fixed, then the mapping $\varphi(\cdot\,, x_0)$ defines a solution curve of the system through the point x_0. If we identify the mapping $\varphi(\cdot\,, x_0)$ with its graph, then the trajectory can be visualized as a motion along a graph in $\mathbb{R}^n$ passing through the point x_0. On the other hand, if we think of the point x_0 as varying through a set $\mathbb{K}$ where $\mathbb{K} \subseteq \mathbb{R}^n$ is the domain of the vector field f, then the flow of the system $\varphi_t : \mathbb{K} \to \mathbb{R}^n$ can be viewed as the motion of all the points in the set $\mathbb{K}$.

Definition 1. *A point $x_0 \in \mathbb{R}^n$ is called an ω-limit point of $x \in \mathbb{R}^n$, denoted by $\omega(x)$, if there exist a sequence $\{t_i\}$, $t_i \to \infty$, such that*

$$\varphi(t_i, x) \to x_0. \tag{1.4}$$

Similarly, an α-limit point of $x \in \mathbb{R}^n$ is a point $x_0 \in \mathbb{R}^n$ denoted by $\alpha(x)$ such that

$$\varphi(t_i, x) \to x_0. \tag{1.5}$$

for a sequence $\{t_i\}$, with $t_i \to -\infty$

Reproduced with permission of the copyright owner. Further reproduction prohibited without permission.

Definition 2. *The set of all ω-limit points of a flow or map is called the ω-limit set. Similarly the set of all α-limit points of a flow or ma is called the α-limit set.*

Definition 3. *A point x_0 is called non-wandering if the following holds.*

Flows*: For any neighborhood U of x_0 and $T > 0$, there exist some t with $|t| > T$ such that*

$$\varphi(t, U) \cap U \neq \emptyset.$$

Maps*: for any neighborhood U of x_0, there exist some n with $n \neq 0$ such that*

$$g^n(U) \cap U \neq \emptyset.$$

Definition 4. *The set of all non-wandering points of a map or a flow is called the* non-wandering set *of that particular map or flow.*

As mentioned earlier, as $t \to \infty$ the dynamical system will reach its steady state behavior, which is often a fixed point, a limit cycle or some attracting set. Loosely speaking, an attractor is a set to which all neighboring trajectories converge. More precisely, an attracting set A is an invariant set contained in an open set U such that for any trajectory $\varphi(t, x_0)$ starting in U, the distance from $\varphi(t, x_0)$ to A tends to 0 as $t \to \infty$. An attractor is a minimal attracting set. We now present the formal definitions.

Reproduced with permission of the copyright owner. Further reproduction prohibited without permission.

Definition 5. *A closed invariant set $A \subset \mathbb{R}^n$ is called an attracting set if there is some neighborhood U of A such that:*

Flows:

$$\forall x \in U, \quad \forall t \geq 0 \qquad \varphi(t,x) \in U \quad and \quad \varphi(t,x) \to A \quad as \quad t \to \infty. \tag{1.6}$$

Maps:

$$\forall x \in U, \quad \forall t \geq 0 \qquad g^n(x) \in U \quad and \quad g^n(x) \to A \quad as \quad t \to \infty. \tag{1.7}$$

There is no universally accepted definition for chaos, but there is large consensus that every chaotic system satisfies certain properties. The essential ingredients of a chaotic system are:

1. **Aperiodic long-term behavior**: Given a random initial condition, the probability of occurrence of trajectories which do not settle down to fixed points, periodic orbits, or quasi-periodic orbits is nonzero.

2. **Deterministic**: System has no random or noisy parameters and the irregular behavior of the system arises from the nonlinearity of the system.

3. **Sensitive dependence on initial conditions**: Nearby trajectories separate exponentially fast.

One of the most basic tools for studying the stability and bifurcation of periodic orbits of dynamical systems, in particular chaotic systems, is the Poincaré map or

Reproduced with permission of the copyright owner. Further reproduction prohibited without permission.

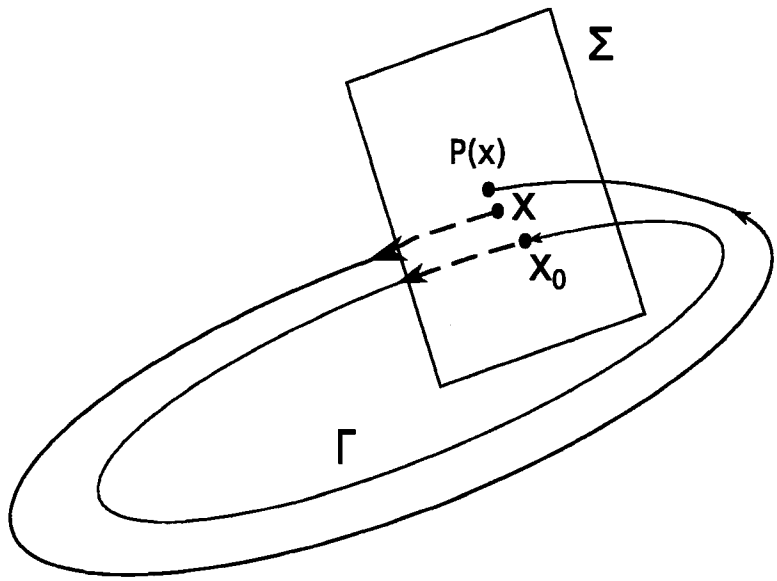

Figure 1-5. The Poincaré map.

the first return map. The idea of the Poincaré map is simple. Suppose that Γ is a periodic orbit through the point x_0 for the system

$$\dot{x} = f(x), \tag{1.8}$$

and suppose that Σ is a hyperplane perpendicular to Γ at x_0. Here $f \in C^1(E)$ where E is an open subset of $\mathbb{R}^n$. For any point $x \in \Sigma$ sufficiently close to x_0, the solution of (1.8) through x, $\varphi_t(x)$, will cross Σ again at a point $P(x)$ near x_0. The mapping $x \mapsto P(x)$ is called the Poincaré map. Fig. 1-5 shows a plot of this map.

The Poincaré map can be used to determine the stability of a periodic orbit of the dynamical system (1.8). Assume that (1.8) has a periodic orbit of period T, passing through a point $x_0 \in E$,

Reproduced with permission of the copyright owner. Further reproduction prohibited without permission.

$$\varphi(t, x_0) = \gamma(t), \quad 0 \leq t \leq T. \tag{1.9}$$

The *linearization* of (1.8) about Γ is defined as the non-autonomous linear system

$$\dot{x} = A(t)x, \tag{1.10}$$

where

$$A(t) = Df\left(\gamma(t)\right). \tag{1.11}$$

The $n \times n$ matrix $A(t)$ is a continuous $T-$periodic function of t for all $t \in \mathbb{R}$. The equation (1.10) is called the *variational flow* of (1.8). A *fundamental matrix* for (1.10) is a nonsingular $n \times n$ matrix $\Phi(t)$ which satisfies the matrix differential equation

$$\dot{\Phi}(t) = A(t)\Phi, \tag{1.12}$$

for all $t \in \mathbb{R}$. The columns of $\Phi(t)$ are linearly independent solutions of (1.10) and the solution of (1.10) satisfying the initial condition $x(0) = x_0$ is given by

$$x(t) = \Phi(t)\Phi^{-1}(0)x_0. \tag{1.13}$$

Reproduced with permission of the copyright owner. Further reproduction prohibited without permission.

For a periodic matrix $A(t)$ we have the following result known as *Floquet's Theorem.* A proof of the theorem can be found, for example, in [21].

Theorem 6. *If $A(t)$ is a continuous, $T-$periodic matrix, then for all $t \in \mathbb{R}$ any fundamental matrix for (1.10) can be written in the form*

$$\Phi(t) = Q(t)e^{Bt}, \tag{1.14}$$

where $Q(t)$ is a nonsingular, differentiable, $T-$periodic matrix and B is a constant matrix. Furthermore, if $\Phi(0) = I$ then $Q(0) = I$.

It can be shown that if $\Phi(t)$ is a fundamental matrix for (1.10) which satisfies $\Phi(0) = I$, then $\|DP(x_0)\| = \|\Phi(T)\|$ for any point $x_0 \in \Gamma$ where P denotes the Poincaré map [21]. It then follows from Theorem 6 that $\|DP(x_0)\| = \|e^{BT}\|$. The eigenvalues of e^{BT} are given by $e^{\lambda_j T}$ where λ_j, $j = 1, \cdots, n$, are the eigenvalues of the matrix B. The eigenvalues of B are called *characteristic exponents* of $\gamma(t)$ and the eigenvalues of e^{Bt} are called the *characteristic multipliers* of $\gamma(t)$. It is well known that if $\|DP(x_0)\| < 1$, then the periodic orbit $\gamma(t)$ is asymptotically stable.

In the next section we present a control scheme for stabilizing the unstable periodic orbits of chaotic systems. The technique allows for creation of thousands of approximate periodic orbits. We will then investigate the properties of these orbits and discuss their applications.

Reproduced with permission of the copyright owner. Further reproduction prohibited without permission.

CHAPTER 2

CUPOLETS

2.1 Introduction

In this chapter, we will introduce a control scheme for stabilizing the unstable periodic orbits of chaotic systems and discuss the properties of these orbits. The technique allows for creation of thousands of periodic orbits. These chaotic unstable periodic orbits are called cupolets. In chapter 3 we will discuss the properties of cupolets and we will show how cupolets can be passed through a phase transformation to a *compact cupolet* state that possesses a wavelet-like structure.

The chaotic control approach is adapted from a communication scheme developed by Hayes, Grebogi, and Ott, HGO [12, 13]. In their paper, the authors used small perturbations to steer the trajectories of the double scroll oscillator around each of the two loops in the attractor. In this way an analog signal is obtained and the bit value can be determined by observing whether the oscillation is above or below a reference value. This scheme was not meant to be secure. However, Parker and Short [28] later showed that this scheme can be adapted for secure communication. In the course of this work, they discovered that the receiver can be initialized remotely by sending sequences of initializing codes that would cause the chaotic system to

Reproduced with permission of the copyright owner. Further reproduction prohibited without permission.

stabilize onto a cupolet regardless of the initial state of the system. Furthermore, this process allowed for the creation of tens of thousands of unique cupolets.

The key point in this method is that all these different dynamical behaviors are easily accessible via small controls. We implement this technique in order to produce cupolets which are essentially approximate periodic orbits of the chaotic system. The orbits are produced with small perturbations which in turn suggests that these orbits might not be very far away from true periodic orbits. We will investigate more on this in chapter 4.

2.2 Generating Controlled Stabilized Periodic Orbits

In this section we present a way of producing *controlled periodic orbits.* in [12], HGO introduced a control scheme that can be utilized to induce a chaotic system to produce a signal bearing a desired information stream. In this section, we will show how this realization that chaos can be controlled with small perturbations can be utilized to drive a chaotic system onto a periodic orbit. The controls we use are arbitrarily small. Consequently, these controls cannot grossly alter the topological structure of the orbits on the chaotic attractor.

In their paper, HGO controlled the double scroll oscillator to follow a prescribed symbolic sequence which contains the encoded information. Figure 2-1 (a) shows a schematic diagram of the circuit generating the double scroll chaotic attractor. The nonlinearity comes from a nonlinear negative resistance represented by the function g in Figure 2-1 (b).

Reproduced with permission of the copyright owner. Further reproduction prohibited without permission.

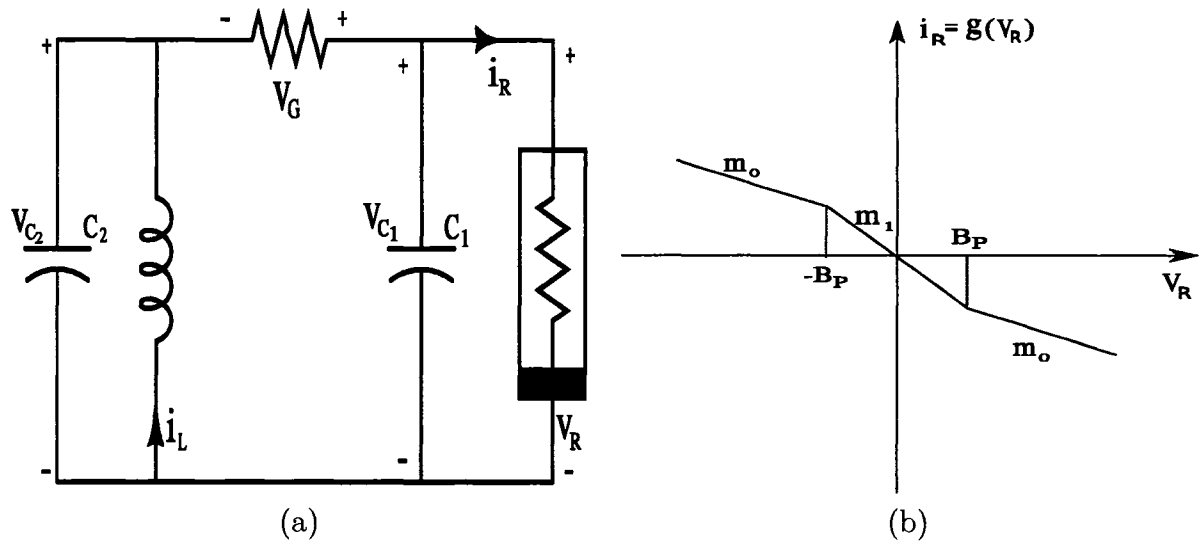

Figure 2-1. Double scroll oscillator. (a) Electrical schematic and (b) nonlinear negative resistance g.

The differential equations describing the double scroll oscillator are:

$$\begin{aligned} C_1\dot{v}_{C_1} &= G(v_{C_2} - v_{C_1}) - g(v_{C_1}), \\ C_2\dot{v}_{C_2} &= G(v_{C_1} - v_{C_2}) + i_L, \\ L\dot{i}_L &= -v_{C_2}, \end{aligned} \tag{2.1}$$

where

$$g(v) = \begin{cases} m_1 v, & \text{if } -B_p \le v \le B_p, \\ m_0\,(v + B_p) - m_1 B_p, & \text{if } v \le -B_p, \\ m_0\,(v - B_p) + m_1 B_p, & \text{if } v \ge B_p, \end{cases} \tag{2.2}$$

with parameter values, $C_1 = \frac{1}{9}$, $C_2 = 1$, $L = \frac{1}{7}$, $G = 0.7$, $m_0 = -0.5$, $m_1 = -0.8$, and $B_p = 1$. The attractor of this system contains two loops, each of which surrounds an unstable fixed point. Fig. 2-2 shows a typical trajectory of this system.

Reproduced with permission of the copyright owner. Further reproduction prohibited without permission.

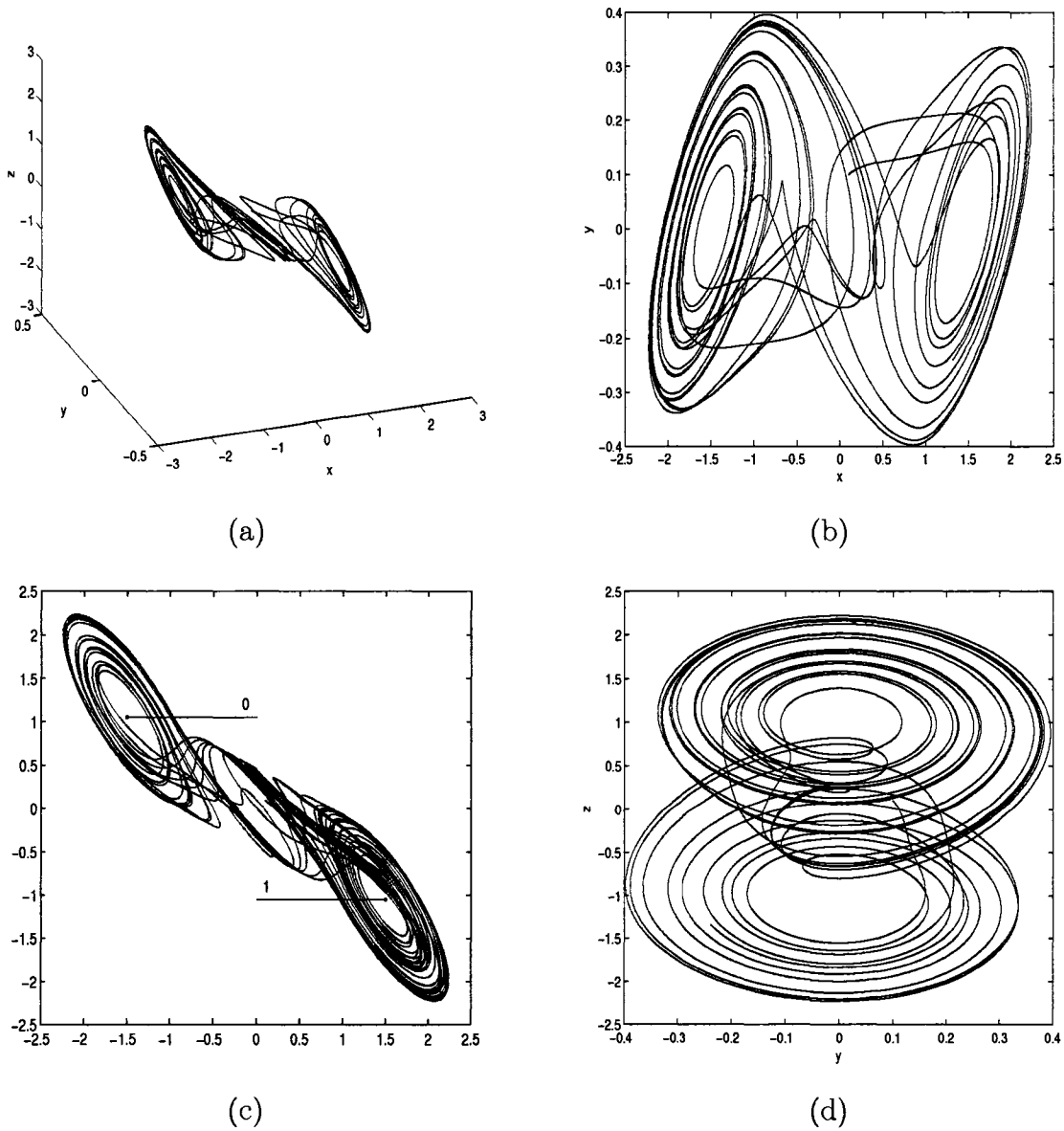

Figure 2-2. (a) The Attractor of the Double Scroll oscillator and its projections to (b) $x - y$, (c) $x - z$ and (d) $y - z$ planes. Here $x = v_{c_1}$, $y = v_{c_2}$ and $z = i_L$. The straight lines in part (c) of the figure are the Poincaré cross sections.

Reproduced with permission of the copyright owner. Further reproduction prohibited without permission.

To generate the desired symbolic sequence, a Poincaré surface of section is defined on each lobe by

$$i_L = \pm GF, \quad |v_{C_1}| \leq F, \tag{2.3}$$

where $F = \frac{B_P(m_0 - m_1)}{(G+m_0)}$. These half-planes intersect the attractor with an edge at the unstable point at the center of each lobe. The Poincaré surface is two dimensional, but because the attractor is also nearly two dimensional close to this surface, the intersection between the attractor and the Poincaré surface is approximately one dimensional. The asterisks in Fig. 2-3 mark the intersection of the trajectory with the Poincaré half plane. This set of points may be approximated quite accurately by a line extending from the unstable fixed point fitted with the least squares method. Fig. 2-3 shows a top view of this line.

This line segment is then partitioned into M bins and the distance x from the center of each bin to the center of the corresponding lobe is recorded. Each one of these points is then used as a starting point and computer simulations are run without control. The obtained trajectory will result in a symbolic sequence which is the sequence of lobes visited by the trajectory. These symbolic sequences are associated with their start point and then stored in a bit register where 0 and 1 values are recorded each tile a Poincaré surface is crossed. The symbolic state of the system can be represented by a function r which maps the symbolic state space coordinate x

Reproduced with permission of the copyright owner. Further reproduction prohibited without permission.

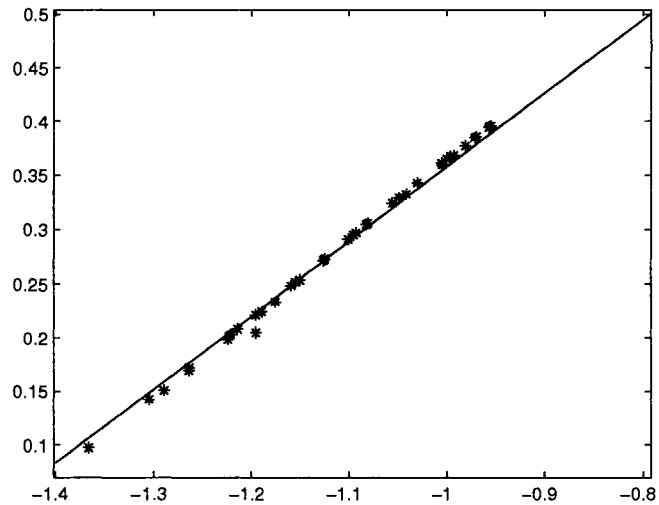

Figure 2-3. Top view of the intersection of the Poincaré surface with one of the lobes of the double scroll attractor. The asterisks show the places where the trajectory pierces the Poincaré surface.

on the Poincaré surface to a binary representation of the symbol sequence obtained from x. More precisely, if x results in a binary sequence $b_1 b_2 b_3 \ldots$, this sequence is mapped to the binary decimal $0.b_1 b_2 b_3 \ldots$, and $r(x)$ is defined by

$$r(x) = \sum_{n=1}^{\infty} \frac{b_n}{2^n}, \tag{2.4}$$

This function $r(x)$ is referred to as the *coding function.* Fig 2-4 shows a plot of this function.

In practice the coding function $r(x)$ has to be truncated to some finite value N. Given a point x_0 on the Poincaré line, there exists a neighborhood $N_\delta(x_0)$, $\delta > 0$ of the point x_0 on the Poincaré line such that for any point $x \in N_\delta(x_0$, the sym-

Reproduced with permission of the copyright owner. Further reproduction prohibited without permission.

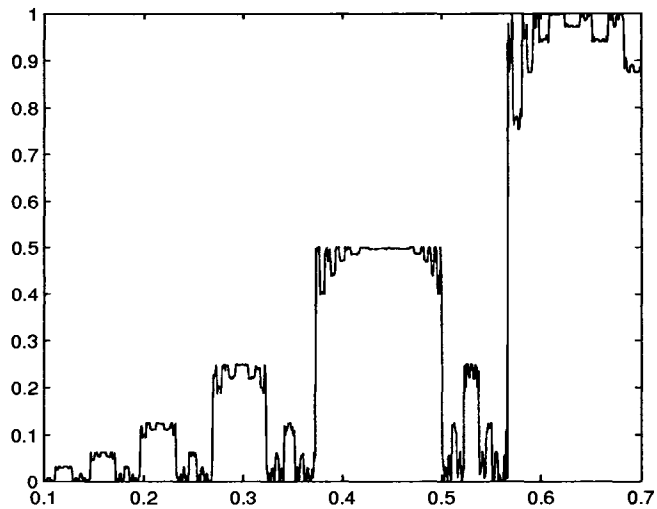

Figure 2-4. Coding function $r(x)$

bolic sequence of x is the same as the symbolic sequence of x_0 for N loops around the attractor. This truncated version of the coding function $r(x)$ is denoted by $r_N(x)$.

$$r_N(x) = \sum_{n=1}^{N} \frac{b_n}{2^n} \tag{2.5}$$

In order to control the system to follow a desired symbolic sequence, we run the simulation and wait until the trajectory crosses a Poincaré surface, say at x_0. Recall that the symbolic sequence of x_0 up to N loops around the attractor is given by $r_N(x)$. The goal is to steer the future trajectory through x_0 so that it will trace out the desired symbolic sequence. So, if the last digit of the symbolic sequence of x_0 is different from the first digit of the desired sequence, we can search $r_N(x)$ for nearest point on the section which has the same symbolic sequence as x_0 except

Reproduced with permission of the copyright owner. Further reproduction prohibited without permission.

for the last digit. More precisely, we look for an x_1 on the Poincaré line such that $|r_N(x_0) - r_N(x_1)| = 2^{-N}$. This is guaranteed to occur in an adjacent level of the $r_N(x)$ section. So the perturbations are guaranteed to be small and the trajectory is then perturbed so that it starts at x_1.

If the last digit of the symbolic sequence of x_0 is the same as the first digit of the desired sequence, we let the trajectory pass through unperturbed. In a situation like this the trajectory may be reset to the center of whatever bin it is in without changing the dynamics for the N loops. This resetting process may be thought of as applying *microcontrols*. This has the effect of removing any accumulation of round off error and minimizing the effect of sensitive dependence on initial conditions when the simulations are run.

The process of perturbing or not perturbing the trajectory can be described by a binary sequence with 1 meaning apply the control and 0 meaning no control. It was shown by Parker and Short[28] that this binary sequence bears no correlation to the original message and hence if an identical transmitter and receiver are used, the communication can be achieved by transmitting the control sequence only. However, in order to make the system work, the transmitter and the receiver must be initialized to the same state. It was discovered that this could be achieved without knowledge of the initial state of the transmitter and receiver. To do this, a control sequence is repeatedly applied to the system. It was found that independent of the initial state of the system, the trajectory will closes up on itself. The obtained controlled periodic orbit is independent of the choice of initial condition and so it turns out that there

Reproduced with permission of the copyright owner. Further reproduction prohibited without permission.

is usually a unique correlation between a control sequence and a particular periodic orbit. This makes remote initialization of the receiver possible by transmitting the same initializing sequence that was used to bring the transmitter to the initial state.

At a fundamental level, when the binary sequence of controls are applied in this manner, there are only a finite number of orbits on the attractor, so the periodicity of the dynamics would eventually be guaranteed even if no controls were applied. However, when the initializing controls are applied, the system rapidly stabilizes onto the periodic orbits that we call cupolets. Fig. 2-5 shows a few cupolets.

We have found the cupolets to be useful in a variety of applications, such as signal processing, data and music compression and image processing. In chapter 3, we investigate the properties of the cupolets and show how they can be utilized to approximate discrete signals.

Reproduced with permission of the copyright owner. Further reproduction prohibited without permission.

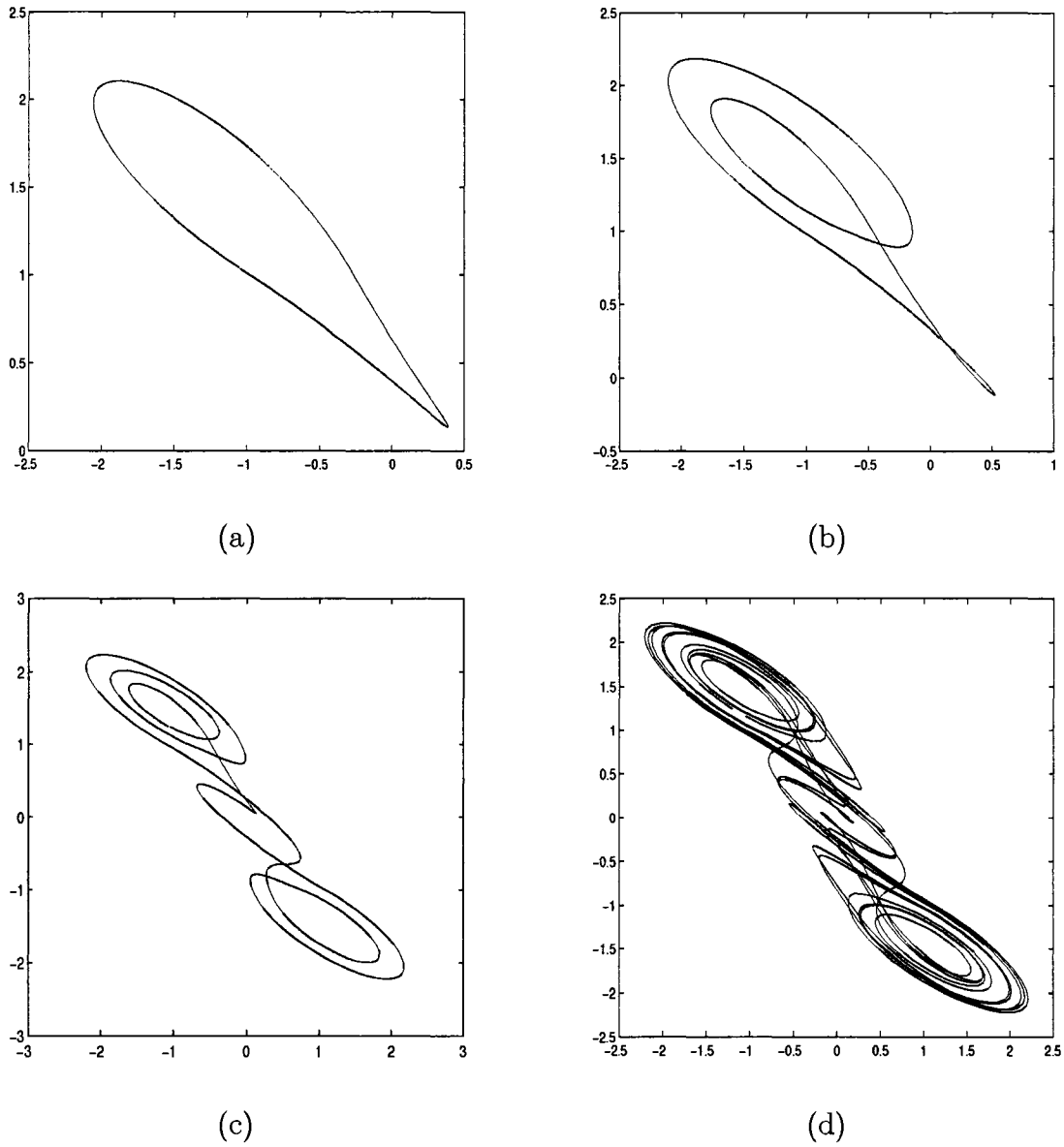

Figure 2-5. This figure shows a few of the cupolets of the double scroll system with different periods. The control sequences applied to obtain the cupolets are, (a)00, (b)11, (c) 01 and (d) 001.

Reproduced with permission of the copyright owner. Further reproduction prohibited without permission.

CHAPTER 3

ADAPTIVE MULTIRESOLUTION ANALYSIS

3.1 Introduction

In this chapter we show that cupolets can be used effectively to produce an adaptive basis for the space of real-valued functions of a discrete variable. From this basis, we construct a multiresolution analysis which allows for the approximation of signals at different resolutions and we apply it to image compression. This adaptive multiresolution analysis provides an interesting continuum between Fourier analysis and wavelet analysis.

Two of the most effective signal analysis techniques for compression are windowed Fourier and wavelet transforms. The building blocks of windowed Fourier analysis are *sines* and *cosines* or their complex equivalents, and when applied to signal processing of digital data, the analysis is done with sliding data windows. The fundamental idea behind wavelets is analysis based on scale. Wavelet analysis can be thought of as an alternative to classical Fourier analysis. In wavelet analysis the building block is called a mother wavelet and is generally compact and oscillatory. There are three basic wavelet operators that play the role of sliding windows in Fourier analysis. These operators are translation by h, defined by $(\tau_h f)(x) = f(x-h)$,

Reproduced with permission of the copyright owner. Further reproduction prohibited without permission.

dilation by $r > 0$, defined by $(\rho_r f)(x) = f(rx)$, and modulation by m, defined by $(\mu_m f)(x) = e^{imx} f(x)$. These operators are then applied to the mother wavelet to produce other wavelets.

We will now show that cupolets can be used in a similar manner to produce a multiresolution analysis. In fact, cupolets can be transformed between an oscillatory state similar to the sinusoidal basis of the Fourier analysis and a compact cupolet state that is wavelet-like.

We denote the space of real-valued $N-$ periodic functions of a discrete variable by $\tilde{\mathbb{R}}^N$, i.e.,

$$\tilde{\mathbb{R}}^N = \{f : \mathbb{N} \to \mathbb{R} \mid f(n+N) = f(n),\ n \in \mathbb{N}\}.$$

Here N represents the number of discrete samples in one period of the function.

Suppose that $\gamma(t) \in (\tilde{\mathbb{R}}^3)^N$ is a periodic orbit of chaotic system,

$$\dot{x} = f(x), \tag{3.1}$$

Here

$$\tilde{\mathbb{R}}^3)^N == \left\{f : \mathbb{N} \to \mathbb{R}^{\nvDash} \mid f(n+N) = f(n),\ n \in \mathbb{N}\right\}. \tag{3.2}$$

Assume that $\gamma(t) = (x(t), y(t), z(t))$. We take one of the components of γ, say x and compute its discrete Fourier transform $\hat{x}$. Let α_k represent the Fourier coefficients

Reproduced with permission of the copyright owner. Further reproduction prohibited without permission.

of the signal x. More specifically

$$\alpha_k = \frac{1}{2\pi}\hat{x}\left(\frac{2\pi}{N}k\right) = \frac{1}{N}\sum_{n=0}^{N-1} x(n)\exp\left(-ik\left(\frac{2\pi}{N}\right)n\right).$$

For a real valued signal $x \in \tilde{\mathbb{R}}^N$, the Fourier coefficients α_k, $k = 0, \cdots, N-1$, are complex valued numbers

$$\alpha_k = |\alpha_k| \exp(i\varphi(k)),$$

where $\varphi(k)$ in the above equation is the phase term. To convert the cupolet into a compact state we perform a phase transformation on the cupolet, designed to align all of the frequency components so that they add constructively at the center of the window. In order to concentrate the energy of the cupolet at the $p-th$ position of the window, we change the phase term to $2\pi k\frac{p}{N}$. For the case $p = \frac{N}{2}$, this gives a final phase term of the form πk . Define $\tilde{\alpha}_k$ as

$$\tilde{\alpha}_k = |\alpha_k| \exp(i\pi k),$$

and define the signal $\tilde{x} \in \tilde{\mathbb{R}}^N$ by

$$\tilde{x}(n) = \sum_{k=1}^{N} \tilde{\alpha}_k \exp\left(ik\left(\tfrac{2\pi}{N}\right)n\right) \quad \text{for} \quad n = 0, \cdots, N-1.$$

Reproduced with permission of the copyright owner. Further reproduction prohibited without permission.

In this way we obtain a discrete periodic signal $\tilde{x}$ with period N, that has most of its energy concentrated in the center of the window. Figure 3-1 shows a few examples of cupolets and their corresponding compact form.

We call these wavelet-like signals *compact cupolets.*

In the following, we present three different approaches to the construction of an adaptive multiresolution analysis from compact cupolets. In the first approach, we construct the basis using a recursive process similar to the process of creating a Walsh basis [2]. In the second approach, we present a definition of a *partial periodic multiresolution analysis* and discuss the properties of the basis elements at different resolution-levels. In the third, a periodic multiresolution analysis is constructed with each resolution-level being created by translations of an appropriately chosen scaling function. In each case we will approximate arbitrary signals at different resolution-levels and compress a sample image.

3.2 A Walsh Transform-like approach

In this section, we show how the method of creating a Walsh basis can be used with compact cupolets to approximate elements of the space of discrete functions over $N = 2^n$ samples, $\tilde{\mathbb{R}}^N$. Let ψ_0 be a given compact cupolet defined over a sample window, and assume $N = 2^n$ samples are taken in the window. We define ψ_0 to be zero outside the window. Define a sequence of functions ψ_j, $j = 0, 1, \cdots, n-1$, as follows.

Reproduced with permission of the copyright owner. Further reproduction prohibited without permission.

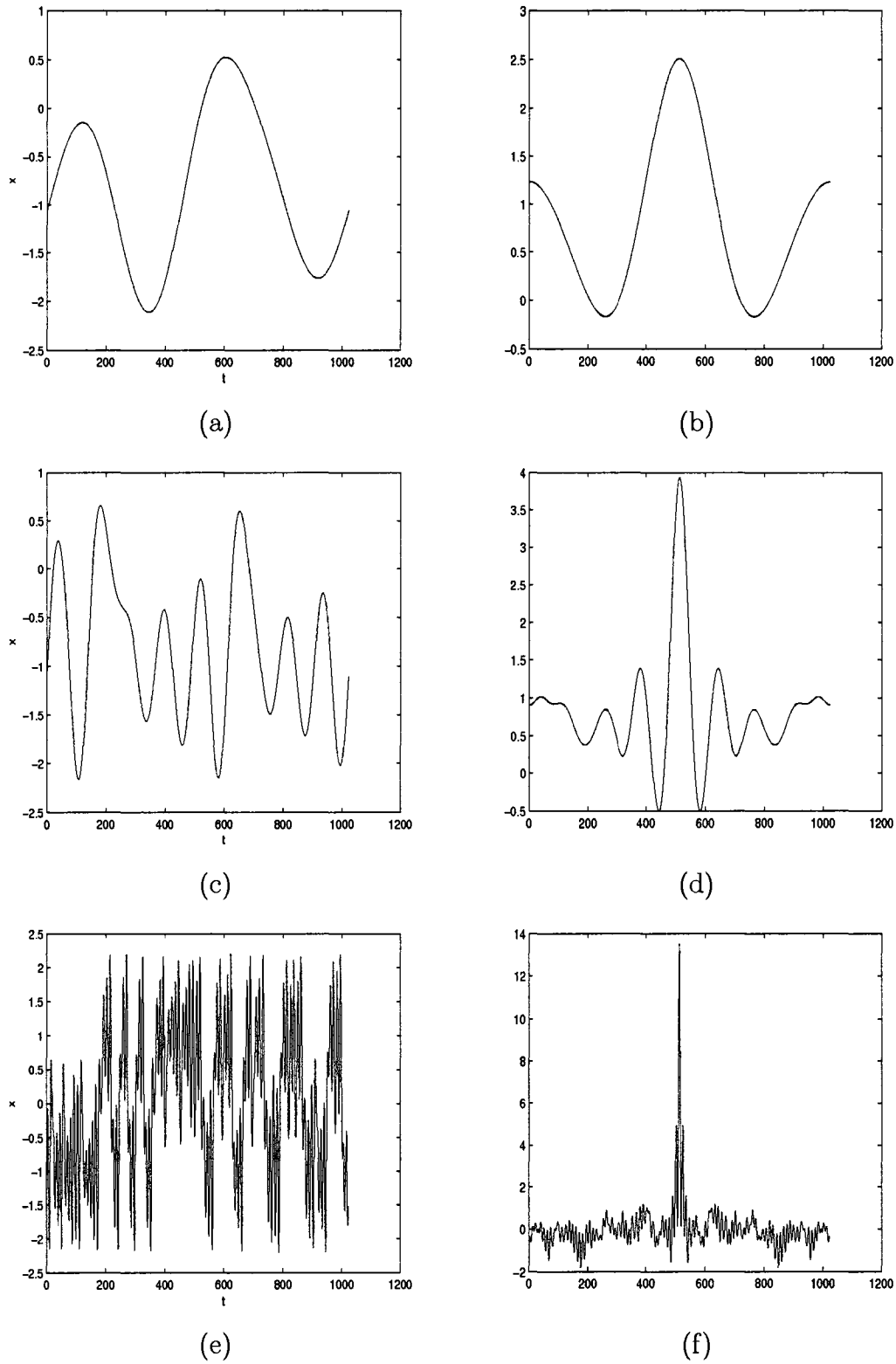

Figure 3-1. The compact cupolets in the second column of this figure are created by using the phase transformation to compact form of the corresponding cupolets in the first column of the figure.

Reproduced with permission of the copyright owner. Further reproduction prohibited without permission.

$$
\begin{aligned}
\psi_{2j}(x) &= \psi_j(2x) + (-1)^j \psi_j\left[2\left(x - \tfrac{N}{2}\right)\right], \\
\psi_{2j+1}(x) &= \psi_j(2x) - (-1)^j \psi_j\left[2\left(x - \tfrac{N}{2}\right)\right],
\end{aligned}
\tag{3.3}
$$

In (3.3) we take x to range over the N samples in the sample window, and remember that the extension of the function is zero outside the window. Let $\Psi = [\Psi_1|\cdots|\Psi_{n-1}]$ where Ψ_j, $j = 1, \cdots, n-1$ is a matrix whose columns are $\psi_{2^{j-1}}, \cdots, \psi_{2^j-1}$, i.e., $\Psi_j = \begin{bmatrix} \psi_{2^{j-1}} & \cdots & \psi_{2^j-1} \end{bmatrix}$. One can easily verify that the columns of Ψ_j construct an orthogonal set. Let V^j be the closure of the linear span of the columns of Ψ_j. In this way we obtain a sequence of linear spaces $V^0 \subset V^1 \subset \cdots \subset V^{n-1} = \tilde{\mathbb{R}}^{2^n}$. The basis elements for the space V^2 are shown in Figure 3-2. A direct application of this basis produces a fair representation of images; however there are strong, persistent artifacts where the basis functions overlap, so a direct use of this adapted Walsh transform is not optimal. Instead we extend the technique as described below.

Next, given an integer $0 \leq j \leq n-2$, we complexify the basis elements in the space V^j as follows. Assume that $\hat{\Psi}_j$ is a matrix whose columns are the Fourier coefficients of the corresponding column in Ψ_j, i.e.,

$$
\hat{\Psi}_j = \begin{bmatrix} \hat{\psi}_{2^{j-1}} & \cdots & \hat{\psi}_{2^j-1} \end{bmatrix}, \tag{3.4}
$$

where $\hat{\psi}_k$, $k = 2^{j-1}, \cdots, 2^j - 1$ are column vectors containing the Fourier coefficients

Reproduced with permission of the copyright owner. Further reproduction prohibited without permission.

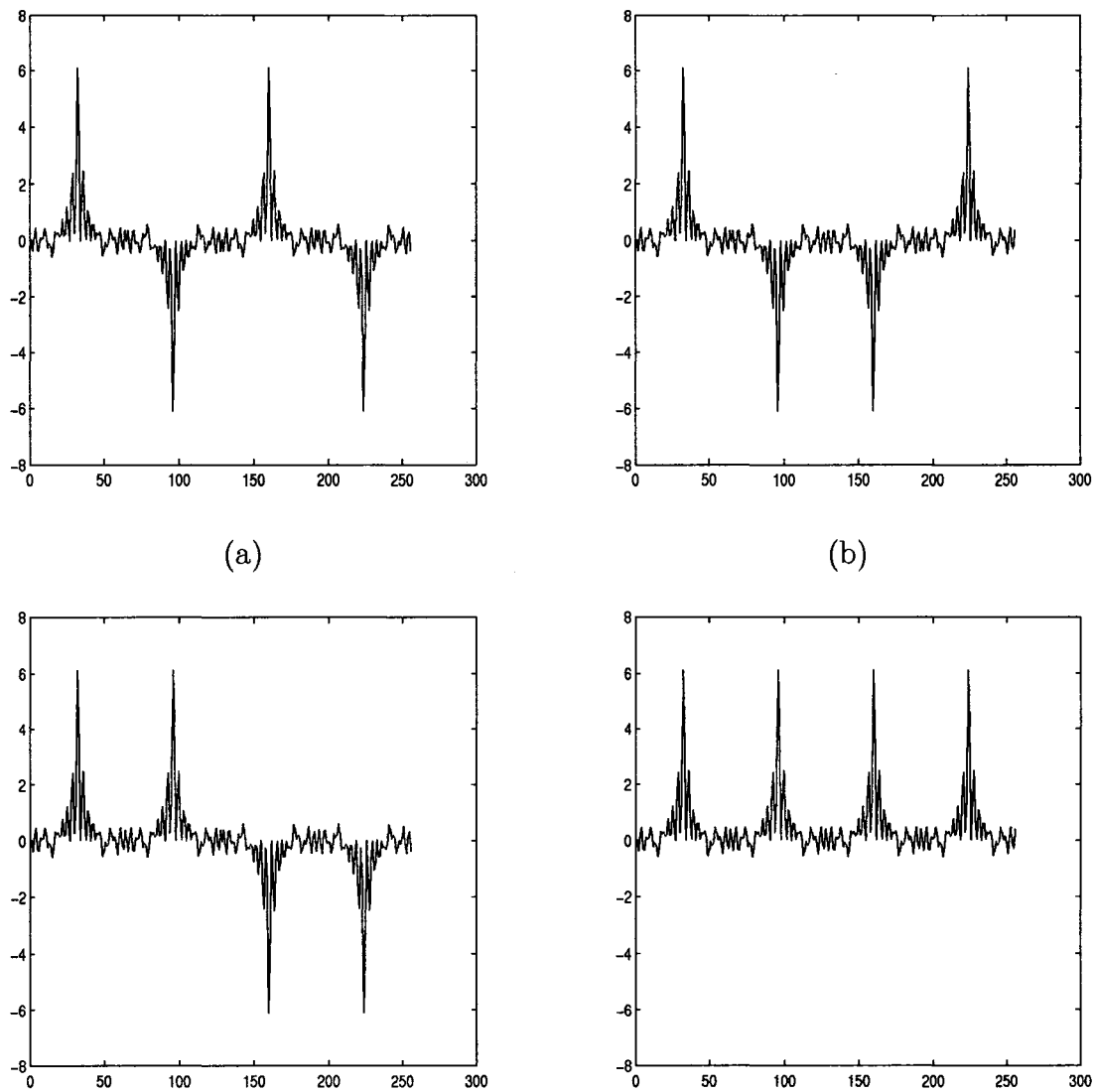

Figure 3-2. Basis element for the space V^2.

Reproduced with permission of the copyright owner. Further reproduction prohibited without permission.

of ψ_k. We then write $\hat{\Psi}_j$ as

$$\hat{\Psi}_j = \hat{\Psi}_j^+ + \hat{\Psi}_j^-, \tag{3.5}$$

where $\hat{\Psi}_j^+$ and $\hat{\Psi}_j^-$ are two matrices whose columns consist of positive frequencies and negative frequencies of columns of $\hat{\Psi}_j$. More precisely, if $\hat{\Psi}_j$ is represented by the matrix

$$\hat{\Psi}_j = \begin{bmatrix} a_{00} & a_{10} & \cdots & a_{(2^j-1)0} \\ a_{01} & a_{11} & \cdots & a_{(2^j-1)1} \\ \vdots & \vdots & & \vdots \\ \bar{a}_{02} & \bar{a}_{12} & \cdots & \bar{a}_{(2^j-1)2} \\ \bar{a}_{01} & \bar{a}_{11} & \cdots & \bar{a}_{(2^j-1)1} \end{bmatrix}, \tag{3.6}$$

then,

$$\hat{\Psi}_j^+ = \begin{bmatrix} a_{00} & a_{10} & \cdots & a_{(2^j-1)0} \\ a_{01} & a_{11} & \cdots & a_{(2^j-1)1} \\ \vdots & \vdots & & \vdots \\ 0 & 0 & \cdots & 0 \\ 0 & 0 & \cdots & 0 \end{bmatrix} \text{ and } \hat{\Psi}_j^- = \begin{bmatrix} 0 & 0 & \cdots & 0 \\ 0 & 0 & \cdots & 0 \\ \vdots & \vdots & & \vdots \\ \bar{a}_{02} & \bar{a}_{12} & \cdots & \bar{a}_{(2^j-1)2} \\ \bar{a}_{01} & \bar{a}_{11} & \cdots & \bar{a}_{(2^j-1)1} \end{bmatrix}. \tag{3.7}$$

We then take the inverse Fourier transform of the columns of the matrices $\hat{\Psi}_j^+$ and

Reproduced with permission of the copyright owner. Further reproduction prohibited without permission.

$\hat{\Psi}_j^-$ to obtain two new matrices Ψ_j^+ and Ψ_j^- with complex elements. Note that

$$\Psi_j = \Psi_j^+ + \Psi_j^-. \tag{3.8}$$

We now create a $(2^n \times 2^{j+1})$ –complex matrix Φ_j by filling the first half of the columns with the columns of Ψ_j^+ and the second half of the columns with the columns of Ψ_j^- but reversing the order of the columns. More precisely,

$$\Phi_j = \begin{bmatrix} \Psi_j^+(0,0) & \cdots & \Psi_j^+(0,2^j-1) & \Psi_j^-(0,2^j-1) & \cdots & \Psi_j^-(0,0) \\ \Psi_j^+(1,0) & \cdots & \Psi_j^+(1,2^j-1) & \Psi_j^-(1,2^j-1) & \cdots & \Psi_j^-(1,0) \\ \vdots & & \vdots & \vdots & & \vdots \\ \Psi_j^+(2^n-2,0) & \cdots & \Psi_j^+(2^n-2,2^j-1) & \Psi_j^-(2^n-2,2^j-1) & \cdots & \Psi_j^-(2^n-2,0) \\ \Psi_j^+(2^n-1,0) & \cdots & \Psi_j^+(2^n-1,2^j-1) & \Psi_j^-(2^n-1,2^j-1) & \cdots & \Psi_j^-(2^n-1,0) \end{bmatrix}.$$

Here $\Psi_j^{\pm}(l,k)$ means the $(l,k)-th$ element of the matrices $\Psi_j^{\pm}$.

Given a function $f \in \tilde{\mathbb{R}}^{2^n}$ representing $N = 2^n$ samples of a signal, we then try to obtain the best approximation to f in the least squares sense using the columns of the matrix Φ_j. One way this can be achieved is by performing a *singular value decomposition, SVD*, of the matrix Φ_j and solving the system of the linear equations

$$\Phi_j \vec{c} = f, \tag{3.9}$$

where $\vec{c}$ is the vector of coefficients and f is viewed as a column vector. In Figures

Reproduced with permission of the copyright owner. Further reproduction prohibited without permission.

3-3 and 3-4 two different compact cupolets are used to approximate the arbitrary signal f at different resolution-levels. We can see that in the first level, the overall structure of the signal f is fit reasonably well but the finer structures of the signal are not fit until we move to higher levels.

Fundamentally, when approximating a given signal f with a given compact cupolet c, the complexification process will introduce a complex number α such that

$$f \approx \alpha c^{+} + \bar{\alpha} c^{-}. \tag{3.10}$$

Here $\bar{\alpha}$ denotes the complex conjugate of α. The term $\alpha c^{+} + \bar{\alpha} c^{-}$ can be viewed as a nonlinear phase deformation of the compact cupolet c that will result in the best approximation of the signal.

This method can be used in image compression as follows. Given an image, we first transform it to a color space such as $YCbCr$ or YUV. For the ease of computations we assume that the image has side lengths equal to powers of 2. We then use a scanning method to scan each layer of the image. In this way we obtain 3 one-dimensional signals representing each layer of the image. Using similar techniques as in windowed Fourier analysis we partition these signals into desirable windows and represent each window using our compact cupolet transform. Figure 3-5 shows compressions of a sample image along with the original image. The size of the image used is 256×256 and the size of the windowed data is a single scan line or 256. The compressions are

Reproduced with permission of the copyright owner. Further reproduction prohibited without permission.

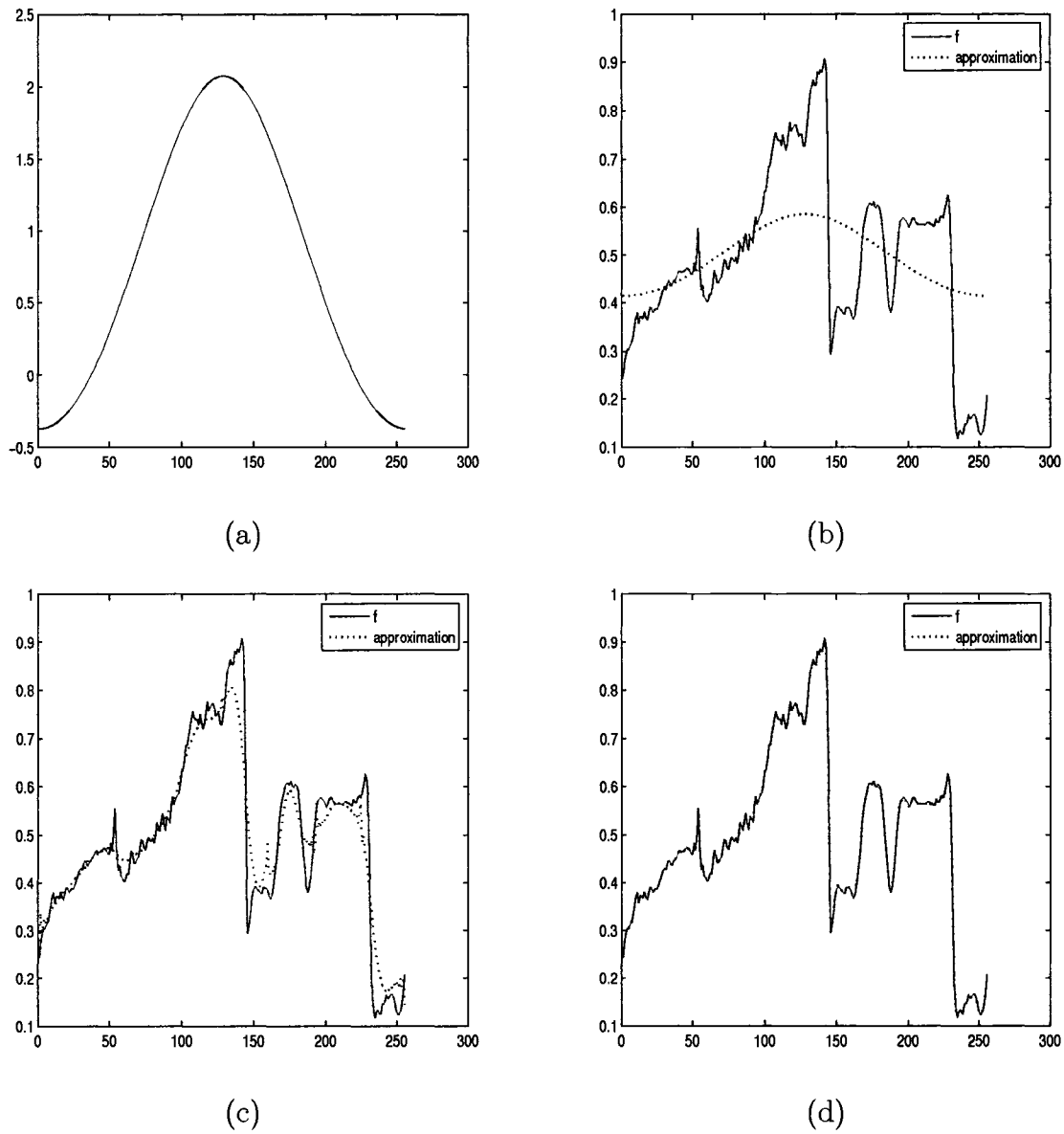

Figure 3-3. An arbitrary signal f is approximated using the compact cupolets shown in (a). There are 256 sample points in the signal f. The approximations are done at levels 0, 4, and 8. The number of basis elements for each of these resolution-level is 1, 16, and 256 respectively.

Reproduced with permission of the copyright owner. Further reproduction prohibited without permission.

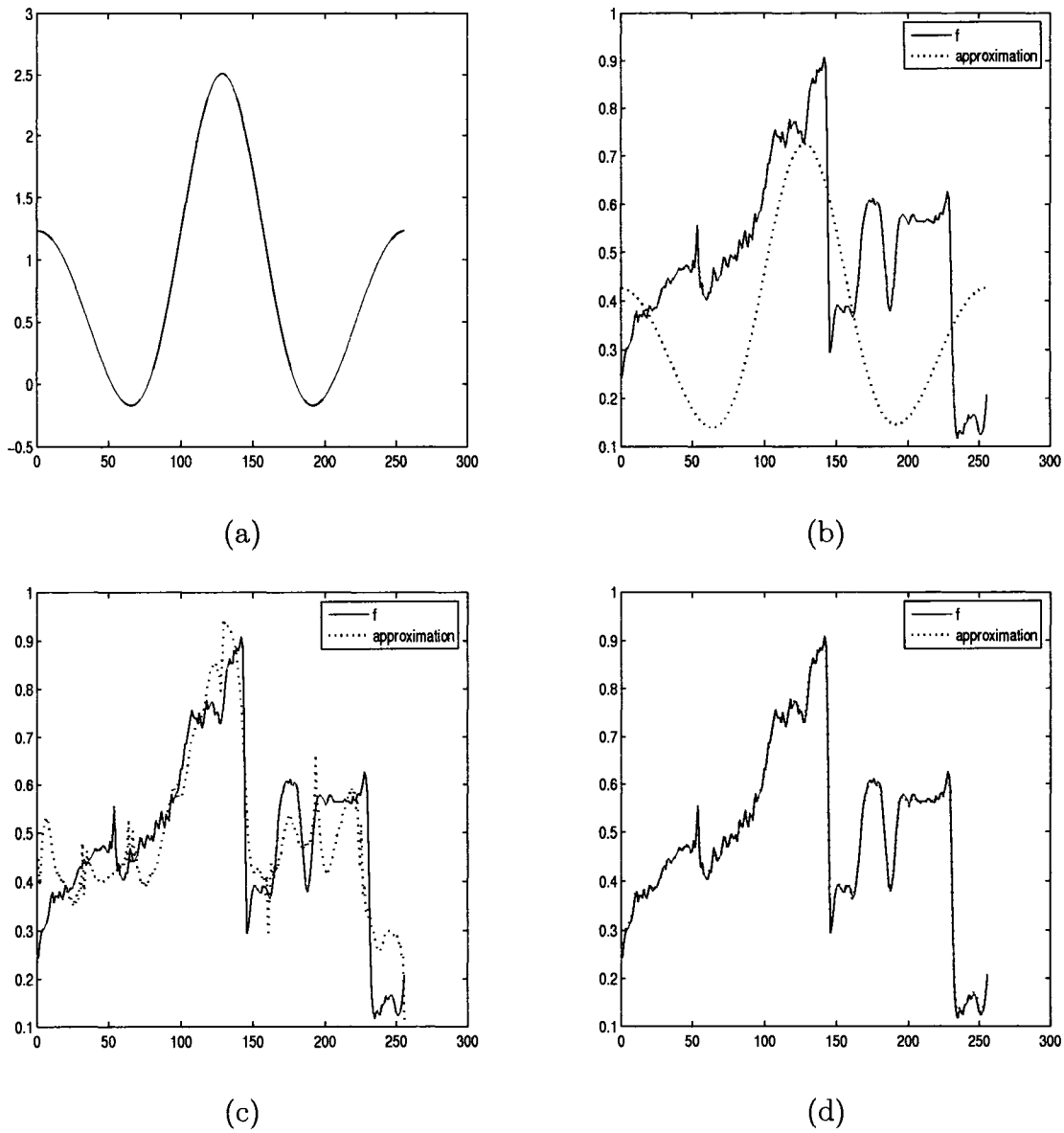

Figure 3-4. An arbitrary signal f is approximated using the compact cupolets shown in (a). There are 256 sample points in the signal f. The approximations are done at levels 0, 4, and 8. The number of basis elements for each of these resolution-level is 1, 16, and 256 respectively.

Reproduced with permission of the copyright owner. Further reproduction prohibited without permission.

done in resolution-levels 4, 6 and 8. The number of basis elements per data window is 15, 63 and 254.

There are several other possible ways of implementing this method for image compression such as using different scanning techniques or creating two dimensional bases. In the next section we present another method for creating a multiresolution analysis.

3.3 Partial Periodic Multiresolution Analysis

In this section, we define a *Partial Periodic Multiresolution Analysis (PPMRA)* and we show how the compact cupolets can be used to construct a $PPMRA$. Our approach to the construction of $PPMRA$ is inspired by the work of Petukhov [22]. In this section the basis functions are sampled $N = 2^n$ times in a data window, but we assume that they are extended periodically outside of the window. So, whenever an index ranges beyond N, the value is taken from the periodic extension.

Definition 7. *A sequence of linear function spaces* $\{V^j\}_{j=s}^{n}$, $s \geq 0$, *is called a* partial periodic multiresolution analysis, PPMRA, *of the space* $\tilde{\mathbb{R}}^N$, $N = 2^n$ *if the following conditions are satisfied:*

1. $V^s \subset V^{s+1} \subset \cdots \subset V^j \subset \cdots V^n = \tilde{\mathbb{R}}^{\mathbb{N}}$; $\dim V^j = 2^j$, $j = s, \cdots, n$.

2. *If* $f(x) \in V^j$, *then* $f(2x) \in V^{j+1}$.

3. *If* $f(x) \in V^{j+1}$, *then there exists* $g(x) \in V^j$ *such that* $g(2x) = f(x) + f(x + \frac{N}{2})$.

Reproduced with permission of the copyright owner. Further reproduction prohibited without permission.

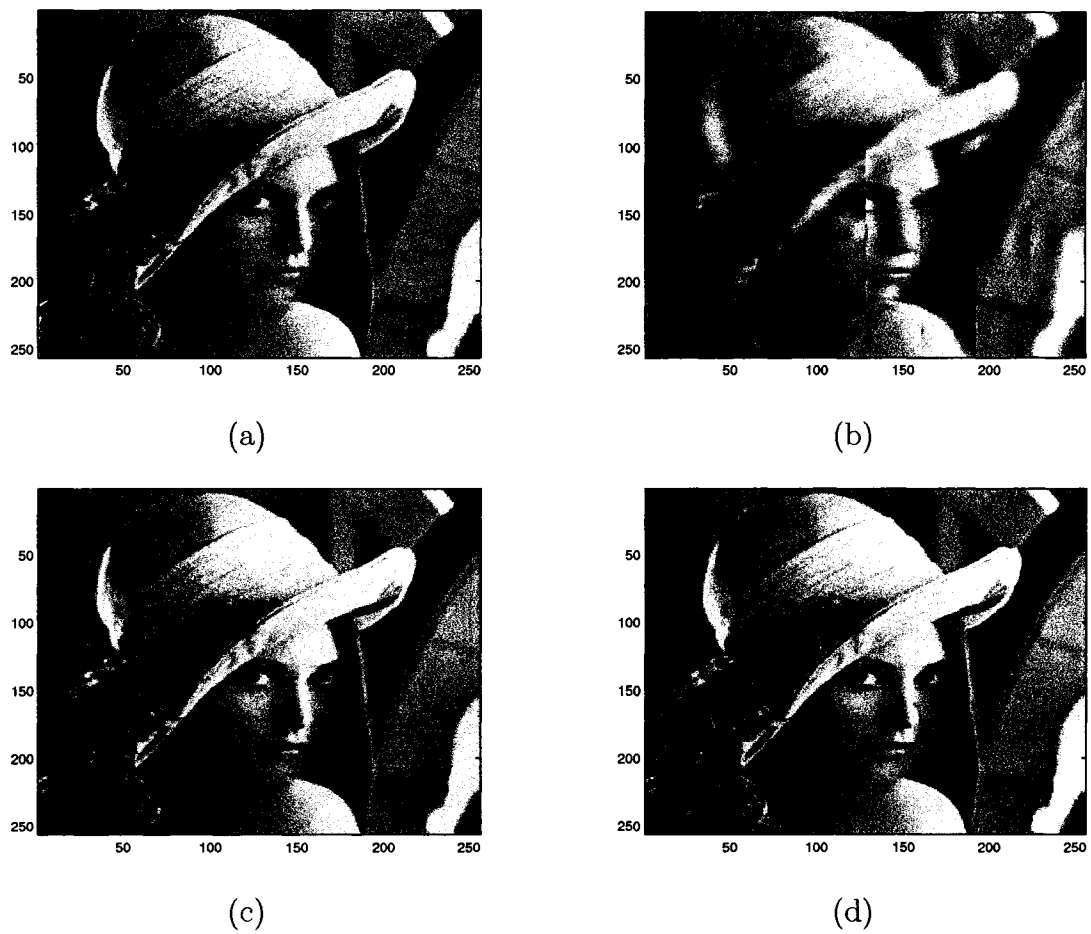

Figure 3-5. (a) Original 256 × 256 Image, (b) fourth resolution-level with 16 basis elements, (c) Sixth resolution-level with 63 basis elements and (d) eighth resolution-level with 254 basis elements. The size of the windowed data is one scan line (256).

Reproduced with permission of the copyright owner. Further reproduction prohibited without permission.

4. *The spaces V^j, $j = s, \cdots, n$, are invariant under the shift by 2^{n-j} samples i.e., for any function $f \in V^j$ and any $k \in \mathbb{Z}$ we have $f(x + k2^{n-j}) \in V^j$.*

Note that the index s may be strictly bigger that 0, i.e., the first resolution-level may include more than 1 basis element. This is because the shifts at levels lower than s may result in a degenerate cupolet representation. Also, property (3) above defines the relationship between a finer and coarser resolution. This process can be thought of as an up-sampling of the finer resolution, and then truncation to N samples. For a given cupolet, and a fixed sample window length, a set of sampled versions will exist that preserve the cupolet structure. This defines the total number of available resolutions. More precisely, for $N = 2^n$ and a cupolet that must have 2^k samples to preserve its structure, the number P of non-degenerate resolutions is given by the formula

$$P = 1 + \log_2\left(\frac{2^n}{2^k}\right) = 1 + n - k. \tag{3.11}$$

For a function $\varphi^l \in V^l$, $l = s, \cdots, n$, we denote by $\vec{\varphi}^l$ the vector function

$$\vec{\varphi}^l(x) = \left(\varphi^l(x), \varphi^l\left(x - 2^{n-l}\right), \cdots, \varphi^l\left(x - \left(2^l - 1\right)2^{n-l}\right)\right)^T.$$

Reproduced with permission of the copyright owner. Further reproduction prohibited without permission.

In order to construct the basis for each resolution-level with a given compact cupolet γ, we first rescale and resample the compact cupolet as follows. For the given compact cupolet γ, assume that it is sampled $N = 2^n$ times over the data window. Let $\varphi^s = \gamma$. The scaling function φ^s and its shift define the coarsest resolution-level. The next finer resolution level is defined by regenerating (resampling) γ so that it has $\frac{N}{2}$ samples. We then define

$$\varphi^{s+1}(m) = \begin{cases} \gamma(m) & \text{for} \quad 0 \leq m \leq \frac{N}{2} - 1. \\ 0 & \text{for} \quad \frac{N}{2} \leq k < N. \end{cases} \tag{3.12}$$

This process continues up to the finest available resolution. At this level choose an integer $\tilde{n} < n$ and regenerate the compact cupolet γ with $2^{\tilde{n}}$ points and define the function $\varphi^{s+P}(m) = \varphi^n(m)$ by,

$$\varphi^{s+P}(m) = \varphi^n(m) = \begin{cases} \gamma(m) & \text{for} \quad 0 \leq m \leq 2^{\tilde{n}} - 1, \\ 0 & \text{for} \quad 2^{\tilde{n}} \leq m < 2^n, \end{cases} \tag{3.13}$$

The functions $\varphi^i(m)$, $i = s, s+1, \cdots, s+P$ are normalized by dividing them with their Euclidian norm. Figure 3-6 shows a few of the functions φ^n and γ for the case $n = 10$ and $\tilde{n} = 7$. Note that the finest resolution-level has 2^n basis elements.

Reproduced with permission of the copyright owner. Further reproduction prohibited without permission.

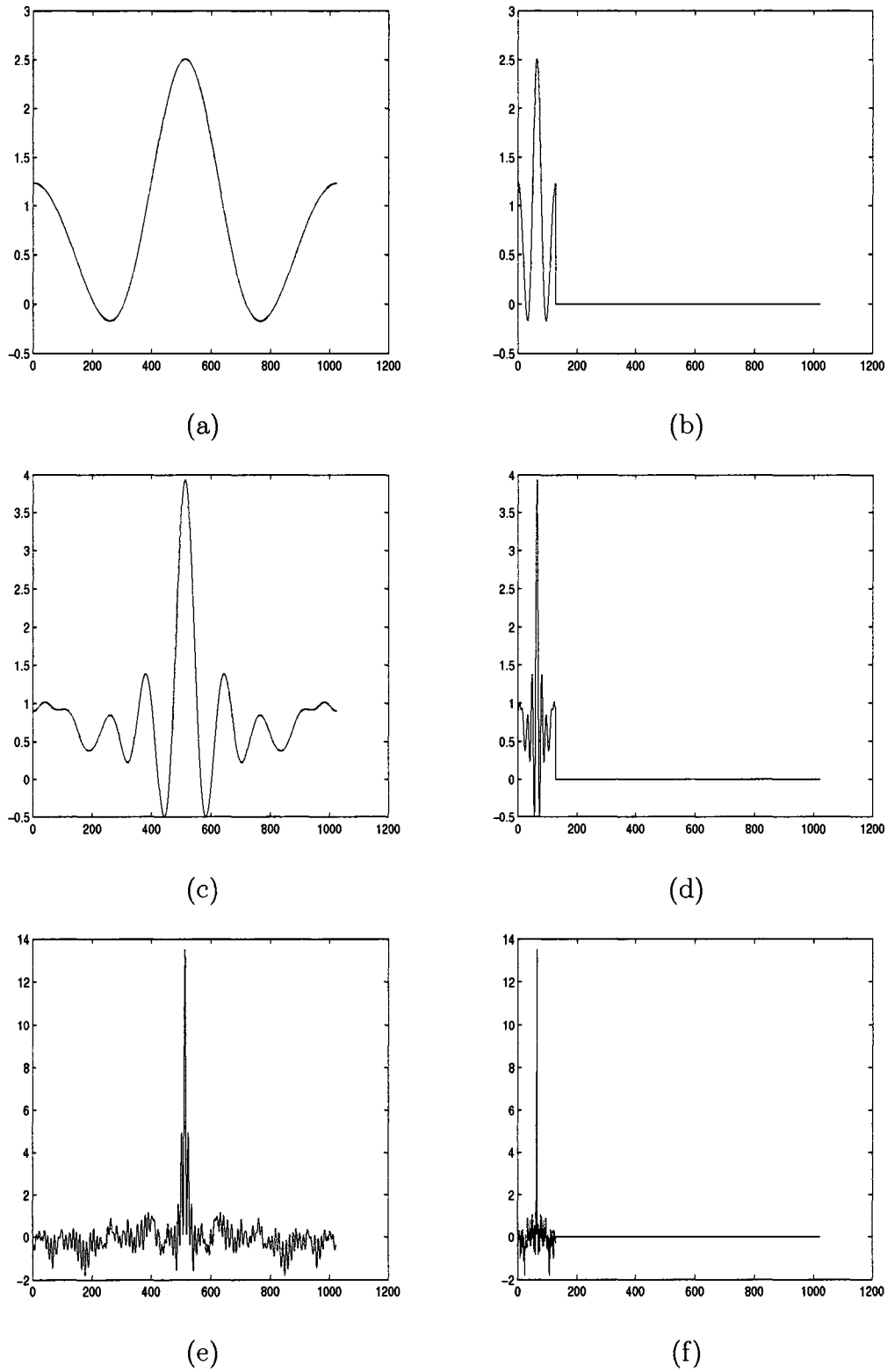

Figure 3-6. The functions in the first column of the figure represent examples of compact cupolets at the coarsest resolution. The versions in the second column of the figure, correspond to the level 4 scaling function.

Reproduced with permission of the copyright owner. Further reproduction prohibited without permission.

The scaling functions satisfy the following recursion relation:

$$\varphi^{j-1}(2m) = \varphi^{j}(m) + \varphi^{j}\left(m + 2^{n-1}\right), \qquad j = s+1, \cdots n. \tag{3.14}$$

At each resolution-level j we construct a linearly independent set by shifting the corresponding scaling function by 2^{n-j} units. Let $span(\vec{\varphi}^j)$ denote the subspace V^j spanned by the components of $\vec{\varphi}^j$. This space can be used to approximate all the functions $f \in \tilde{\mathbb{R}}^N$ in a least squares sense. More precisely, suppose that M^j is a matrix whose columns are the components of $\vec{\varphi}^j$. Then to get an approximation of f in the space V^j we solve the set of linear equations,

$$M^j X = f, \tag{3.15}$$

in the least squares sense. Here $X = (x_1, \cdots, x_{2^j})$ are the coefficients. In this way we get that

$$f(x) \approx \sum_{m=1}^{2^j} x_m \varphi^j\left(x + m2^{n-j}\right). \tag{3.16}$$

We now show how the $PPMRA$ can be utilized in compressing a signal. Suppose $f \in \tilde{\mathbb{R}}^N$ is an arbitrary signal. In order to approximate this signal in the space V^j,

Reproduced with permission of the copyright owner. Further reproduction prohibited without permission.

we first compute the scaling function φ^j and form a matrix M^j whose columns are shifted versions of the scaling function φ^j. For the $j-th$ resolution-level, we shift the scaling function φ^j by $m2^{n-j}$, for $m = 0, 1, \cdots, 2^j - 1$. More precisely, let

$$M^j = \left[\varphi^j(\cdot),\ \ \varphi^j(\cdot + 2^{n-j}),\ \ \cdots,\ \ \varphi^j(\cdot + (2^j - 1)2^{n-j})\right], \tag{3.17}$$

where

$$\varphi^j\left(\cdot + m2^{n-j}\right) = \left(\varphi^j\left(1 + m2^{n-j}\right), \varphi^j\left(2 + m2^{n-j}\right), \cdots, \varphi^j\left(2^n + m2^{n-j}\right)\right)^T.$$

In practice, when we are doing the computations, the matrix M^j may not be of full rank. To overcome this problem we perform a singular value decomposition of the matrix M^j. Assume that

$$M^j = UWV^T. \tag{3.18}$$

Here, U and V are orthogonal matrices. The degree of singularity of the matrix M^j can be determined by monitoring the diagonal elements of the matrix W which are close to zero (up to machine precision). We choose a sufficiently small positive number ε and replace the zero diagonal elements with ε. This gives us a new matrix W which in turn gives rise to a nonsingular matrix $\tilde{M}^j$. The new columns of the matrix $\tilde{M}^j$ are very similar to the old ones except for some small changes. We use

Reproduced with permission of the copyright owner. Further reproduction prohibited without permission.

the new matrix $\tilde{M}^j$ to solve the linear equation

$$\tilde{M}^j X = f. \tag{3.19}$$

The solution X of the above equation can be interpreted as the spectrum of the compact cupolet transformation of the signal f. It appears that this spectrum of the signal f has very desirable structure for compression purposes. Figure 3-7 shows an arbitrary signal f and its approximations at different resolution-levels. The actual length of the signal used is 256 samples and there are 4 different resolution-levels available. The number of basis elements in the resolution-levels are 32, 64, 128 and 256 respectively. The spectral values of a typical signal f are oscillatory and bounded by an envelope function (see Figure 3-8). This envelope function is almost periodic and has only low frequency components.

A more robust variation in approximating a signal is to form a basis matrix as follows. Assume that there are a total number of 2^k basis elements, of length 2^n, available in the coarsest resolution-level. This will give us a total number of $n - k + 1$ available resolution-levels. The goal is to pick certain basis elements from each resolution-level and construct a new basis matrix. In this way, we will obtain a matrix that will be able to fit the coarser structure as well as the fine structures in a given signal. To do this, we select a subset of the columns from the M^j matrices at each resolution- level. Since M^k has 2^k columns, we can choose 2^l columns, $l < k$,

Reproduced with permission of the copyright owner. Further reproduction prohibited without permission.

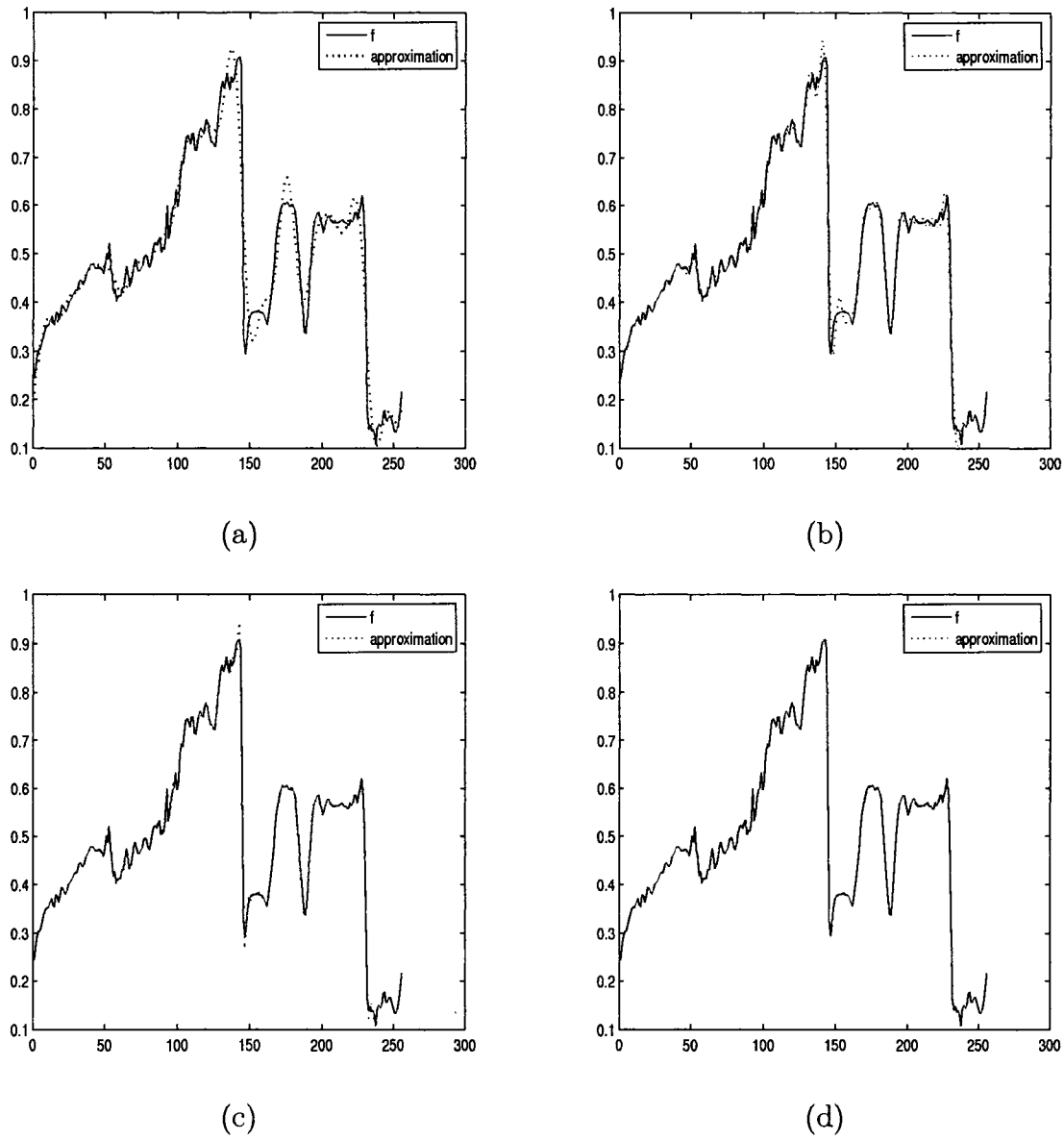

Figure 3-7. These figures illustrate approximations of an arbitrary signal f. There are 4 different available resolution-levels and the number of basis elements in the resolution-levels are 32, 64, 128 and 256 respectively.

Reproduced with permission of the copyright owner. Further reproduction prohibited without permission.

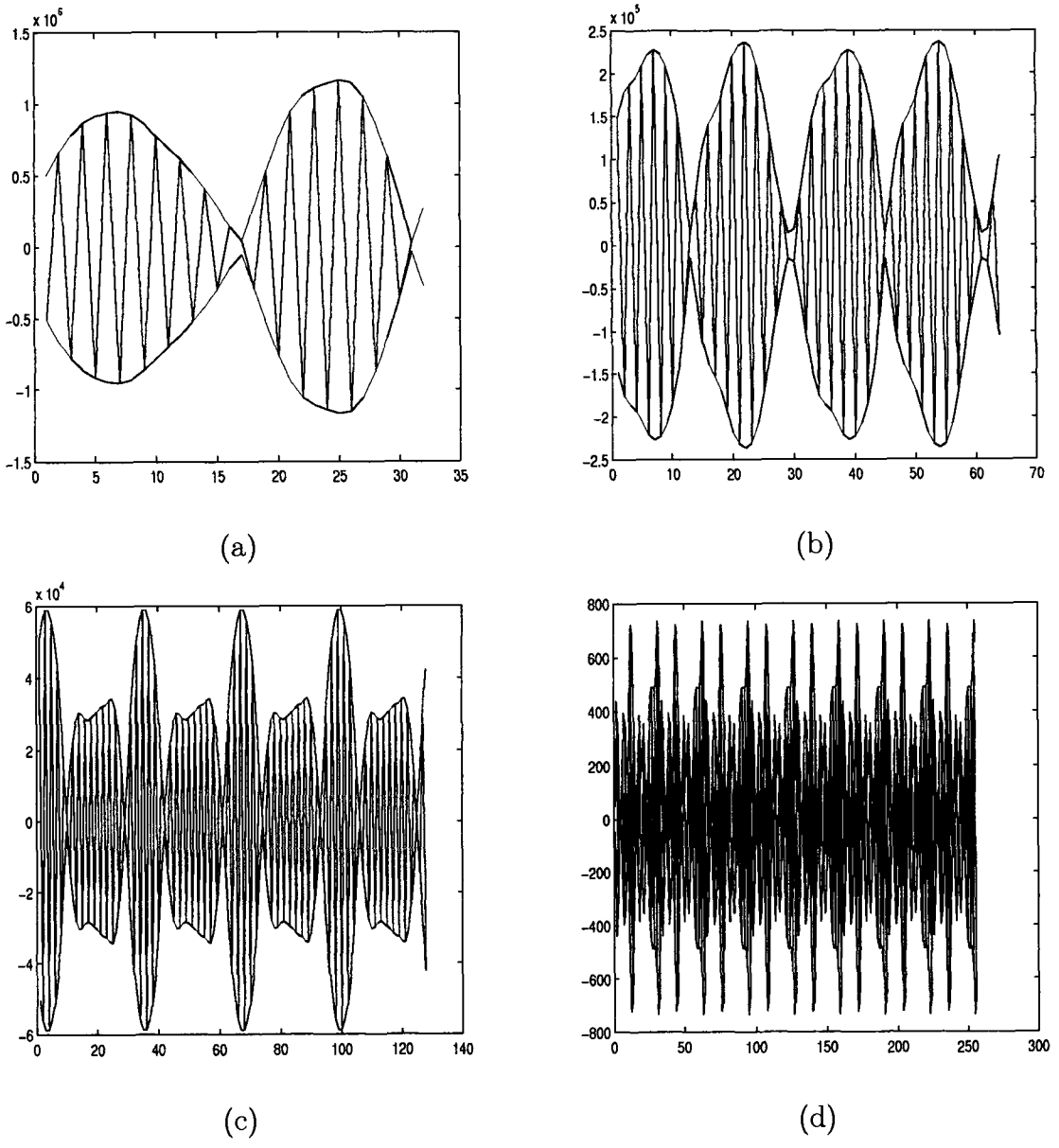

Figure 3-8. These figures illustrate spectral values as well as the enclosing envelop function of the signal f in Figure (3-7) in the 4 available resolution-levels.

Reproduced with permission of the copyright owner. Further reproduction prohibited without permission.

and define a matrix W^1 by

$$\begin{aligned} W^1 &= \big[\varphi^k(\cdot + 0 \times 2^{k-l}2^{n-k}), \varphi^k(\cdot + 1 \times 2^{k-l}2^{n-k}), \cdots \\ &\qquad \cdots, \varphi^k(\cdot + (2^l - 1) \times 2^{k-l}2^{n-k})\big] \\ &= \big[\varphi^k(\cdot + 0 \times 2^{n-l}), \varphi^k(\cdot + 1 \times 2^{n-l}), \cdots \\ &\qquad \cdots, \varphi^k(\cdot + (2^l - 1) \times 2^{n-l})\big]. \end{aligned}$$

We then define a sequence of matrices $\{W^j\}_{j=2}^{n-k+1}$ by picking 2^{j+l-1} columns from the $(k+j-1)-th$ basis matrix M^{k+j-1}

$$\begin{aligned} W^j &= \big[\varphi^{k+j-1}(\cdot + 0 \times 2^{k-l}2^{n-(k+j-1)}), \cdots \\ &\quad \cdots, \varphi^{k+j-1}(\cdot + 1 \times 2^{k-l}2^{n-(k+j-1)}), \cdots \\ &\quad \cdots, \varphi^{k+j-1}(\cdot + (2^{j+l-1} - 1) \times 2^{k-l}2^{n-(k+j-1)}\big] \\ &= \big[\varphi^{k+j-1}(\cdot + 0 \times 2^{n-j-l+1}), \cdots \\ &\quad \cdots, \varphi^{k+j-1}(\cdot + 1 \times 2^{n-j-l+1}), \cdots \\ &\quad \cdots, \varphi^{k+j-1}(\cdot + (2^{j+l-1} - 1) \times 2^{n-j-l+1}\big]. \end{aligned}$$

for $j = 2, \cdots, n-k+1$. We then complexify these newly obtained matrices using the same technique described in the previous section and then we insert a column of *ones* at the beginning of the matrix. When we perform a least squares approximation with this matrix, the compact cupolets will go through a nonlinear phase deformation that will adjust the compact cupolets to approximate the signal in the best possible way for this one-parameter phase deformation. In order to get higher resolution-levels, the same process can be applied by picking more basis elements from each resolution-level, i.e., by choosing a smaller step size. Figure 3-9 shows the

Reproduced with permission of the copyright owner. Further reproduction prohibited without permission.

approximation of an arbitrary signal using this method. The total number of basis elements used is 4, 8 and 16 respectively and the number of samples in the signal is 256. The convergence is extremely rapid for such a small number of basis elements.

Similarly, we can use this technique in image compression. Figure 3-10 shows the successive approximation of a sample image. The size of the image is 256×256 and the processing is done on single scan lines, so the length of the windowed data is 256. The number of basis elements used in each level is 24, 56 and 120 per window respectively. We observe that by adding the phase deformation freedom, the image reconstruction becomes of significantly higher quality using fewer basis elements. This effect is particularly noticeable on full-sized images.

The number of different compact cupolets that can be utilized is practically infinite. Compact cupolets have rich structure and a wide array of oscillatory behaviors. By adding a pre-selection step to choose the most appropriate cupolet, more rapid convergence is expected. This demonstrates the potential for the use of the compact cupolets in different areas of signal processing.

3.4 Scaling and Shifting

In this section we present a third approach to creating a multiresolution analysis using the compact cupolets. The approach is based on scaling and shifting a given compact cupolet. Let c_1^1 be a compact cupolet of length 2^n. We can view c_1^1 as the scaling function for our lowest (coarsest) resolution-level. In fact c_1^1 will be representing the lowest frequencies in the spectrum of a given signal of length 2^n. Let V^1 be

Reproduced with permission of the copyright owner. Further reproduction prohibited without permission.

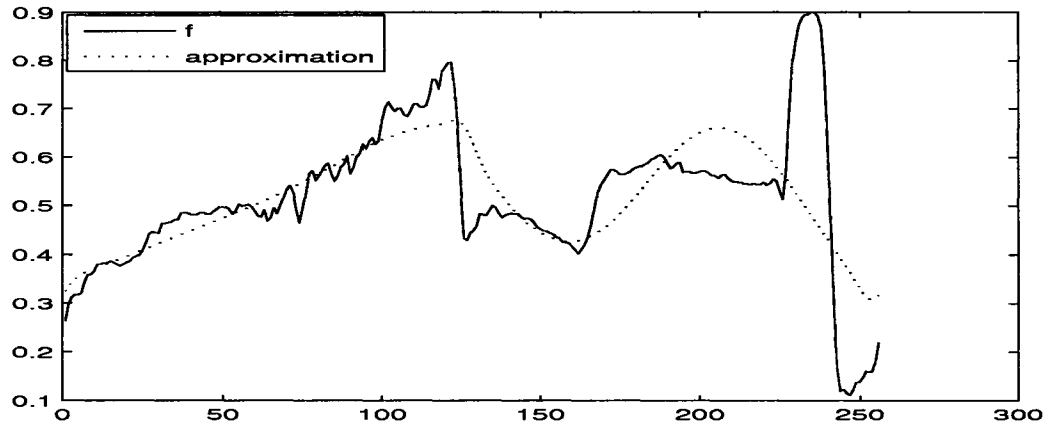

(a)

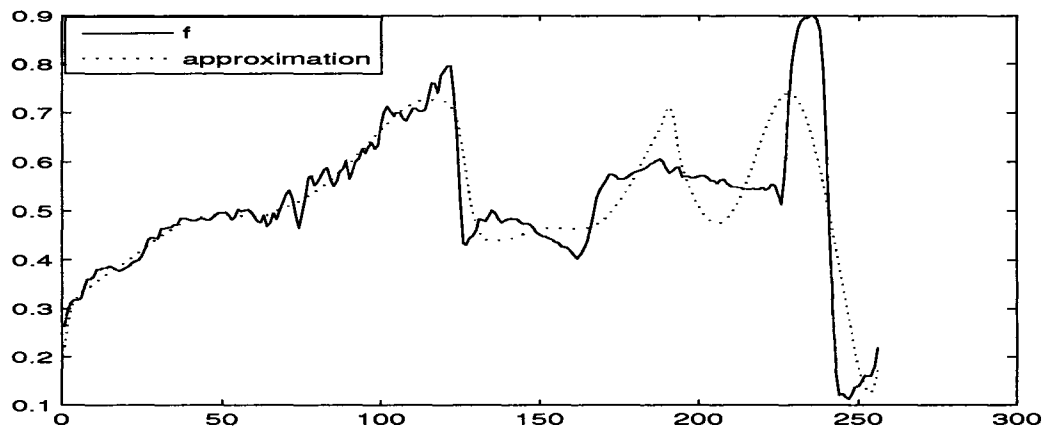

(b)

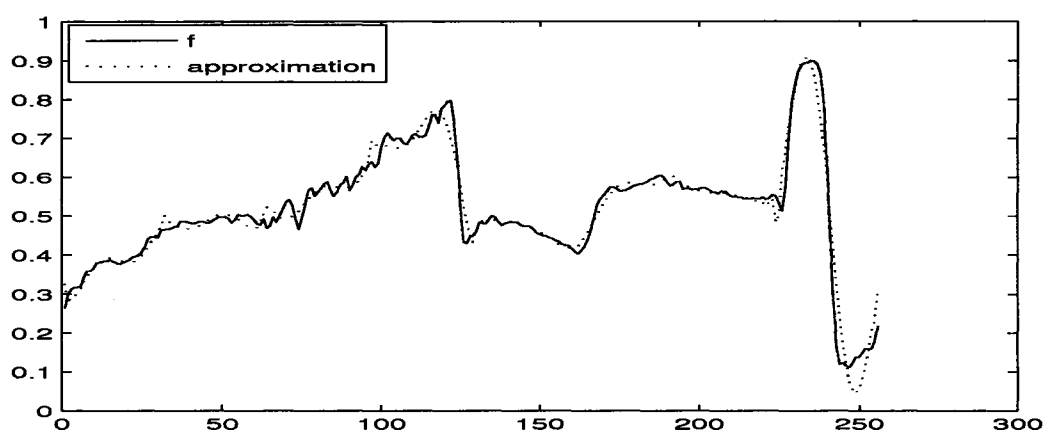

(c)

Figure 3-9. The total number of basis elements used is 4, 8 and 16 respectively.

Reproduced with permission of the copyright owner. Further reproduction prohibited without permission.

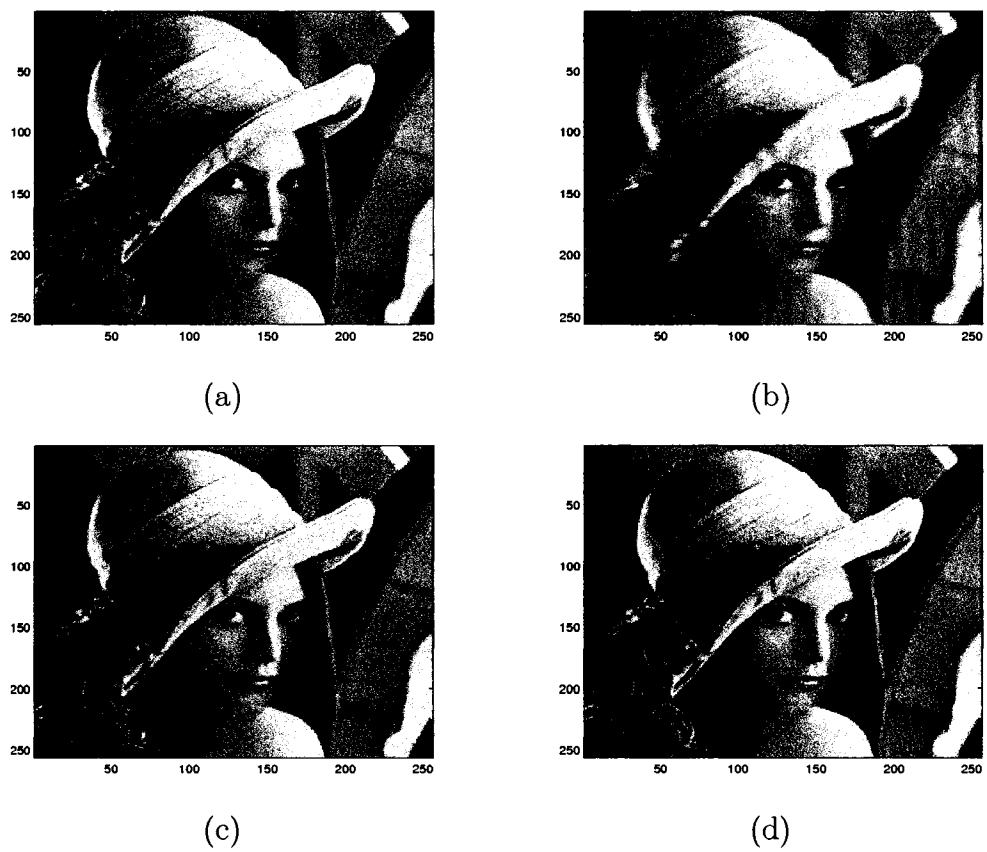

Figure 3-10. (a) Original 256×256 Image, (b) level 2, (c) level 3 and (d) level 4. The size of the windowed data is 256 and the number of basis elements used in each resolution-level is 24, 54 and 120 per window.

Reproduced with permission of the copyright owner. Further reproduction prohibited without permission.

the closure of the linear space spanned by the vector c_1^1. We then define the higher (finer) resolution-levels V^j, $j = 2, \cdots, 2^{n-1}$ by introducing appropriate versions of the scaling function in each resolution-level. The scaling functions c_j^1, $j = 2, \cdots, 2^{n-1}$ are defined recursively as follows. In order to obtain the scaling function c_j^1, we regenerate the original compact cupolet with step size 2^{j-1} times bigger than the original step size. This will result in a down-sampling of the compact cupolet c_1^1. If the windowed data is of length 2^n, we can shift the down-sampled compact cupolet by 2^{n-j} points at a time, thus obtaining 2^j orthogonal vectors $c_j^1, c_j^2, \cdots, c_j^{2^j}$. Similarly, define V^j to be the closure of the linear span of the orthogonal vectors $c_j^1, c_j^2, \cdots, c_j^{2^j}$. This process will give us a total number of n available resolution-levels. In order to approximate a given signal f, up to the $k-th$ resolution-level, we construct a $2^n \times (2^k - 1)$ matrix M by

$$M = \left[V^1, \ V^2, \ \cdots, \ V^k \right],$$

and then in a manner similar to the previous sections, we complexify this matrix and insert a column of *ones* at the beginning of the complexified matrix. Figure 3-11 shows the successive approximations of an arbitrary signal f. The length of the signal f is 256 and the approximations are done up to resolution-levels 2, 5 and 7. The number of basis elements in the resolution-levels is 3, 31 and 127 respectively.

Reproduced with permission of the copyright owner. Further reproduction prohibited without permission.

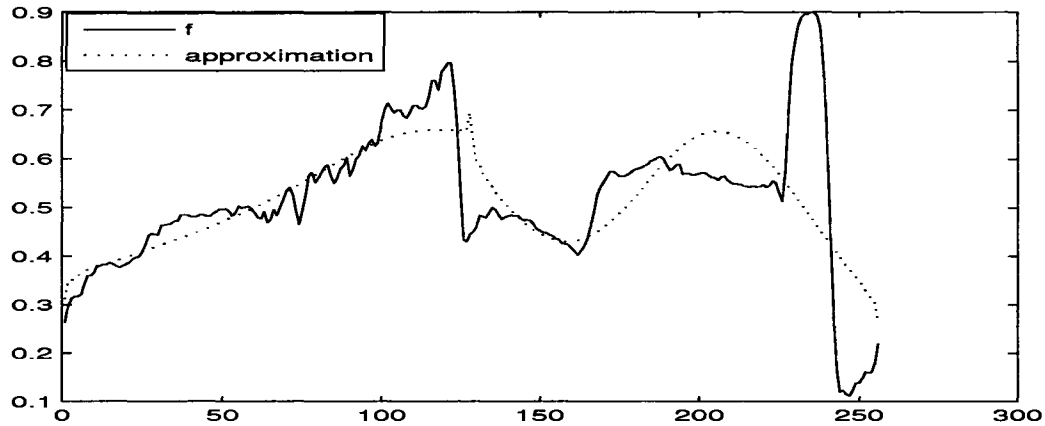

(a)

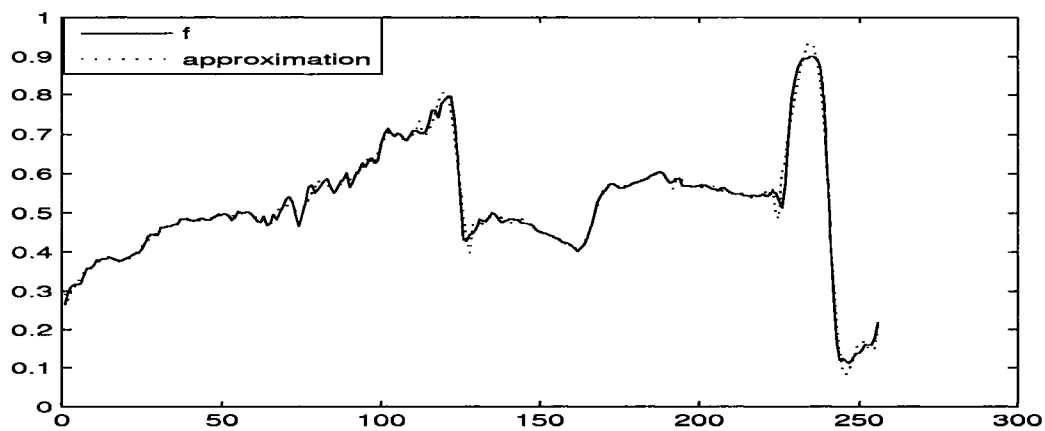

(b)

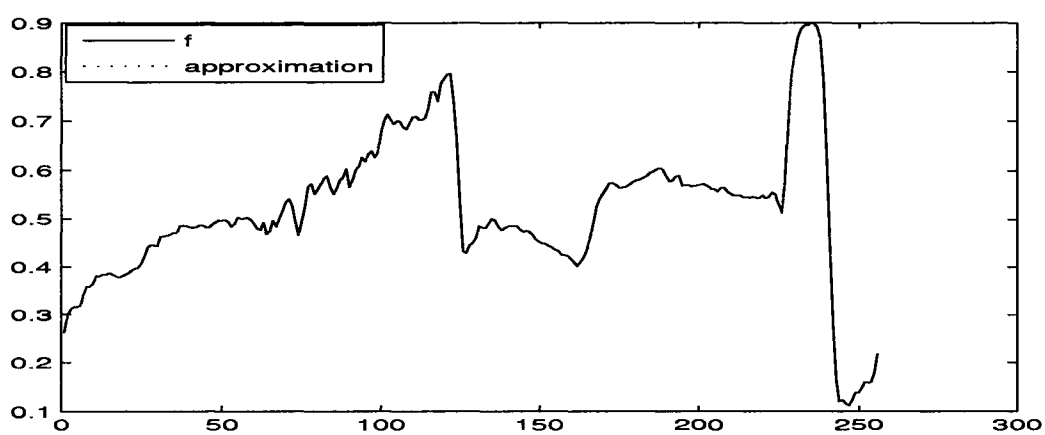

(c)

Figure 3-11. The length of the signal f is 256 and the approximations are done up to resolution-levels (a) 3, (b) 5 and (c) 7. The number of basis elements used in each case is 7, 31 and 127 respectively.

Reproduced with permission of the copyright owner. Further reproduction prohibited without permission.

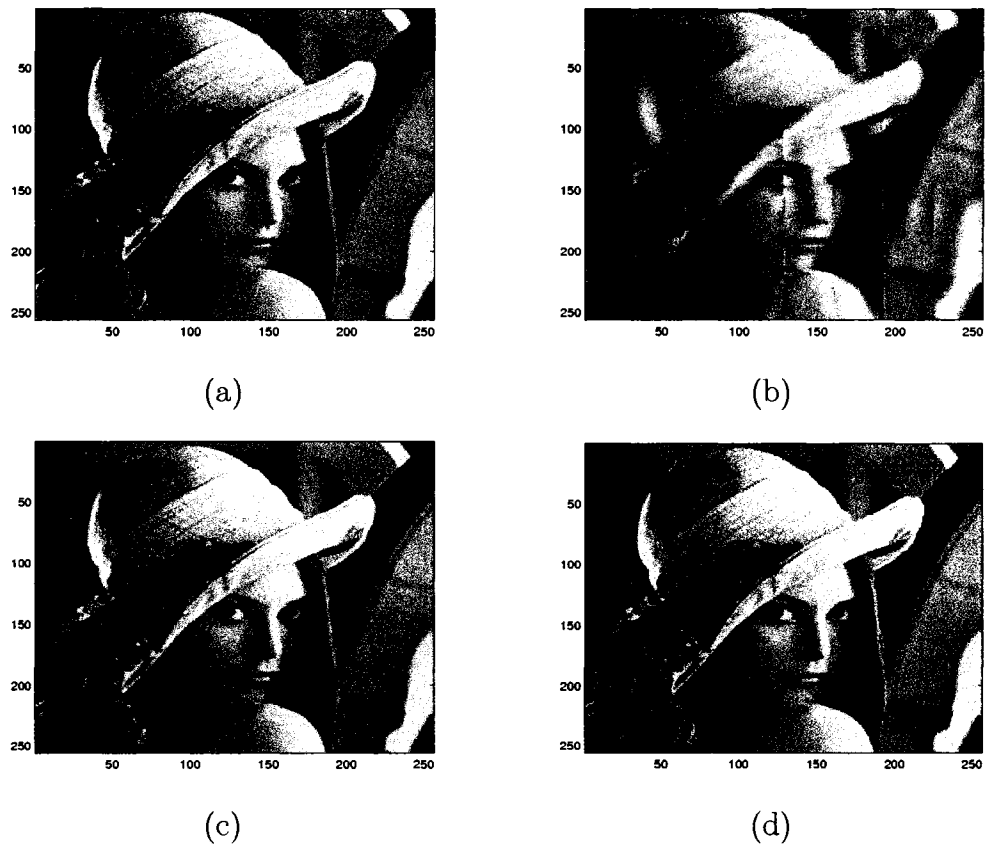

Figure 3-12. (a) Original 256×256 Image, (b) reconstruction up to resolution level 4, (c) reconstruction up to resolution-level 6 and (d) reconstruction up to resolution-level 7. The length of the windowed data is 256 and the number of basis elements used in each resolution-level is 15, 63 and 127 per windowed data respectively.

Similarly, we can implement this technique in image compression. Figure 3-12 shows the successive approximations of a sample image in different resolution-levels. The size of the original image is 256×256, the length of the data window is 256 and the number of basis elements used in each resolution-level is 15, 63 and 127 per data window respectively.

Reproduced with permission of the copyright owner. Further reproduction prohibited without permission.

We believe that cupolets have the potential to provide a framework for developing new techniques in signal processing that bridge the gap between Fourier analysis and wavelet analysis. The rich structure of cupolets allows for processing global as well as the local behavior of discrete signals. The potential exists for a beneficial interchange between chaotic systems and the processing of discrete signals but there is much more work left to be done.

Several different approaches of using cupolets in multiresolution analysis were presented in this chapter. In our initial investigations, the most efficient approach is that which produced Figure 3-10. However, in the next stage of research, it will be important to consider secondary compression of the coefficients, and one can see that things like the regular envelope structure of Figure 3-8 may allow for greater efficiency overall. Hence, it is important not to limit the focus on only one approach. Further research will investigate these issues, as well as looking at the evolution of the cupolet transform coefficients over a sequence of frames from video data.

On the more theoretical side, we can investigate the question of shadowability of cupolets by true unstable periodic orbits. By establishing the relationship between cupolets and shadowing, a deeper understanding of the structure of attractors may be achieved, while also providing a practical means to generate shadows of unstable periodic orbits. Certain restrictive results have been achieved in this area, such as the periodic shadowing theorem of Coomes, Koçak and Palmer [4], while other shadowing results such as the containment method [9] are not directly applicable

Reproduced with permission of the copyright owner. Further reproduction prohibited without permission.

to periodic orbits. In the next chapter, we will present a new tool to verify the shadowability in such cases.

In summary, the study of periodic orbits of chaotic systems appears to be extremely promising from both theoretical and applied perspectives. It will be interesting to see if technological developments benefit more from using chaos to produce periodicity than from the typical aperiodic dynamics.

Reproduced with permission of the copyright owner. Further reproduction prohibited without permission.

CHAPTER 4

THEORETICAL RESULTS

4.1 Introduction

Computational techniques are among the most important tools in understanding and analyzing the nature of chaotic systems of ordinary differential equations and computer simulations have greatly broadened our understanding in the field. However, since chaotic systems exhibit sensitive dependence on initial conditions, it is important to develop analytical techniques to verify the reliability of computer generated trajectories of such systems [10]. It is very interesting to know if a computer generated orbit is tracked closely by a true orbit of the dynamical system, perhaps with a slightly different initial condition. This true orbit, if it exists, is called a shadow and the computer generated orbit is then said to be shadowable by a true orbit. It was proved by Anosov and Bowen in their famous shadowing lemma [1] that if Λ is a hyperbolic set for a diffeomorphism ϕ , then the orbits of ϕ are shadowable in some neighborhood of the set Λ. Later Frank and Selgrade extended this result to hyperbolic sets of vector fields [6].

- S

Reproduced with permission of the copyright owner. Further reproduction prohibited without permission.

- U

The hyperbolicity is very difficult to verify in general and many chaotic systems do not possess this property. In [3], Coomes, Koçak and Palmer, CKP, proved a shadowing theorem that does not require the assumption of hyperbolicity. The idea of their theorem is as follows. Suppose that $\varphi_t(x)$ denotes the flow of a dynamical system $\dot{x} = f(x)$ where f is a C^2 vector field on $\mathbb{R}^n$. Suppose that δ is a positive number and $\{y_i\}_{i=0}^{N}$ is a computer generated orbit of the dynamical system with associated times $\{h_i\}_{i=0}^{N-1}$, and error bound δ, i.e. $\|\varphi_{h_i}(y_i) - y_{i+1}\| \leq \delta$ for $i = 0, \cdots, N-1$. This computer generated orbit is referred to as a *δ-pseudo orbit.* They then choose Poincaré surfaces at each point y_i on the δ-pseudo orbit normal to the vector field at that point. The problem then becomes finding a true orbit of the dynamical system that passes through some local neighborhoods of the points of the δ-pseudo orbit on the Poincaré surfaces. This approach reduces to proving the existence of a fixed point of a suitably chosen map. In their paper, CKP utilized the Brouwer fixed point theorem. The Brouwer fixed point theorem requires the map to be non-expansive in order to have a fixed point. This puts a serious restrictions on the allowed numerical integration error δ.

In some application of chaos, for example in communications, encoding and stabilization of unstable periodic orbits (see Chapter 1), we have to perturb the trajectories by small amounts in order to make the trajectory follow a desired symbolic dynamics. These perturbations can be considered as external numerical error that happens at

Reproduced with permission of the copyright owner. Further reproduction prohibited without permission.

some points along the orbits. These types of external errors are generally much larger than δ and the conditions of the shadowing theorem of CKP cannot be satisfied.

The method of containments introduced by Grebogi, Hammel, Yorke and Sauer, GHYS, [9] does not depend too much on the integration error δ. The idea of the containment method is as follows. Consider a sequence of parallelograms around each point on the δ-pseudo orbit. Each parallelogram is projected to the next parallelogram by the flow of the dynamical system and as long as the intersections of the parallelograms make a plus sign shape, a shadow of the δ-pseudo orbit can be obtained via the backward flow. For this method to work the system needs to be pseudo hyperbolic. GHYS used this method to show the shadowability of two dimensional chaotic maps. Later, Hayes and Jackson generalized this to higher dimensional flows [7, 8].

In this chapter we present two new shadowing theorems for periodic and non-periodic shadowing of pseudo orbits of ordinary differential equations that reduces the restrictions on the error bound δ. Also, new notions of periodic and non-periodic shadowing of pseudo orbits of autonomous system of ordinary differential equations are defined. We begin this chapter by introducing the quantities and reviewing the background material required in our shadowing theorems.

4.2 Background Materials

In this section we provide the background materials and present the definitions and quantities required in our shadowing theorems. We will define the notion of

Reproduced with permission of the copyright owner. Further reproduction prohibited without permission.

pseudo-hyperbolicity and briefly discuss the containment method of GHYS. We will also discuss the fixed point method of CKP. Both methods have some advantages and disadvantages. For example, both methods do not require the system to be hyperbolic. Instead, they use the assumption of pseudo-hyperbolicity. One advantage of the containment method over the fixed point method is that, unlike the latter it does not put restrictive bounds on the computational error δ. On the other hand, with a a slight modification, the fixed point method can handle the periodic shadowing where as the containment method is limited to non-periodic shadowing [4].

In this chapter our intention is to prove general periodic and non-periodic shadowing theorems that take advantage of both methods and improve the points of weakness. We also require the systems to be pseudo-hyperbolic. The numerical verification of our methods is similar to that of the containment method where some interval arithmetic and Validate ODE integration is required [17].

4.2.1 Definitions

In this chapter all norms are assumed to be Euclidian norms unless otherwise stated. By a *solution* we mean a continuous exact or approximated solution curve, an *orbit* is a discrete set of points on a solution, and a *trajectory* refers to either an orbit or a solution depending on the context. For a given positive number δ, the notion of a δ-pseudo orbit is defined in order to provide a measure of closeness of a computer generated orbit to a true underlying orbit. More precisely, assume that $f : \mathbb{R}^n \to \mathbb{R}^n$ is a C^1 vector field. Consider the autonomous differential equation

Reproduced with permission of the copyright owner. Further reproduction prohibited without permission.

$$\dot{x} = f(x), \tag{4.1}$$

with the associated flow $\varphi_t(x) = \varphi(t, x)$. Consider a sequence of points $\{x_i\}_{i=0}^{N}$ on the solution $x(t) = \varphi_t(x_0)$ of system (4.1) with $x_{i+1} = x(t_{i+1}) = \varphi_{t_i}(x_i)$ for $i = 0, 1, \cdots, N-1$. Here $\{t_i\}_{i=0}^{N-1}$, is a sequence of time steps. We can view the solution $x(t)$ as an iterative map defined by $x_{i+1} = \varphi_{t_i}(x_i)$.

In practice, when a close form solution is not available, a *numerical method* such as a *Runge-Kutta* method is used to approximate the solution $x(t)$. In this way we obtain a sequence of points $\{y_i\}_{i=0}^{N}$ in $\mathbb{R}^n$ with y_i approximating x_i and a sequence of positive numbers $\{h_i\}_{i=1}^{N-1}$ with h_i approximating t_i.

In order to have a measure the accuracy of a computer generated orbit, the notion of *δ-pseudo orbit* is defined to provide a measure of closeness of the computed orbit to the true orbit. More precisely,

Definition 8. *For a given positive number δ, a sequence of points $\{y_i\}_{i=0}^{N}$ with $f(y_i) \neq 0$ is said to be a δ-pseudo orbit of (4.1) if there is an associated sequence $\{h_i\}_{i=0}^{N-1}$ of positive times such that*

$$\|y_{i+1} - \varphi_{h_i}(y_i)\| \leq \delta \quad for \;\; i = 0, \cdots, N-1. \tag{4.2}$$

Definition 9. *For a given positive number δ, a sequence of points $\{y_i\}_{i=0}^{N}$ with $f(y_i) \neq 0$ is said to be a δ-pseudo periodic orbit of (4.1) if there is an associated*

Reproduced with permission of the copyright owner. Further reproduction prohibited without permission.

sequence $\{h_i\}_{i=0}^{N}$ *of positive times such that*

$$\|y_{i+1} - \varphi_{h_i}(y_i)\| \leq \delta \quad for \;\; i = 0, \cdots, N-1, \tag{4.3}$$

and

$$\|y_0 - \varphi_{h_N}(y_N)\| \leq \delta. \tag{4.4}$$

It is well known that due to sensitive dependence on initial conditions in chaotic systems, the computer generated orbits may be faraway from the true underlying orbit that starts from the same initial condition. The notion of ε-*shadowing* is defined in order to verify, whether there exist some other true orbit of the system possibly with a different initial condition that stays closed to the computer generated one. More precisely,

Definition 10. *For a given positive number* ε*, an orbit of (4.1) is said to* ε*-shadow a* δ*-pseudo orbit* $\{y_i\}_{i=0}^{N}$ *with associated times* $\{h_i\}_{i=0}^{N-1}$ *if there are points* $\{x_i\}_{i=0}^{N}$ *on the true orbit and times* $\{t_i\}_{i=0}^{N-1}$ *with* $\varphi_{t_i}(x_i) = x_{i+1}$ *such that*

$$\|x_i - y_i\| \leq \varepsilon \quad for \;\; i = 0, \cdots, N, \tag{4.5}$$

and

$$|t_i - h_i| \leq \varepsilon \quad for \;\; i = 0, \cdots, N-1. \tag{4.6}$$

The constant ε in the above definition is referred to as the *shadowing distance.* This definition of ε-shadowing may be generalized by allowing the shadowing distance ε to vary from point to point along the δ-pseudo orbit. More precisely,

Reproduced with permission of the copyright owner. Further reproduction prohibited without permission.

Definition 11. *For a given sequence of positive numbers $\{\varepsilon_i\}_{i=0}^N$, an orbit of (4.1) is said to $\{\varepsilon_i\}_{i=0}^N$-shadow a δ-pseudo orbit $\{y_i\}_{i=0}^N$ with associated times $\{h_i\}_{i=0}^{N-1}$ if there are points $\{x_i\}_{i=0}^N$ on the true orbit and times $\{t_i\}_{i=0}^{N-1}$ with $\varphi_{t_i}(x_i) = x_{i+1}$ such that*

$$\|x_i - y_i\| \leq \varepsilon_i \quad for \;\; i = 0, \cdots, N, \tag{4.7}$$

and

$$|t_i - h_i| \leq \varepsilon_i \quad for \;\; i = 0, \cdots, N-1. \tag{4.8}$$

Note that for

$$\varepsilon = \max_{0 \leq i \leq N} \varepsilon_i, \tag{4.9}$$

a $\{\varepsilon_i\}_{i=0}^N$-shadow of the δ-pseudo orbit $\{y_i\}_{i=0}^N$ is also an ε-shadow of the δ-pseudo orbit.

In a similar manner, we can define the notion of ε-shadowing for the periodic case.

Definition 12. *For a given positive number ε, an periodic orbit of (4.1) is said to ε-shadow a δ-pseudo periodic orbit $\{y_i\}_{i=0}^N$ with associated times $\{h_i\}_{i=0}^N$ if there are points $\{x_i\}_{i=0}^N$ on the true orbit and times $\{t_i\}_{i=0}^N$ with $\varphi_{t_i}(x_i) = x_{i+1}$, $i = 0, \cdots, N-1$,*

Reproduced with permission of the copyright owner. Further reproduction prohibited without permission.

and $\varphi_{t_N}(x_N) = x_0$ *such that*

$$\|x_i - y_i\| \leq \varepsilon \quad for \;\; i = 0, \cdots, N, \tag{4.10}$$

and

$$|t_i - h_i| \leq \varepsilon \quad for \;\; i = 0, \cdots, N. \tag{4.11}$$

Similar to the non-periodic case, this definition of ε-shadowing may be generalized as follows.

Definition 13. *For a given sequence of positive numbers* $\{\varepsilon_i\}_{i=0}^N$*, a periodic orbit of (4.1) is said to* $\{\varepsilon_i\}_{i=0}^N$*-shadow a* δ*-pseudo periodic orbit* $\{y_i\}_{i=0}^N$ *with associated times* $\{h_i\}_{i=0}^N$ *if there are points* $\{x_i\}_{i=0}^N$ *on the true orbit and times* $\{t_i\}_{i=0}^N$ *with* $\varphi_{t_i}(x_i) = x_{i+1}$*,* $i = 0, \cdots, N-1$*, and* $\varphi_{t_N}(x_N) = x_0$ *such that*

$$\|x_i - y_i\| \leq \varepsilon_i \quad for \;\; i = 0, \cdots, N, \tag{4.12}$$

and

$$|t_i - h_i| \leq \varepsilon_i \quad for \;\; i = 0, \cdots, N-1. \tag{4.13}$$

Again, for

$$\varepsilon = \max_{0 \leq i \leq N} \varepsilon_i, \tag{4.14}$$

a $\{\varepsilon_i\}_{i=0}^N$-shadow of the δ-pseudo periodic orbit $\{y_i\}_{i=0}^N$ is also an ε-shadow of the δ-pseudo periodic orbit.

Reproduced with permission of the copyright owner. Further reproduction prohibited without permission.

We now define *hyperbolicity* and *pseudo-hyperbolicity* of a dynamical system. A system of ODE's is said to be hyperbolic if for any given solution $y(t)$ of the system, a δ perturbation of the solution at time $t = t_0, z(t_0) = y(t_0) + \delta$ produces a new solution $z(t)$ that either converges or diverges exponentially to $y(t)$ depending on whether the perturbation δ is on the stable or unstable manifold of the solution $y(t)$ respectively. More precisely,

Definition 14. *A set Λ is called hyperbolic for system (4.1) if*

1. *Λ is compact and φ-invariant.*

2. *There exist numbers $C > 0$, $\lambda_0 \in (0,1)$, and continuous families of linear subspaces $S(p)$ and $U(p)$ of $\mathbb{R}^n$ for each $p \in \Lambda$ such that,*

   (a) *The families S and U are $D\varphi$-invariant, i.e.,*

$$\begin{aligned} D\varphi_t(p)U(p) &= U(\varphi_t(p)), \\ D\varphi_t(p)S(p) &= S(\varphi_t(p)), \end{aligned}$$

   for $p \in \Lambda$ and for $t \in \mathbb{R}$. Here D denotes the derivative with respect to the spatial variable.

   (b) *For $p \in \Lambda$, we have,*

$$\begin{aligned} S(p) \oplus U(p) &= \mathbb{R}^n \quad \text{if} \quad f(p) = 0, \\ S(p) \oplus U(p) \oplus < f(p) > &= \mathbb{R}^n \quad \text{if} \quad f(p) \neq 0. \end{aligned}$$

Reproduced with permission of the copyright owner. Further reproduction prohibited without permission.

Here $< f(p) >$ denotes the one dimensional linear space spanned by $f(p)$.

(c) The following inequalities hold,

$$\begin{aligned} \|D\varphi_t(p)\,v\| &\leq C\lambda_0^t\,\|v\| \quad \textit{for} \quad v \in S(p) \quad , \quad t \geq 0, \\ \|D\varphi_t(p)\,v\| &\leq C\lambda_0^{-t}\,\|v\| \quad \textit{for} \quad v \in U(p) \quad , \quad t \geq 0. \end{aligned}$$

See [23].

The constants C, λ_0 are called the hyperbolicity constants of Λ and the families S and U are called the hyperbolic structure of Λ. The hyperbolicity forces the angle between the stable and the unstable manifolds to be bounded away from 0 [9].

We do not intend to use the assumption of hyperbolicity, but we require the system to exhibit pseudo-hyperbolicity. A system of ODE's is pseudo hyperbolic if trajectories of the system tend to have solutions to the variational equation of the system which can be split into two classes, one of which tends to expand exponentially, while the other tends to contract exponentially, both simultaneously and for nontrivial lengths of time. In other words, the system behaves like a hyperbolic system for finite but nontrivial periods of time [8].

4.2.2 Fixed Point Theorems

In this section we review some of the fixed point theorems that are used in CKP shadowing theorems as well as our shadowing results. Fixed point theorems play a fundamental role in existence and uniqueness theorems in ordinary differential equations.

Reproduced with permission of the copyright owner. Further reproduction prohibited without permission.

Suppose that (X, d) is a complete metric space and $f : X \to X$ is any function.

Definition 15. *The function f is said to satisfy a Lipschitz condition with constant K if*

$$d(f(x), f(y)) \leq Kd(x, y), \tag{4.15}$$

holds for all $x, y \in X$. If $K < 1$, then f is called a contraction mapping.

The following theorem is called *The Principle of Contraction Mapping* .

Theorem 16. *If f is a contraction mapping with constant K on a complete metric space (X, d), then there exist a unique fixed point x_0 of f and if $\tilde{x}$ is any point in X and $\tilde{x}_n = f^n(\tilde{x})$ then*

- $d(\tilde{x}_n, x_0) \leq \frac{K^n}{1-K}$,
- $\lim_{n\to\infty} \tilde{x}_n = x_0$.

The following theorem is a modification of Newton Bisection method. See [3] for a proof.

Theorem 17. *Let X and Y be finite-dimensional topological vector spaces of the same dimension. Let B be an open subset of X and let $\mathcal{G} : B \to Y$ be a mapping of class C^2 with the following properties*

- *The derivative $D\mathcal{G}(v_0)$, $v_0 \in B$ has an inverse $\mathcal{K}$,*

Reproduced with permission of the copyright owner. Further reproduction prohibited without permission.

- *The set B contains the closed ball $N_\varepsilon(v_0)$ centered at v_0 with radius*

$$\varepsilon = 2\|\mathcal{K}\|\|\mathcal{G}(v_0)\|, \tag{4.16}$$

- *The inequality*

$$2M\|\mathcal{K}\|^2\|\mathcal{G}(v_0)\| < 1, \tag{4.17}$$

holds, where

$$M = \max_{v \in N_\varepsilon(v_0)} \|D^2\mathcal{G}(v)\|. \tag{4.18}$$

Then the equation

$$\mathcal{G}(v) = 0, \tag{4.19}$$

has a unique solution in the ball $N_\varepsilon(v_0)$.

In our shadowing theorem we utilize a generalized version of the Schauder fixed point theorem obtained by Browder in 1967 [15].

Theorem 18. ***(Browder)*** *Let X be a locally convex topological linear space, C a compact convex subset of X and $f : C \to X$ be a continuous mapping. Suppose that for each u in the boundary of C there is an element $v \in C$ and a $\lambda > 0$ (both v and λ depending on u) such that*

$$f(u) = u + \lambda(v - u). \tag{4.20}$$

Then f has a fixed point in C.

Reproduced with permission of the copyright owner. Further reproduction prohibited without permission.

The same result holds if we replace $\lambda > 0$ with $\lambda < 0$. The equation (4.20) can be reformulated as

$$u - f(u) \in \mathbb{R}^+ (u - C) \quad \text{for all } u \in \partial C. \tag{4.21}$$

Here ∂C denotes the boundary of the set C. For example consider a cube C in $\mathbb{R}^2$ as shown in Figure (4-1). Let u be a point on the boundary of the cube C. For example if u is on the top edge of the cube, the condition

$$u - f(u) \in \mathbb{R}^+ (u - C),$$

implies that $u - f(u)$ belongs to the top half plane in $\mathbb{R}^2$.

4.2.3 Method of containment

In this section we give an informal description of containment method. Containment was first introduced by Grebogi, Hammel, Yorke and Sauer, GHYS [9], for proving the existence of finite time shadows of two dimensional orbits. It was then generalized to higher dimensions by Hayes and Jackson [8, 7]. The containment method is a simple, elegant method for verification of the existence of true orbits of the system near computer generated orbits. It will provide a distance between the true orbit and the approximate one. We restrict our attention to two dimensional orbits for ease of presentation.

Reproduced with permission of the copyright owner. Further reproduction prohibited without permission.

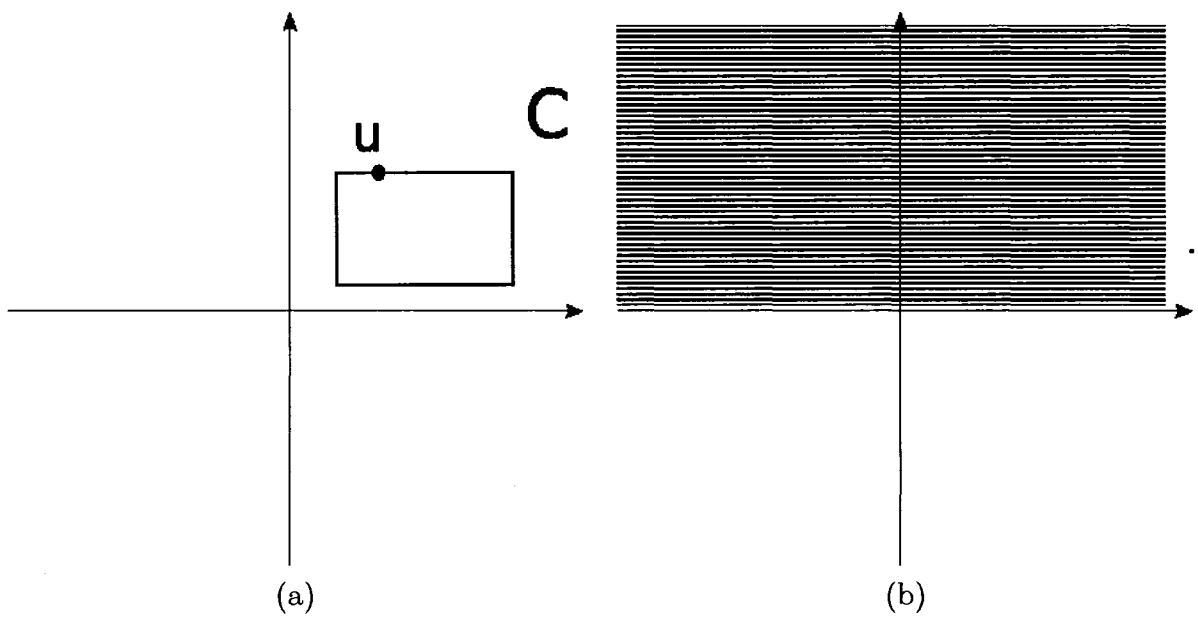

Figure 4-1. Geometric interpretation of the Browder fixed point theorem. For example if the point u on the boundary of the box C lives on the upper edge of the box as shown in part (a) of the figure, then the map $u - f(u)$ has to live in the upper half plane in $\mathbb{R}^2$, i.e., the dashed area shown if part (b) of the figure.

Reproduced with permission of the copyright owner. Further reproduction prohibited without permission.

Assume that $f : \mathbb{R}^3 \to \mathbb{R}^3$ is a C^1 vector field and consider the autonomous differential equation (4.1), with the associated flow $\varphi_t(x) = \varphi(t, x)$. This system is required to be pseudo-hyperbolic. Assume that $\{y_i\}_{i=0}^N$ is a δ-pseudo orbit of this system with associated times $\{h_i\}_{i=0}^{N-1}$. Then the set of points $\{y_i\}_{i=0}^N$ is a pseudo-hyperbolic set for (4.1). This means that at each point y_i we will have a contracting direction and an expanding direction. Perturbations to the point y_i along the expanding direction will diverge from each other while perturbations along the contracting direction will converge to each other on average. The containment process consists of building a parallelogram M_i around each point y_i with the following property. Each parallelogram has two sides $C_i^{\pm}$ approximately normal to the contracting direction at y_i. The sides C_i^+ and C_i^- should be separated from each other. The other two sides $E_i^{\pm}$ of the parallelogram M_i are approximately normal to the expanding direction and are also separated from each other. The maximum value of the diameters of the parallelograms M_i will be the shadowing distance ε.

In order to prove the existence of a shadow, the image $\varphi(M_i)$ of the parallelogram M_i under the flow φ must intersect M_{i+1} such that their intersection makes a plus sign. In other words, the image of the contracting sides of M_i under φ should not intersect the contracting sides of M_{i+1} and the image of the expanding sides of M_i under φ should not intersect the expanding sides of M_{i+1}. Figure 4-2 illustrates this process. To ensure this property, GHYS require a bound on the second derivative of φ. The amounts of the expansion and contraction also need to be bounded away from the range of the machine precision. Next consider a continuous curve γ_i in M_i

Reproduced with permission of the copyright owner. Further reproduction prohibited without permission.

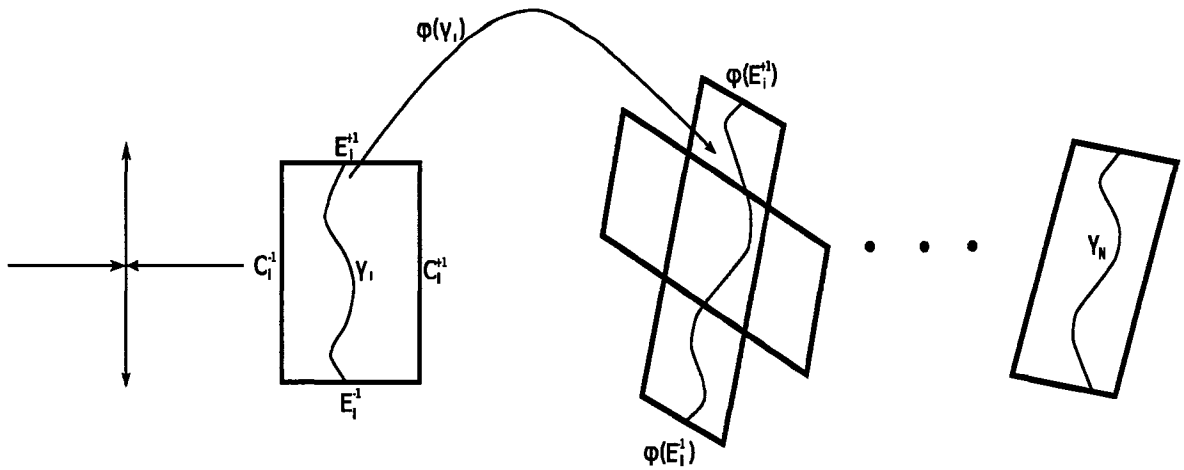

Figure 4-2. Containment Method

connecting the expanding sides E_i^+ and E_i^-. The image $\varphi(\gamma_i)$ of γ_i under φ is a curve lying in $\varphi(M_i)$. In particular there is a section of $\varphi(\gamma_i)$ lying in M_{i+1} connecting the expanding sides at two points. Let γ_{i+1} be this part of $\varphi(\gamma_i)$. Continuing in this way along the δ-pseudo orbit $\{y_i\}_{i=0}^N$, we obtain a sequence of curves $\{\gamma_i\}_{i=0}^N$ with γ_i lying wholly in M_i and connecting the expanding sides $E_i^\pm$ for $i = 0, \cdots, N$. Choose a point x_N on γ_N and trace it backward via φ^{-1}. In this way we obtain an orbit $\{x_i\}_{i=0}^N$ of (4.1) with $x_i \in \gamma_i \subset M_i$ for $i = 0, \cdots, N$. Thus $\{x_i\}_{i=0}^N$ is an ε-shadow of $\{y_i\}_{i=0}^N$.

We note that the angle between the stable and the unstable directions should be bounded away from 0. If the angle gets too small then the parallelogram M_i loses one dimension and image $\varphi(M_i)$ of M_i under φ will fail to make a plus sign with M_{i+1}. This will happen when the angle becomes comparable with the error δ. Hence the more accurate the orbit, the longer it can be shadowed.

Reproduced with permission of the copyright owner. Further reproduction prohibited without permission.

4.2.4 A fixed point method

In this section we review the shadowing theorems obtained by Coomes, Koçak and Palmer, CKP [3, 4], based on fixed point theory. The rough idea is to choose Poincaré surfaces at each point y_i on the δ-pseudo orbit $\{y_i\}_{i=0}^N$, normal to the vector field at that point and prove the existence of a true orbit of the dynamical system that passes through some local neighborhoods of the points y_i on the Poincaré surfaces. In their paper, CKP reduced this problem to proving the existence of a fixed point of a suitably chosen map $\mathcal{G}$. For a fixed point theorem, CKP utilized the Brouwer fixed point theorem. As our approach is very similar to this one, we will shortly discuss the methods here. We will first review the shadowing theorem for aperiodic orbits and then discuss the periodic shadowing theorem.

4.2.4.1 Non-periodic shadowing

In this section we discuss the non-periodic shadowing theorem obtained by CKP [3]. This result is one of the most impressive tools for verifying the shadowability of non-periodic δ-pseudo orbits.

Consider the autonomous system

$$\dot{x} = f(x), \tag{4.22}$$

Suppose that δ is a positive number and $\{y_i\}_{i=0}^N$ is a δ-pseudo orbit of (4.22) with

Reproduced with permission of the copyright owner. Further reproduction prohibited without permission.

associated times $\{h_i\}_{i=0}^{N-1}$. Let

$$h_{\max} = \max_{0 \le i \le N-1} h_i,$$

and let

$$h_{\min} = \min_{0 \le i \le N-1} h_i.$$

If we choose a fixed time step, then all h_i's will be a same number h. Consider the variational flow

$$\begin{aligned} \dot{Y} &= Df(\varphi_t(y_i))Y, \\ Y(0) &= I, \end{aligned} \tag{4.23}$$

where I is the identity matrix. This system is the linearization of (4.22) around the solution $\varphi_t(y_i)$. Let

$$Y_i = D\varphi_t(y_i), \quad i = 0, \cdots, N, \tag{4.24}$$

be the fundamental matrix of solutions of the variational system. Next consider a sequence of hyperplanes H_i passing through y_i and orthogonal to $f(y_i)$. The hyperplanes H_i can be thought of as Poincaré surfaces. Assume that S_i is an $n \times (n-1)$ matrix whose columns form an orthogonal basis for the hyperplane H_i. In their paper, CKP chose initial coordinate systems on each hyperplane H_i and then used

Reproduced with permission of the copyright owner. Further reproduction prohibited without permission.

the Gram-Schmidt orthogonalization to obtain orthogonal bases for the hyperplanes. This method does not provide natural coordinate systems for the hyperplanes and ignores the rotations of the flow of the system. As mentioned earlier, the problem of establishing the existence of true orbits near δ-pseudo orbits is reduced to establishing the existence of a fixed point of a suitably chosen map. This map, which will be defined shortly, is essentially a combination of forward and backward flows of the original system and the variational equation. Choosing the coordinate systems on the hyperplanes in a way consistent with these flows will prevent the rotations of the flows from causing the map to expand and hence increase the chances of obtaining a fixed point. In our theorems in sections 4.3.1 and 4.3.2 we will introduce a way to obtain coordinates consistent with the flow of the system.

The hyperplane H_i can be identified with $\mathbb{R}^{n-1}$ via the transformation $x \mapsto y_i + S_i x$. Define

$$A_i = S_{i+1}^T Y_i S_i, \quad i = 0, \cdots, N-1. \tag{4.25}$$

Here S_{i+1}^T is the transpose of the matrix S_{i+1}. Geometrically, A_i is Y_i restricted to H_i and then projected to H_{i+1}.

The problem of finding a shadow of the δ-pseudo orbit $\{y_i\}_{i=0}^N$ can be formulated as follows. For a given positive number ε, CKP look for a true orbit $\{x_i\}_{i=0}^N$ of (4.22) with the associated times $\{t_i\}_{i=0}^{N-1}$ such that,

1. $x_i \in H_i$ for $i = 0, \cdots, N$,

Reproduced with permission of the copyright owner. Further reproduction prohibited without permission.

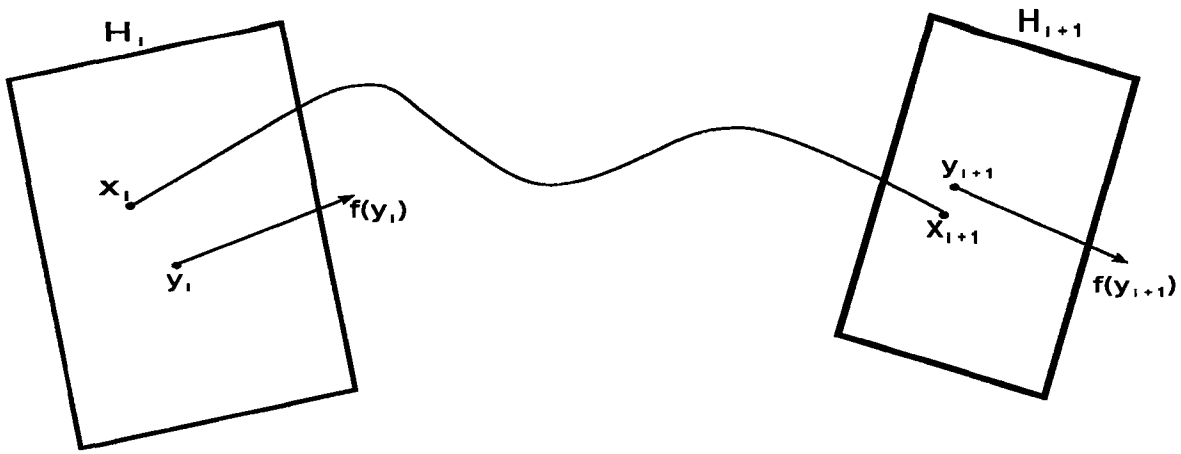

Figure 4-3. Pseudo orbit y_k and shadowing orbit x_k.

2. $\varphi_{t_i}(x_i) = x_{i+1}$ for $i = 0, \cdots, N-1$,

3. $\|x_i - y_i\| \leq \varepsilon$ for $i = 0, \cdots, N$,

4. $|h_i - t_i| \leq \varepsilon$ for $i = 0, \cdots, N-1$.

The points x_i can be represented by

$$x_i = y_i + S_i w_i, \tag{4.26}$$

for some w_i in $\mathbb{R}^{n-1}$. Let $\mathbb{X} = \mathbb{R}^N \times (\mathbb{R}^{n-1})^{N+1}$ with norm

$$\left\| \left(\{s_i\}_{i=0}^{N-1}, \{w_i\}_{i=0}^{N} \right) \right\| = \max \left\{ \max_{0 \leq i \leq N-1} |s_i|, \max_{0 \leq i \leq N} \|w_i\| \right\}, \tag{4.27}$$

and let $\mathbb{Y} = (\mathbb{R}^n)^N$ with norm

$$\left\| \{g_i\}_{i=0}^{N-1} \right\| = \max_{0 \leq i \leq N-1} \|g_i\|. \tag{4.28}$$

Reproduced with permission of the copyright owner. Further reproduction prohibited without permission.

Let U be an open convex set containing the set

$$\bigcup_{i=0}^{N} \varphi([0, h_{\max}], y_i). \tag{4.29}$$

For this set U, define

$$M_0 = \sup_{x \in U} \|f(x)\|, \quad M_1 = \sup_{x \in U} \|Df(x)\|, \quad M_2 = \sup_{x \in U} \left\|D^2 f(x)\right\|,$$

$$\Delta = \inf_{0 \le i \le N} \|f(y_i)\|, \quad \Theta = \sup_{0 \le i \le N-1} \|Y_i\|,$$

and choose a positive number ε_0 in the interval $(0, h_{\min})$ with the following property:

$$\varphi_t(x) \in U \qquad \text{for} \quad t \in [0, \alpha], \tag{4.30}$$

provided that $\|x - y_k\| \le \varepsilon_0$. Here $\alpha = h_{\max} + \varepsilon_0$.

Let B be an open set in $\mathbb{X}$ with radius ε_0 and assume that $v = \left(\{s_i\}_{i=0}^{N-1}, \{w_i\}_{i=0}^{N}\right)$ is a point in B. Define the function $\mathcal{G} : B \to \mathbb{Y}$ by

$$(\mathcal{G}(v))_i = y_{i+1} + S_{i+1} w_{i+1} - \varphi_{s_i}(y_i + S_i w_i) \quad \text{for} \quad i = 0, \cdots, N-1. \tag{4.31}$$

Now let

$$L = I - A_N \cdots A_0. \tag{4.32}$$

Reproduced with permission of the copyright owner. Further reproduction prohibited without permission.

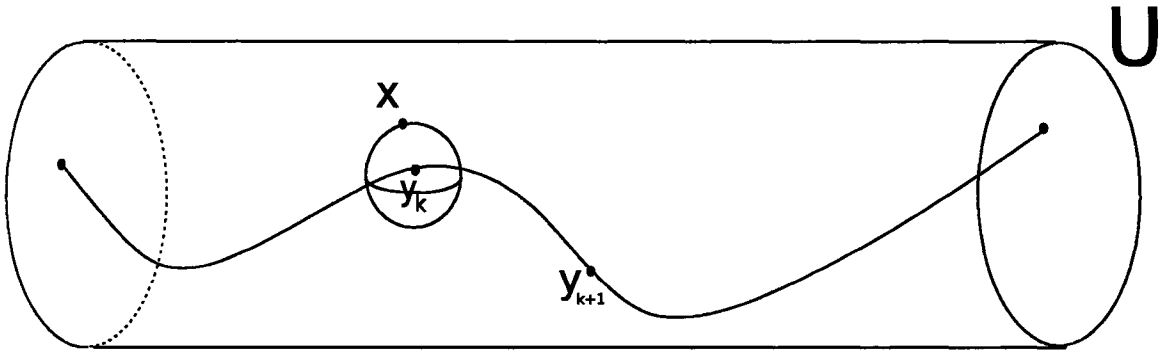

Figure 4-4. The convex set U containing the $\delta-$ pseudo orbit $\{y_k\}_{k=0}^{N}$.

CKP, require this map to be invertible. Since the Brouwer fixed point theorem requires the map to be non-expansive, they have utilized the inverse of the map L to obtain a Newton bisection method which in turn is used to prove the existence of a zero of the map $\mathcal{G}$. Obviously the problem will be solved if we find a zero of the map $\mathcal{G}$. For this to happen, a few inequalities on the error δ are required.

Theorem 19. *Let $\{y_i\}_{i=0}^{N}$ be a δ-pseudo orbit of the autonomous system $\dot{x} = f(x)$ and let*

$$C = \max\left\{\Delta^{-1}\left(\Theta\left\|L^{-1}\right\| + 1\right), \left\|L^{-1}\right\|\right\}. \tag{4.33}$$

If δ satisfies the inequalities

1. $C(M_1 + 1)\delta \leq \frac{1}{2}$,
2. $4\delta C < \min\left\{\min_{0\leq i\leq N-1} h_i, \varepsilon_0\right\}$,
3. $8\left(M_0 M_1 + 2M_1 e^{2M_1 h} + 2M_2 e^{4M_1 h}\right) C^2 \delta \leq 1$.

Reproduced with permission of the copyright owner. Further reproduction prohibited without permission.

then the δ-pseudo orbit $\{y_i\}_{i=0}^N$ is ε-shadowed by a true orbit $\{x_i\}_{i=0}^N$ with $\varepsilon \leq 4C\delta$.

The third condition of the above theorem shows that δ has to be very small in order to control the exponential parts of the condition. In practice these conditions are difficult to meet. In particular, in situations such as chaotic communications, encoding using chaos or stabilization of unstable periodic orbits, the error bound δ becomes much bigger than the acceptable error bound of the theorem. (see chapter 1) This dependency on the error bound δ makes the theorem impractical in such situations.

In the next section we discuss the periodic shadowing theorem obtained by CKP [4], which is also one of the most impressive results in shadowing theory.

4.2.4.2 Periodic shadowing

In this section we review a method for periodic shadowing obtained by CKP [4]. This method allows for proving the existence of a true periodic orbit near an approximated one. The method also provides the shadowing distance in terms of computable quantities.

Assume that $\{y_i\}_{i=0}^N$, is a δ-pseudo periodic orbit of (4.22). Let $\{Y_i\}_{i=0}^N$ be a sequence of $n \times n$ matrices that approximate the fundamental matrices of solutions of the variational equation,

$$\begin{aligned} \dot{Y} &= Df\left(\varphi_t\left(y_i\right)\right) Y, \\ Y(0) &= I. \end{aligned} \tag{4.34}$$

Reproduced with permission of the copyright owner. Further reproduction prohibited without permission.

In other words, assume that

$$|Y_i - D\varphi_{t_i}(y_i)| \leq 0 \quad \text{for} \quad 0 \leq i \leq N. \tag{4.35}$$

Assume that H_i, S_i, A_i, $h_{\min}$, $h_{\max}$ and U are defined as in section (4.3.1). Define

$$M_0 = \sup_{x \in U} \|f(x)\|, \quad M_1 = \sup_{x \in U} \|Df(x)\|, \quad M_2 = \sup_{x \in U} \left\|D^2 f(x)\right\|, \tag{4.36}$$

$$\Delta = \inf_{0 \leq i \leq N} \|f(y_i)\|, \quad \Theta = \sup_{0 \leq i \leq N-1} \|Y_i\|. \tag{4.37}$$

Finally let $\varepsilon_0 \in (0, h_{\min})$ be such that if $\|x - y_i\| \leq \varepsilon_0$, then the solution $\varphi_t(x)$ is defined for $t \in [0, \chi]$ and

$$\varphi_t(x) \in U \quad \text{for} \quad t \in [0, \chi], \tag{4.38}$$

where

$$\chi = h_{\max} + \varepsilon_0. \tag{4.39}$$

Theorem 20. *Assume that $\{y_i\}_{i=0}^N$ is a δ-pseudo periodic orbit for the system (4.22) such that the matrix*

$$L = I - A_N \cdots A_0, \tag{4.40}$$

Reproduced with permission of the copyright owner. Further reproduction prohibited without permission.

is invertible. Let

$$C_1 = \max_{0\le i\le N}\left(\|A_{i-1}\cdots A_0\|\|L^{-1}\|\left(1+\sum_{m=1}^{N}\|A_N\cdots A_m\|\right)+\sum_{m=1}^{i}\|A_{i-1}\cdots A_m\|\right),$$

$$C = \max\left(\tfrac{\theta C_1(1+d_1)+1}{\Delta}, C_1\sqrt{1+d_1}\right),$$

$$d_K = C\left(d\left(M_1+\sqrt{1+d_1}\right)+3d1\tfrac{\sqrt{1+d_1}+\Delta^{-1}}{1-d_1(1+\Delta^{-2})}\right),$$

$$\bar{M} = M_0M_1 + 2M_1\exp M_1\chi\sqrt{1+d_1} + M_2\exp 2M_1\chi\left(1+d_1\right). \tag{4.41}$$

Assume that for the introduced quantities the following inequalities hold.

1. $(1+\Delta^{-2})\,d_1 < 1,$
2. $d_K < 1,$
3. $2Cd(1-d_K)^{-1}\sqrt{1+d_1} < \varepsilon_0,$
4. $2\bar{M}C^2d(1-d_K)^{-2} < 1.$

Then there exist a point x_0 and numbers t_i, $i = 0,\cdots,N$, such that the trajectory of x_0 is closed and

$$\|t_i - h_i\|,\ \ \|x_i - y_i\| \le L_0 d \quad \textit{for} \quad i = 0,\cdots,N, \tag{4.42}$$

Reproduced with permission of the copyright owner. Further reproduction prohibited without permission.

where $x_{i+1} = \varphi_{t_i}(x_i)$, *and*

$$L_0 = \frac{2C}{1 - d_K}\sqrt{1 + d_1}. \tag{4.43}$$

Similar to the CKP's non-periodic shadowing theorem, the error δ has to control the exponential part of the constant $\bar{M}$. Again, this makes the theorem impractical in situations where chaos is controlled via small perturbations.

In the next section we introduce new shadowing theorems. The idea is to combine both the containment method and the fixed point method, in conjugation with Browder fixed point theorem, in order to obtain a theorem that can be applied in broader situations.

4.3 Finite time shadowing theorem

We devote this section to new theorems of non-periodic and periodic shadowing. This method provides a possible technique to establish the existence of real trajectories near approximate ones and gives error bounds for the distance between the true and the approximate trajectories in terms of computable quantities associated with the variational flow along the approximated trajectory. We first start with the non-periodic case.

Reproduced with permission of the copyright owner. Further reproduction prohibited without permission.

4.3.1 Non-periodic shadowing theorem

We now present our finite time shadowing theorem. All the index computations are done in the additive group $\mathbb{Z}_{N+1}$, i.e., all index operations are done mod $N+1$.

As mentioned earlier, our motivation is to provide a general purpose shadowing theorem that can be applied in broader situations. The idea of the theorem is similar to the shadowing theorem of CKP discussed in section 4.2.4.1. We will define a map that takes an interval around the points on the δ-pseudo orbit on each of the Poincaré hyperplanes and projects the interval back to itself passing through all the other hyperplanes. The rotations of the flow of the dynamical system are implemented in the definitions of the map. The coordinates are chosen very carefully and are implicitly used in the map. Similar to the CKP method, the existence of a true orbit of the system that will shadow the computer generated δ-pseudo orbit, depends on the existence of a fixed point of our map. For a fixed point theorem, we have chosen a more natural fixed point theorem, i.e., the Browder fixed point theorem 18 that fits naturally with the set up of the problem.

Suppose that δ is a positive number and $\{y_i\}_{i=0}^{N}$ is a δ-pseudo orbit of (4.22) with associated times $\{h_i\}_{i=0}^{N-1}$. Consider the variational flow

$$\begin{aligned} \dot{Y} &= Df\left(\varphi_t\left(y_i\right)\right)Y, \\ Y\left(0\right) &= I, \end{aligned} \tag{4.44}$$

where I is the identity matrix. Recall that this system is the linearization of (4.22)

Reproduced with permission of the copyright owner. Further reproduction prohibited without permission.

around the solution $\varphi_t(y_i)$. Let

$$Y_i = D\varphi_t(y_i), \quad i = 0, \cdots, N, \tag{4.45}$$

be the fundamental matrices of solutions of the above variational systems.

Similar to the shadowing theorems of CKP, we consider a sequence of hyperplanes H_i passing through y_i and orthogonal to $f(y_i)$ as Poincaré surfaces and assume that S_i is an $n \times (n-1)$ matrix whose columns form an orthogonal basis for the hyperplane H_i. We choose the matrices S_i in a way consistent with the flow of the system. The *Singular Value Decomposition, SVD*, provides one way of obtaining appropriate basis matrices S_i's. First choose a coordinate system with origin at y_i and the $n-th$ axis in the $f(y_i)$ direction. Assume that Γ is the projection of the representation of Y_i in the new coordinates into the hyperplane H_i. Performing a singular value decomposition on the matrix Γ, we obtain two orthogonal matrices U and V and a diagonal matrix W such that

$$\Gamma = UWV^T. \tag{4.46}$$

The Null space of the matrix V is spanned by the unit vector along the $f(y_i)$ direction. The columns of V whose same numbered diagonal elements of the matrix W are nonzero, are an orthonormal basis for the Poincaré surface H_i. Choose S_i to be the $n \times (n-1)$ matrix whose columns are this orthonormal basis for the hyperplane

Reproduced with permission of the copyright owner. Further reproduction prohibited without permission.

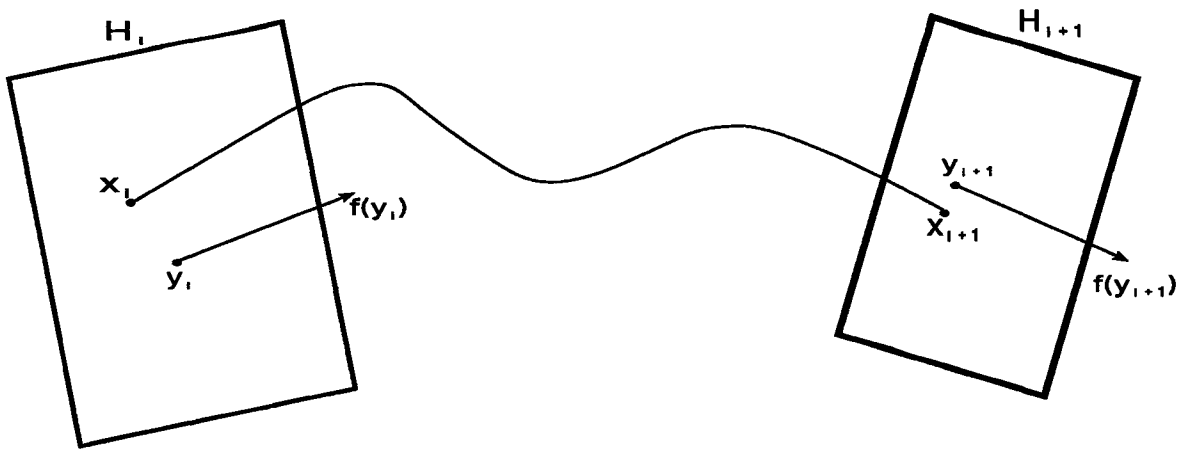

Figure 4-5. Pseudo orbit y_k and shadowing orbit x_k.

H_i. Recall that the hyperplane H_i can be identified with $\mathbb{R}^{n-1}$ via the transformation $x \mapsto y_i + S_i x$. For the ease of notation, we denote $y_i + S_i x$ by $\tilde{x}$. Define the matrices A_i, $i = 0, \cdots, N$, to be

$$A_i = S_{i+1}^T Y_i S_i. \tag{4.47}$$

Here S_{i+1}^T is the transpose of the matrix S_{i+1}. Recall that the matrices A_i can be geometrically interpreted as a map that restricts Y_i to H_i and then projects it to H_{i+1}. We require the matrices A_i to be invertible.

problem of finding a shadow of the δ-pseudo orbit $\{y_i\}_{i=0}^N$ can be formulated as follows. For a given sequence $\{\varepsilon_i\}_{i=0}^N$ of positive numbers, we are looking for a true orbit $\{x_i\}_{i=0}^N$ of (4.22) with the associated times $\{t_i\}_{i=0}^{N-1}$ such that,

1. $x_i \in H_i$ for $i = 0, \cdots, N$,

Reproduced with permission of the copyright owner. Further reproduction prohibited without permission.

2. $\varphi_{t_i}(x_i) = x_{i+1}$ for $i = 0, \cdots, N-1$,

3. $\|x_i - y_i\| \leq \varepsilon_i$ for $i = 0, \cdots, N$.

4. $|h_i - t_i| \leq \varepsilon_i$ for $i = 0, \cdots, N-1$.

The point x_i can be represented by

$$x_i = \tilde{w}_i = y_i + S_i w_i,$$

for some w_i in $\mathbb{R}^{n-1}$. Let $\mathbb{X} = (\mathbb{R}^{n-1})^{N+1}$ with the norm

$$\left\| \{w_i\}_{i=0}^{N} \right\| = \max_{0 \leq i \leq N} \|w_i\|, \tag{4.48}$$

Define the map $\mathcal{G} : \mathbb{X} \to \mathbb{X}$ to be $\mathcal{G} = (g_0, \cdots, g_N)$ with

$$g_i(w_0, \cdots, w_N) = w_i - S_i^T \left[\varphi_{t_{i-1}}(\tilde{w}_{i-1}) - y_i\right], \tag{4.49}$$

for $i = 0, \cdots, N-1$ and

$$g_N(w_0, \cdots, w_N) = w_N. \tag{4.50}$$

Here t_i is the time required for the point $\tilde{w}_i$ on the hyperplane H_i to go to the next hyperplane H_{i+1} via φ. The time $t_i = t_i(\tilde{w}_i)$ depends on the point $\tilde{w}_i$, but for the ease of notation we do not explicitly write this dependency.

Reproduced with permission of the copyright owner. Further reproduction prohibited without permission.

Geometrically we can think of the map $S_i^T\left[\varphi_{t_{i-1}}\left(\tilde{w}_{i-1}\right)-y_i\right]$ as a map which projects the image of the hyperplane H_{i-1} under the flow φ to the hyperplane H_i.

The derivative of the map $\mathcal{G}$ at point 0 is given by

$$D\mathcal{G}\left(0\right)=\begin{bmatrix} -A_0 & I & 0 & \cdots & 0 & 0 \\ 0 & -A_1 & I & \cdots & 0 & 0 \\ \vdots & \vdots & \ddots & \ddots & \vdots & \vdots \\ 0 & 0 & 0 & \cdots & -A_{N-1} & I \\ 0 & 0 & 0 & \cdots & 0 & I \end{bmatrix}. \tag{4.51}$$

Note that $D\mathcal{G}\left(0\right)$ is an invertible matrix. We can easily show that the inverse operator $D\mathcal{G}\left(0\right)^{-1}$ is given by

$$\begin{aligned} \xi_i &= \left(D\mathcal{G}\left(0\right)^{-1}\left(v_0,\cdots,v_N\right)\right)_i \\ &= A_i^{-1}\left(A_{i+1}^{-1}\left(\cdots A_{N-2}^{-1}\left(A_{N-1}^{-1}\left(v_N-v_{N-1}\right)-v_{N-2}\right)\cdots v_{i+1}\right)-v_i\right), \end{aligned}$$

for $i=0,\cdots,N-1$ and

$$\xi_N=\left(D\mathcal{G}\left(0\right)^{-1}\left(v_0,\cdots,v_N\right)\right)_N=v_N.$$

Here $(v_0,\cdots,v_N)$ and $(\xi_0,\cdots,\xi_N)$ are two points in $\mathbb{X}$ and $D\mathcal{G}\left(0\right)^{-1}\left(v_0,\cdots,v_N\right)=(\xi_0,\cdots,\xi_N)$.

Given a sequence $\{\varepsilon_i\}_{i=0}^N$ of positive numbers, let $\tilde{\varepsilon}=\max\limits_{0\le i\le N}\varepsilon_i$ and let $C\left(\varepsilon_i\right)$ denote the cube centered at the origin in $\mathbb{R}^{n-1}$ and side lengths equal to ε_i. Define the

Reproduced with permission of the copyright owner. Further reproduction prohibited without permission.

compact convex set $\mathbb{B}$ to be

$$\mathbb{B} = \prod_{i=0}^{N} C(\varepsilon_i). \tag{4.52}$$

Here $\prod$ denotes the Cartesian product. We restrict the map $\mathcal{G}$ to the compact convex set $\mathbb{B}$.

Now define the map $\mathcal{F} : \mathbb{B} \to \mathbb{X}$ to be

$$\mathcal{F}(w) = D\mathcal{G}(0)^{-1}\mathcal{G}(\tilde{w}), \tag{4.53}$$

and define the map $\mathcal{H} : \mathbb{B} \to \mathbb{X}$ to be

$$\mathcal{H}(w) = w - \mathcal{F}(w), \tag{4.54}$$

for $w = (w_0, \cdots, w_N)$ in $\mathbb{B}$. We note that the problem of finding a shadow of the δ-pseudo orbit $\{y_i\}_{i=0}^{N}$ is solved if we can show the existence of a fixed point of the map $\mathcal{H}$. In order to obtain a set of conditions under which the map $\mathcal{H}$ has a fixed point, we apply the Browder fixed point theorem (18) to this map along with the compact convex set $\mathbb{B}$. Assume that $u = (u_0, \cdots, u_N) \in \partial\mathbb{B}$. Let $\zeta_i : \mathbb{X} \to \mathbb{R}^{n-1}$ be

$$\zeta_i(w) = w_i - A_i^{-1} S_{i+1}^{T} (\varphi_{t_i}(\tilde{w}_i) - y_{i+1}), \tag{4.55}$$

Reproduced with permission of the copyright owner. Further reproduction prohibited without permission.

for $i = 0, \cdots, N$. Here $w = (w_0, \cdots, w_N)$ is a point in $\mathbb{X}$. We can easily verify that if $\xi = (\xi_0, \cdots, \xi_N) = \mathcal{F}(u)$, then $\mathcal{H}(u) = (u_0 - \xi_0, \cdots, u_N - \xi_N)$ with

$$u_i - \xi_i = \zeta_i(u) + A_i^{-1}\zeta_{i+1}(u) + \cdots + A_i^{-1}A_{i+1}^{-1}\cdots A_{N-2}^{-1}\zeta_{N-1}(u), \tag{4.56}$$

for $i = 0, \cdots, N-1$ and

$$u_N - \xi_N = 0. \tag{4.57}$$

The boundary of the set $C(\varepsilon_i)$, i.e., $\partial C(\varepsilon_i)$ consists of $2(n-1)$ faces in $\mathbb{R}^{n-1}$. In particular we may consider the set $C(\varepsilon_i)$ as the Cartesian product of its faces. If we denote the $k-th$ face by F_i^k, then,

$$C(\varepsilon_i) = \prod_{k=0}^{2(n-1)} F_i^k,$$

We now check the conditions of the Browder fixed point theorem for our map $\mathcal{H}$ on $\partial\mathbb{B}$. Consider the space $\mathbb{R}^{n-1}$ with the infinity norm $\|\cdot\|_\infty$. For each $0 \leq j \leq N$, define the set $\mathbb{B}_j$ to be

$$\mathbb{B}_j = C(\varepsilon_0) \times \cdots \times C(\varepsilon_{j-1}) \times \partial C(\varepsilon_j) \times C(\varepsilon_{j+1}) \times \cdots \times C(\varepsilon_N) \tag{4.58}$$

and define the mapping $\mathcal{F}_j : \mathbb{B}_j \to \mathbb{R}^{n-1}$ by

$$\mathcal{F}_j = \left(\mathcal{F}|_{\mathbb{B}_j}\right)_j, \tag{4.59}$$

Reproduced with permission of the copyright owner. Further reproduction prohibited without permission.

where $\left(\mathcal{F}|_{\mathbb{B}_j}\right)_j$ denotes the $j-th$ component of the map $\mathcal{F}$ restricted to $\mathbb{B}_j$. For an arbitrary point $\tilde{u} = (u_0, \cdots, u_N) \in \partial\mathbb{B}$, there exists at least one $0 \leq j \leq N$, such that $u \in \mathbb{B}_j$, i.e., $u_k \in \partial C(\varepsilon_j)$. In particular if $u_j = \left(u_j^1, \cdots, u_j^{n-1}\right)$, we get that u_j^k is either ε_j or $-\varepsilon_j$ for some $1 \leq k \leq n-1$. In order for (4.21) to be satisfied, we need to have that $(\mathcal{F}(u))_j^k \geq 0$ or $(\mathcal{F}(u))_j^k \leq 0$ depending on $u_j^k = \varepsilon_j$ or $u_j^k = -\varepsilon_j$. This needs to be true for all $0 \leq j \leq N$ and for all $1 \leq k \leq n-1$ which in turn implies that the image F_j^k of the $k-th$ face of the cube $C(\varepsilon_j)$ under the map $\mathcal{F}_k$, i.e., $\mathcal{F}_k(F_j^k)$, has to live in the same half-space as F_j^k. In order to verify this condition we need to use interval arithmetic and a validate numerical ODE solver. The computations are quite similar to the containment method.

In order to obtain a shadowing distance ε, we need to estimate the times that it takes to go from the neighborhood $C(y_i, \varepsilon_i)$ on the hyperplane H_i to the next hyperplane H_{i+1} under the flow φ. The hyperplane H_i can be described as

$$H_i = \{x \in X \ ; \ G_k(x) = 0\}, \tag{4.60}$$

where $G_k : \mathbb{R}^n \to \mathbb{R}$ is a linear functional defined by

$$G_k(x) = \langle x | f(y_k) \rangle . \tag{4.61}$$

Reproduced with permission of the copyright owner. Further reproduction prohibited without permission.

Let $(x_1, \cdots, x_n) \in \mathbb{R}^n$ and let $x_{n+1} = G_k(x)$. Define a function $\hat{f} : \mathbb{R}^n \to \mathbb{R}^{n+1}$ by $\hat{f} = (f, f_{n+1})$, where f is the vector field of the system (4.22) and

$$f_{n+1}(x_1, \cdots, x_n) = \dot{G}_k(x) = \langle f(x) | f(y_k) \rangle . \tag{4.62}$$

We now introduce the new system of differential equations

$$\dot{x} = \hat{f}(x) . \tag{4.63}$$

Interchanging the role of the independent variable t with the new variable x_{n+1}, we obtain the following new system

$$\begin{aligned} \frac{dx_1}{dx_{n+1}} &= \frac{f_1}{f_{n+1}}, \\ &\vdots \\ \frac{dx_n}{dx_{n+1}} &= \frac{f_n}{f_{n+1}}, \\ \frac{dt}{dx_{n+1}} &= \frac{1}{f_{n+1}}, \end{aligned} \tag{4.64}$$

Let $v = (v_1, \cdots, v_{n+1}) = (x_1, \cdots, x_n, t)$ and let $g : \mathbb{R}^{n+1} \to \mathbb{R}^{n+1}$ be the function

$$g = \left(\frac{f_1}{f_{n+1}}, \cdots, \frac{f_n}{f_{n+1}}, \frac{1}{f_{n+1}} \right) . \tag{4.65}$$

Then the system (4.64) can then be written as

Reproduced with permission of the copyright owner. Further reproduction prohibited without permission.

$$\dot{v} = g(v), \tag{4.66}$$

which is equivalent to (4.63). Denote the flow of this system by $\psi_{x_{n+1}}(v)$. We are interested in the behavior of this flow between the hyperplanes H_i and H_{i+1}. Note that in this new system the hyperplane H_{i+1} is defined by $v_{n+1} = 0$. Let U be an open convex set containing the set $\bigcup_{i=0}^{N} \varphi([0, h_{\max}], y_i)$. Choose a positive number ε_* in the interval $(0, h_{\min})$ with the property that $\varphi_t(x) \in U$ for $t \in [0, \alpha]$, provided that $\|x - y_k\| \leq \varepsilon_*$. Here $\alpha = h_{\max} + \varepsilon_*$. Then define a convex open set $\tilde{U}$ with

$$\widetilde{U} = \{(x, t) \ ; \ x \in U \ and \ t \in [0, h_{\max} + \varepsilon_*]\}, \tag{4.67}$$

and let

$$M = \sup_{v \in \widetilde{U}} \|D\psi(v)\|. \tag{4.68}$$

If we denote the coordinates of the points y_i and $y_i + S_i w_i$ on the hyperplane H_i by $(y_i^1, \cdots, y_i^n)$ and $(z_i^1, \cdots, z_i^n)$ respectively, then their corresponding representation in the new system are $\alpha = (y_i^1, \cdots, y_i^n, 0)$ and $\beta = (z_i^1, \cdots, z_i^n, 0)$ respectively. Also

$$|t_i - h_k| \leq \|\psi_0(\alpha) - \psi_0(\beta)\|_\infty \leq \|D\psi_0\| \, \|\alpha - \beta\|_\infty \leq M\varepsilon_i. \tag{4.69}$$

Define

$$\varepsilon = \max\left\{\max_{0 \leq i \leq N} M\varepsilon_i, \tilde{\varepsilon}\right\}. \tag{4.70}$$

Reproduced with permission of the copyright owner. Further reproduction prohibited without permission.

This ε is the shadowing distance. So we have proved the following theorem.

Theorem 21. *Assume that δ is a positive number and $f : \mathbb{R}^n \to \mathbb{R}^n$ is a C^2 vector field such that the dynamical system*

$$\dot{x} = f(x),$$

is pseudo-hyperbolic. Let $\{y_k\}_{k=0}^{N}$ be a δ-pseudo orbit of this system with associated times $\{h_k\}_{k=0}^{N-1}$. For a given sequence $\{\varepsilon_j\}_{j=0}^{N}$ of positive numbers, let $C(\varepsilon_j)$ denote the cube in $\mathbb{R}^{n-1}$ centered at the origin with side lengths ε_j. Let

$$\mathbb{B}_j = C(\varepsilon_0) \times \cdots \times C(\varepsilon_{j-1}) \times \partial C(\varepsilon_j) \times C(\varepsilon_{j+1}) \times \cdots \times C(\varepsilon_N).$$

Define $\mathcal{G} = (g_0, \cdots, g_N)$ with $g_i(w_0, \cdots, w_N) = w_i - S_i^T\left[\varphi_{t_{i-1}}(\tilde{w}_{i-1}) - y_i\right]$, for $i = 0, \cdots, N-1$ and $g_N(w_0, \cdots, w_N) = w_N$. Let $\mathcal{F}(w) = D\mathcal{G}(0)^{-1}\mathcal{G}(\tilde{w})$. Assume that $u = (u_0, \cdots, u_N) \in \mathbb{B}_j$ for some $0 \le j \le N$. Then for the mapping $\mathcal{F}_j = \left(\mathcal{F}|_{\mathbb{B}_j}\right)_j$, if $(\mathcal{F}(u))_j^k \ge 0$ or $(\mathcal{F}(u))_j^k \le 0$ depending on $u_j^k = \varepsilon_j$ or $u_j^k = -\varepsilon_j$, for all $0 \le j \le N$ and for all $1 \le k \le n-1$, the δ-pseudo orbit can be $\{\varepsilon_j\}_{j=0}^{N}$-shadowed by a true orbit of the system.

4.3.2 Periodic shadowing theorem

In this section we present our finite time periodic shadowing theorem. The theorem provides the shadowing distance in terms of computable quantities from the

Reproduced with permission of the copyright owner. Further reproduction prohibited without permission.

vector field and the variational flow of the system.It is generally very difficult to prove the existence of a certain periodic orbit in a chaotic system and stabilization and computational techniques are normally used to obtain periodic orbits. Shadowing techniques are among the most useful and practical tools in proving the existence of periodic orbits. Many of the quantities and constants are similar to the pervious section. Recall that all the index computations are done mod $N+1$.

The periodic shadowing is a simple modification of the non-periodic case. The map $\mathcal{G}$ has to be redefined in order to obtain a closed orbit. Some of the assumptions need to be modified and the conditions of the periodic shadowing theorem are slightly different from the non-periodic case. All other quantities are almost identical to the non-periodic case. In particular the numerical computations are done using the same ideas as in the non-periodic case.

Recall that all norms are assumed to be Euclidian norms unless otherwise stated. Assume that $f : \mathbb{R}^n \to \mathbb{R}^n$ is a C^1 vector field. Consider the autonomous differential equation

$$\dot{x} = f(x) \tag{4.71}$$

with the associated flow $\varphi_t = \varphi(t, \cdot)$. By a periodic orbit we mean a solution $x(t) = \varphi_t(x_0)$, for some $x_0 \in \mathbb{R}^n$ such that there exists a positive number T with

Reproduced with permission of the copyright owner. Further reproduction prohibited without permission.

$$x(t) = x(t+T), \quad \text{for } t \in \mathbb{R}. \tag{4.72}$$

Suppose that δ is a positive number and $\{y_i\}_{i=0}^{N}$ is a δ-pseudo periodic orbit of (4.71) with associated times $\{h_i\}_{i=0}^{N-1}$. Assume that H_i, S_i, Y_i and A_i are defined as in the pervious section. Assume that $\{\varepsilon_i\}_{i=0}^{N}$ is a given sequence of positive numbers and let $\mathbb{X} = (\mathbb{R}^{n-1})^{N+1}$ with the norm

$$\left\| \{w_i\}_{i=0}^{N} \right\| = \max_{0 \le i \le N} \|w_i\|, \tag{4.73}$$

Define the map $\mathcal{G} : \mathbb{X} \to \mathbb{X}$ to be $\mathcal{G} = (g_0, \cdots, g_N)$ with

$$g_i(w_0, \cdots, w_N) = w_{i+1} - S_{i+1}^T \left[\varphi_{t_i}(\tilde{w}_i) - y_{i+1}\right], \tag{4.74}$$

for $i = 0, \cdots, N-1$ and

$$g_N(w_0, \cdots, w_N) = w_0 - S_0^T \left[\varphi_{t_N}(\tilde{w}_N) - y_0\right]. \tag{4.75}$$

Here t_i is the time required for the point $\tilde{w}_i$ on the hyperplane H_i to go to the next hyperplane H_{i+1} via φ. The time $t_i = t_i(\tilde{w}_i)$ depends on the point $\tilde{w}_i$, but for the ease of notation we do not explicitly write this dependency.

Geometrically we can think of the map $S_i^T \left[\varphi_{t_{i-1}}(\tilde{w}_{i-1}) - y_i\right]$ as a map which projects the image of the hyperplane H_{i-1} under the flow φ to the hyperplane H_i.

Reproduced with permission of the copyright owner. Further reproduction prohibited without permission.

The derivative of the map $\mathcal{G}$ at point 0 is given by

$$D\mathcal{G}(0) = \begin{bmatrix} -A_0 & I & 0 & \cdots & 0 & 0 \\ 0 & -A_1 & I & \cdots & 0 & 0 \\ \vdots & \vdots & \ddots & \ddots & \vdots & \vdots \\ 0 & 0 & 0 & \cdots & -A_{N-1} & I \\ I & 0 & 0 & \cdots & 0 & -A_N \end{bmatrix}. \tag{4.76}$$

Define the linear operators $\{L_i\}_0^N$ by

$$L_i = I - A_{i-1}A_{i-2}\cdots A_{i-N-1}, \quad \text{for } i = 0, 1, \cdots, N, \tag{4.77}$$

where all the index computation are done in the additive group $\mathbb{Z}_{N+1}$, i.e., mod $N+1$. Note that the matrix $D\mathcal{G}(0)$ is invertible if and only if one of the operators L_i, $i = 0, 1, \cdots, N$, is invertible. In this case the inverse operator $D\mathcal{G}(0)^{-1}$ is given by

$$\begin{aligned} \xi_i &= \left(D\mathcal{G}(0)^{-1}(v_0, \cdots, v_N)\right)_i \\ &= L_i^{-1} S_i^T [Y_{i-1}Y_{i-2}\cdots Y_{i-N}\left(\tilde{w}_{i-N} - \varphi_{t_{i-N-1}}(\tilde{w}_{i-N-1})\right) \\ &+ Y_{i-1}Y_{i-2}\cdots Y_{i-N+1}\left(\tilde{w}_{i-N+1} - \varphi_{t_{i-N}}(\tilde{w}_{i-N})\right) + \cdots \\ &+ \left(\tilde{w}_i - \varphi_{t_{i-1}}(\tilde{w}_{i-1})\right)], \end{aligned}$$

for $i = 0, \cdots, N$. Here $(v_0, \cdots, v_N)$ and $(\xi_0, \cdots, \xi_N)$ are two points in $\mathbb{X}$ and $D\mathcal{G}(0)^{-1}(v_0, \cdots, v_N) = (\xi_0, \cdots, \xi_N)$.

Reproduced with permission of the copyright owner. Further reproduction prohibited without permission.

Let $\tilde{\varepsilon} = \max_{0 \le i \le N} \varepsilon_i$ and let $C(\varepsilon_i)$ denote the cube centered at the origin in $\mathbb{R}^{n-1}$ with side lengths equal to ε_i. Define the compact convex set $\mathbb{B}$ to be

$$\mathbb{B} = \prod_{i=0}^{N} C(\varepsilon_i). \tag{4.78}$$

Here $\prod$ denotes the Cartesian product. We restrict the map $\mathcal{G}$ to the compact convex set $\mathbb{B}$.

Now define the map $\mathcal{F} : \mathbb{B} \to \mathbb{X}$ to be

$$\mathcal{F}(w) = D\mathcal{G}(0)^{-1} \mathcal{G}(\tilde{w}), \tag{4.79}$$

and define the map $\mathcal{H} : \mathbb{B} \to \mathbb{X}$ to be

$$\mathcal{H}(w) = w - \mathcal{F}(w), \tag{4.80}$$

for $w = (w_0, \cdots, w_N)$ in $\mathbb{B}$. We note that the problem of finding a shadow of the δ-pseudo orbit $\{y_i\}_{i=0}^{N}$ is solved if we can show the existence of a fixed point of the map $\mathcal{H}$.

We now apply the Browder fixed point theorem 18 to the map $\mathcal{H}$ along with the compact convex set $\mathbb{B}$. Assume that $u = (u_0, \cdots, u_N) \in \partial\mathbb{B}$. Let $\zeta_i : \mathbb{X} \to \mathbb{R}^{n-1}$ be

Reproduced with permission of the copyright owner. Further reproduction prohibited without permission.

$$\zeta_i(w) = w_i - A_i^{-1} S_{i+1}^T \left(\varphi_{t_i}(\tilde{w}_i) - y_{i+1}\right), \tag{4.81}$$

for $i = 0, \cdots, N$. Here $w = (w_0, \cdots, w_N)$ is a point in $\mathbb{X}$. We can easily verify that if $\xi = (\xi_0, \cdots, \xi_N) = \mathcal{F}(u)$, then $\mathcal{H}(u) = (u_0 - \xi_0, \cdots, u_N - \xi_N)$ with

$$u_i - \xi_i \;=\; \zeta_i(u) + A_i^{-1}\zeta_{i+1}(u) + \cdots + A_i^{-1}A_{i+1}^{-1}\cdots A_{N-2}^{-1}\zeta_{N-1}(u), \tag{4.82}$$

for $i = 0, \cdots, N$.

The boundary of the set $C(\varepsilon_i)$, i.e., $\partial C(\varepsilon_i)$ consists of $2(n-1)$ faces in $\mathbb{R}^{n-1}$. In particular we may consider the set $C(\varepsilon_i)$ as the Cartesian product of its faces. If we denote the $k-th$ face by F_i^k, then,

$$C(\varepsilon_i) = \prod_{k=0}^{2(n-1)} F_i^k, \tag{4.83}$$

We now check the conditions of the Browder fixed point theorem for our map $\mathcal{H}$ on $\partial\mathbb{B}$. Consider the space $\mathbb{R}^{n-1}$ with the infinity norm $\|\cdot\|_\infty$. For each $0 \le j \le N$, define the set $\mathbb{B}_j$ to be

$$\mathbb{B}_j = C(\varepsilon_0) \times \cdots \times C(\varepsilon_{j-1}) \times \partial C(\varepsilon_j) \times C(\varepsilon_{j+1}) \times \cdots \times C(\varepsilon_N) \tag{4.84}$$

and define the mapping $\mathcal{F}_j : \mathbb{B}_j \to \mathbb{R}^{n-1}$ by

$$\mathcal{F}_j = \left(\mathcal{F}|_{\mathbb{B}_j}\right)_j, \tag{4.85}$$

Reproduced with permission of the copyright owner. Further reproduction prohibited without permission.

where $\left(\mathcal{F}|_{\mathbb{B}_j}\right)_j$ denotes the $j-th$ component of the map $\mathcal{F}$ restricted to $\mathbb{B}_j$. For an arbitrary point $\tilde{u} = (u_0, \cdots, u_N) \in \partial\mathbb{B}$, there exists at least one $0 \leq j \leq N$, such that $u \in \mathbb{B}_j$, i.e., $u_k \in \partial C(\varepsilon_j)$. In particular if $u_j = \left(u_j^1, \cdots, u_j^{n-1}\right)$, we get that u_j^k is either ε_j or $-\varepsilon_j$ for some $1 \leq k \leq n-1$. In order for (4.21) to be satisfied, we need to have that $(\mathcal{F}(u))_j^k \geq 0$ or $(\mathcal{F}(u))_j^k \leq 0$ depending on $u_j^k = \varepsilon_j$ or $u_j^k = -\varepsilon_j$. This needs to be true for all $0 \leq j \leq N$ and for all $1 \leq k \leq n-1$, which in turn implies that the image F_j^k of the $k-th$ face of the cube $C(\varepsilon_j)$ under the map $\mathcal{F}_k$, i.e., $\mathcal{F}_k(F_j^k)$, has to live in the same half-space as F_j^k. In order to verify this condition we need to use interval arithmetic and a validate numerical ODE solver. The computations are quite similar to the containment method.

Similar to the pervious section, we estimate the times that it takes to go from the neighborhood $C(y_i, \varepsilon_i)$ on the hyperplane H_i to the next hyperplane H_{i+1} under the flow φ. This will provide a way to estimate a lower bound for ε_i's.

Let $\psi_{x_{n+1}}(v)$ denote the flow of 4.63. Let U be an open convex set containing the set $\bigcup_{i=0}^{N} \varphi([0, h_{\max}], y_i)$. Choose a positive number ε_* in the interval $(0, h_{\min})$ with the property that $\varphi_t(x) \in U$ for $t \in [0, \alpha]$, provided that $\|x - y_k\| \leq \varepsilon_*$. Here $\alpha = h_{\max} + \varepsilon_*$. Then define a convex open set $\tilde{U}$ with

$$\widetilde{U} = \{(x,t) \ ; \ x \in U \ and \ t \in [0, h_{\max} + \varepsilon_*]\}, \tag{4.86}$$

and let

Reproduced with permission of the copyright owner. Further reproduction prohibited without permission.

$$M = \sup_{v \in \widetilde{U}} \|D\psi(v)\| . \tag{4.87}$$

If we denote the coordinates of the points y_i and $y_i + S_i w_i$ on the hyperplane H_i by $(y_i^1, \cdots, y_i^n)$ and $(z_i^1, \cdots, z_i^n)$ respectively, then their corresponding representation in the new system are $\alpha = (y_i^1, \cdots, y_i^n, 0)$ and $\beta = (z_i^1, \cdots, z_i^n, 0)$ respectively. Also

$$|t_i - h_k| \leq \|\psi_0(\alpha) - \psi_0(\beta)\|_\infty \leq \|D\psi_0\| \, \|\alpha - \beta\|_\infty \leq M\varepsilon_i. \tag{4.88}$$

Define

$$\varepsilon = \max\left\{\max_{0 \leq i \leq N} M\varepsilon_i, \tilde{\varepsilon}\right\}. \tag{4.89}$$

This ε is the shadowing distance. So we have proved the following theorem.

Theorem 22. *Assume that δ is a positive number and $f : \mathbb{R}^n \to \mathbb{R}^n$ is a C^2 vector field such that the dynamical system*

$$\dot{x} = f(x),$$

is pseudo-hyperbolic. Let $\{y_k\}_{k=0}^N$ be a δ-pseudo periodic orbit of this system with associated times $\{h_k\}_{k=0}^N$. For a given sequence $\{\varepsilon_j\}_{j=0}^N$ of positive numbers, let $C(\varepsilon_j)$ denote the cube in $\mathbb{R}^{n-1}$ centered at the origin with side lengths ε_j. Let

$$\mathbb{B}_j = C(\varepsilon_0) \times \cdots \times C(\varepsilon_{j-1}) \times \partial C(\varepsilon_j) \times C(\varepsilon_{j+1}) \times \cdots \times C(\varepsilon_N).$$

Reproduced with permission of the copyright owner. Further reproduction prohibited without permission.

Define $\mathcal{G} = (g_0, \cdots, g_N)$ *with* $g_i(w_0, \cdots, w_N) = w_i - S_i^T \left[\varphi_{t_{i-1}}(\tilde{w}_{i-1}) - y_i\right]$, *for* $i = 0, \cdots, N$. *Let* $\mathcal{F}(w) = D\mathcal{G}(0)^{-1}\mathcal{G}(\tilde{w})$. *Assume that* $u = (u_0, \cdots, u_N) \in \mathbb{B}_j$ *for some* $0 \leq j \leq N$. *Then for the mapping* $\mathcal{F}_j = \left(\mathcal{F}|_{\mathbb{B}_j}\right)_j$, *if* $(\mathcal{F}(u))_j^k \geq 0$ *or* $(\mathcal{F}(u))_j^k \leq 0$ *depending on* $u_j^k = \varepsilon_j$ *or* $u_j^k = -\varepsilon_j$, *for all* $0 \leq j \leq N$ *and for all* $1 \leq k \leq n-1$, *the* δ*-pseudo orbit can be* $\{\varepsilon_j\}_{j=0}^N$*-shadowed by a true orbit of the system.*

Reproduced with permission of the copyright owner. Further reproduction prohibited without permission.

CHAPTER 5

CONCLUSION

We believe that cupolets have the potential to provide a framework for developing new techniques in signal processing that bridge the gap between Fourier analysis and wavelet analysis. The rich structure of cupolets allows for processing global as well as the local behavior of discrete signals. The potential exists for a beneficial interchange between chaotic systems and the processing of discrete signals.

The key point is that the vast dynamical behaviors produced by cupolets, are easily accessible via small controls and can be generated with very few bits of information. We believe that the investigation of properties of cupolets can potentially lead to the creation of new techniques that will impact on next generation technologies, while also enabling us to gain a better understanding of the nature of chaotic systems.

We presented several different approaches for the use of cupolets in image compression. We intend to pursue these different techniques further, until it becomes clear which method will produce the most efficient compression. In the next stage of the research, it is important to examine other constructions of adaptive bases for the space of periodic discrete functions using cupolets. One such construction is a

Reproduced with permission of the copyright owner. Further reproduction prohibited without permission.

two dimensional cupolet transform. Further research will investigate these issues as well as looking at the evolution of the cupolet transform coefficients over a sequence of frames from video data.

On the more theoretical side, our investigations of shadowability of cupolets by true unstable periodic orbits establishes a relationship between cupolets and shadowing. This work will allow formal verification that numerically computed orbits and cupolets are uniformly accurate approximations of true solutions. Further, since the unstable periodic orbits that are associated with cupolets are generally dense on an attractor, an analysis of a set of cupolets can be used to characterize the framework of the attractor. This will result in a deeper understanding of the structure of attractors, while also providing a practical means to generate shadows of unstable periodic orbits.

In summary, the study of periodic orbits of chaotic systems appears to be extremely promising from both theoretical and applied perspectives. It will be interesting to see if technological developments benefit more from using chaos to produce periodicity than from the typical aperiodic dynamics.

Reproduced with permission of the copyright owner. Further reproduction prohibited without permission.

BIBLIOGRAPHY

[1] D. V. Anosov. Geodesic flows and closed riemannian manifolds with negative curvature. *Proceedings of the Steklov Institute of Mathematics*, 90, 1967.

[2] T. Beer. Walsh transforms. *American Journal of Physics*, 49:466–472, 1981.

[3] B. A. Coomes, H. Koçak, and K. J. Palmer. Shadowing orbits of ordinary differential equations. *Journal of Computational and Applied Mathematics*, 52:35–43, 1994.

[4] B. A. Coomes, H. Koçak, and K. J. Palmer. Long periodic shadowing. *Numerical Algorithms*, 14:55–78, 1997.

[5] K. M. Cuomo and A. V. Oppenheim. Chaotic signals and systems for communications. In *Proc. IEEE ICASSP*, 1993.

[6] J. E. Frank and J. F. Selgrade. Hyperbolicity and chaon recurrence. *Journal of Differential Equations*, 26:27–36, 1977.

[7] J. E. Frank and J. F. Selgrade. Rigorous shadowing of numerical solutions of ordinary differential equations by containment. *SIAM Journal on Numerical Analysis*, 41:1948–1973, 2003.

[8] J. E. Frank and J. F. Selgrade. *Rigorous shadowing of Numerical Solutions of Ordinary Differential Equations by Containment.* PhD thesis, University of Toronto, 2003.

[9] C. Grebogi, S. M. Hammel, J. A. Yorke, and T. Sauer. Shadowing of physical trajectories in chaotic dynamics: Containment and refinement. *Physical Review Letters*, 65:1527–1530, 1990.

[10] S. M. Hammel, J. A. York, and C. Grebogi. Do numerical orbitsof chaotic dynamical processes represent true orbits? *Journal of Complexity*, 3:136–145, 1987.

[11] S. M. Hammel, J. A. York, and C. Grebogi. Numerical orbitsof chaotic dynamical processes represent true orbits. *Bulletin of American Mathematical Society*, 19:465–470, 1987.

Reproduced with permission of the copyright owner. Further reproduction prohibited without permission.

[12] S. Hayes, C. Grebogi, and E. Ott. Communicating with chaos. *Physical Review Letters*, 70:3031–3034, 1993.

[13] S. Hayes, C. Grebogi, E. Ott, and A. Mark. Experimental control of chaos for communication. *Physical Review Letters*, 73:1781–1784, 1994.

[14] M. Henon. On the numerical computation of poincaré maps. *Physica D*, 5:412–414, 1982.

[15] V. I. Istratescu. *Fixed point theory : an introduction.* D. Reidel Pub. Co., Hingham, MA, USA, 1981.

[16] N. Metropolis, M. L. Stein, and P. R. Stein. On the finite sets for transformations on the unit interval. *Journal of Combinatorial Theory*, 15:25–44, 1973.

[17] N. S. Nedialkov and K. R. Jackson. Validate solutions of initial value problems for ordinary differential equations. *Applied Mathematics and Computation*, 105:21–68, 2003.

[18] E. Ott, C. Grebogi, and J. A. Yorke. Controlling chaos. *Physical Review Letters*, 64:1196–1199, 1990.

[19] A. T. Parker. *Topics In Chaotic Secure Communication.* PhD thesis, University of New Hampshire, 1999.

[20] L. M. Pecora and T. M. Carroll. Synchronization in chaotic systems. *Physical Review Letters*, 64:821–824, 1990.

[21] L. Perko. *Name of the Book.* Springer-Verlag, New York, NY, USA, 2001.

[22] A. Petukhov. Periodic discrete wavelets. *Algebra i Analiz*, 8:151–183, 1996.

[23] S. Y. Pilyugin. *Shadowing in Dynamical Systems.* Springer-Verlag, New York, NY, USA, 1999.

[24] T. Sauer, C. Grebogi, and J. A. York. How long do numerical chaotic solutions remain valid? *Physical Review Letters*, 79:59–62, 1997.

[25] T. Sauer and J. A. York. Rigorous verification of trajectories for the computer simulations of dynamical systems. *Nonlinearity*, 4:961–979, 1991.

[26] K. M. Short, R. A. Garcia, and M. Daniels. Scalability in koz audio compression technology. *AES 119th Convention preprint:6598*, October 2005.

[27] K. M. Short, R. A. Garcia, M. Daniels, J. Curley, and M. Glover. An introducotion to the koz scalable audio compression technology. *AES 118th Convention preprint:6446*, May 2005.

Reproduced with permission of the copyright owner. Further reproduction prohibited without permission.

[28] K. M. Short and A. T. Parker. Security issues in chaotic communications. Paper presented at the SIAM Conference on Dynamical Systems,Snowbird, UT, May 23-27, 1999.

Reproduced with permission of the copyright owner. Further reproduction prohibited without permission.